Design and Synthesis of Perylenediimide, Naphthalenediimide Based n-Type Organic Semiconducting Polymers, Small molecules: Fabrication of High Performance Organic Field-Effect Transistors

A Thesis Submitted

In Partial Fulfilment of the Requirements

For the Degree of

DOCTOR OF PHILOSOPHY

By

Suresh Vasimalla

Roll No. 11612241

Department of Chemistry
Indian Institute of Technology Guwahati
Guwahati-781039, India
September, 2016

Dedicated To

..... Almighty GOD

TH-1703_11612241

INDIAN INSTITUTE OF TECHNOLOGY GUWAHATI

Department of Chemistry

STATEMENT

I hereby declare that the matter embodied in this thesis is the result of investigations carried out by me in the Department of Chemistry, Indian Institute of Technology Guwahati, Guwahati, India under the supervision of Prof. Parameswar Krishnan Iyer.

In keeping with the general practice of reporting scientific observations, due acknowledgement has been made wherever the work described is based on the findings of other investigators.

Guwahati Suresh Vasimalla

September 2016

TH-1703_11612241

INDIAN INSTITUTE OF TECHNOLOGY GUWAHATI

Department of Chemistry

CERTIFICATE

This is to certify that Mr. Suresh Vasimalla has been working under my supervision since July 2011. I am forwarding his thesis entitled "Design and Synthesis of Perylenediimide, Naphthalenediimide Based n-Type Organic Semiconducting Polymers, Small molecules: Fabrication of High Performance Organic Field-Effect Transistors" being submitted for the Ph.D. degree of this institute. I certify that he has fulfilled all the requirements according to the rules of this institute, and regarding the investigations embodied in his thesis and this work has not been submitted elsewhere for a degree.

Guwahati — Prof. Parameswar Krishnan Iyer

September 2016 — Supervisor

TH-1703_11612241

ACKNOWLEDGEMENT

I express my unfathomable gratitude to my thesis supervisor Prof. Parameswar Krishnan Iyer for his incisive thinking, suggestions and cogent advice throughout whole research period. His constant encouragement, criticisms and painstaking planning have aided a long way for preparation of present thesis. His true scientific spirit, independence and self-reliance have helped me an immense to develop the quality of my research work. I shall remain indebted to him forever.

I would like to thank my doctoral committee members Dr. Mohd Qureshi, Dr. A. N. Panda, Dr. Tapas K. Mandal, Dr. Dipak K. Goswami and Dr. Achal Kumar A. S, for their valuable suggestions and comments during all assessments of the Ph. D. program.

I owe my sincere thanks to my Chemistry labmates Radha Krishna Radha, T. Bheemraju, Sameer Hussain, Anamika Kalitha, Akthar Hussain Malik, Arvind Sain Tanwar, Sayan Roy Chowdhury, P. Gopikrishna, Md. Adil Afroz, Niranjan Mehar, Laxmi Raman Adil, Subratho Mondal, Maimur Hussain, Debasish Barman, Nehal Zehra, Rabindranath Garai, Dr. Priyanka Dutta and device labmates Ashish Singh, Dipjyothi das, Anamika Dey, Rahul Narasimhan, Ramesh Babu Yathirajula, Indrani Medhi, Ritesh Kant Gupta and Nystha Baishya for their help and suggestions during my research period.

I would like to express my profound gratitude to my seniors in Chemistry lab Dr. Prasanth J Gowtham, Dr. Athul Kumar Dwivedi, Dr. Muthuraj Bala, Dr. Jupitara and from device lab Dr. Nimmakayala V. V. Subbarao, Dr. Murali Gedda for their immense support, encouragement and help.

I would like to thank all the faculty members, research scholars, supporting staff of the Department of Chemistry and CIF, IIT Guwahati for their kind cooperation in all respects.

I acknowledge DST and MHRD for fellowship for the entire period of the Ph.D. program.

Finally, I want to convey my sincere gratitude to my family members for their sustained help and encouragement in all my academic ventures. I feel deeply indebted to them for whatever I have achieved so far.

Suresh Vasimalla

TH-1703_11612241

List of Figures

TH-1703_11612241

TH-1703_11612241

List of Tables

TH-1703_11612241

List of Symbols and Abbreviations

HOMO	Highest Occupied Molecular Orbital
LUMO	Lowest unoccupied Molecular Orbital
L	Channel Length
W	Channel width

TH-1703_11612241

nm	Nanometer
µm	Micrometer
eV	Electron volt
V_{DS}	Source-Drain Voltage
V_{GS}	Gate-Source Voltage
V_{TH}	Threshold Voltage
I_{DS}	Source-Drain current
S(V)	Sub-threshold slope
C_i	Capacitance
CuPc	Copper Phthalocyanine
µ	Mobility
THF	Tetrahydrofuran
SAM	Surface Assembled Monolayer
CH	Clockwise Hysteresis
ACH	Anti-clockwise Hysteresis
D-A	Donor-Acceptor
A-A	Acceptor-Acceptor
BCB	divinyltetramethylsiloxanebis-benzocyclobutene
TIPS	Triisopropylsilyl
NMR	Nuclear magnetic resonance
MALDI	Matrix-assisted laser desorption/ionisation
TOF	Time of flight
Hz	Hertz
MHz	Mega hertz
Ph	Phenylene
BT	Benzothiadiazole
m/z	Mass to charge ratio
M_n	Number average molecular weight
M_w	Weight average molecular weight
RCA	Radio corporation of America
mbar	Millibar
rpm	Rotation per minute

TH-1703_11612241

nF	Nano farad
HMDS	Hexamethyldisilazane
XRD	X-ray diffractometer
PL	Photoluminescence
UV-vis	Ultraviolet-visible
TGA	Thermogravimetric analysis
DSC	Differential scanning calorimetry
CV	Cyclic voltammetry
AFM	Atomic force microscopy
POM	Polarisable optical microscope
FE-SEM	Field emission scanning electron microscopy
GPC	Gel permeation chromatography
TBAP	Tetrabutyl ammonium perchlorate
E_g	Band gap
λ	Wavelength
T_d	Degradation temperature
Å	Angstrom
FWHM	Full width at half maximum
s	Singlet
d	Doublet
dd	doublet of doublet
MHz	Megahertz
T	Triplet
Q	Quartet
M	Multiplet
Hz	Hertz
MV/cm	Megavolt per centimetre
PVA	Polyvinyl alcohol
PMMA	Polymethyl methacrylate
MΩ	Mega ohm
mA	Milli ampere
σ_{rms}	Root mean square roughness

TH-1703_11612241

TLM	Transmission line method
R_c	Contact resistance
V_A	Anodization voltage
C-PVA	Crosslinked Polyvinyl alcohol
RH	Relative humidity
OHP	Overhead projector

TH-1703_11612241

Abstract

The whole thesis was organized into five chapters. The first chapter is about the brief introduction about organic field effect transistors and gives some recent developments in the Organic Field-Effect Transistors (OFETs). Next two chapters are about the synthesis of new polymers and fabrication of OFETs. Later two chapters are the device engineering to reduce the operating voltages and to increase the stability. The contents of the individual chapters are as follows

Chapter 1 gives the brief introduction about Organic Field Effect Transistors, fabrication and working principles of OFETs and some recent developments in the synthesis of new materials for the fabrication of high performance n-type organic semiconducting materials. Particularly, the development of Perylenediimide (PDI) and Naphthalenediimide (NDI) based materials as the alternatives for the fullerenes was discussed.

Chapter 2 describes the synthesis of two new n-channel Perylenediimide (PDI) copolymers PDI-Ph, and PDI-BT. Remarkable enhancements in the electron transport behaviour for copolymers were achieved on improving the intermolecular interactions in their thin film structures. These solution processable n-type copolymers having PDI backbone was synthesized in high yields (83-86%) by palladium catalyzed Suzuki coupling reactions. Since these copolymers possess crystalline domains, annealing their films induced crystalline phases in the thin film structures with a very high degree of enhancement in crystallinity. The annealing of films resulted in significant enhancement in the intermolecular interactions in the thin film state on the macro scale, facilitating improved and higher charge carrier transport in annealed devices as compared to the as-spun devices which are having lesser crystalline phases. It is observed that the extended conjugation in the copolymer structures, the efficient intermolecular interactions in the thin film state, and the formation of crystalline domains in the copolymers after annealing are responsible for the enhanced device performance. These copolymers demonstrated electron mobility as high as 0.04 cm^2 /Vs and 0.032 cm^2 /Vs for PDI-Ph and PDI-BT are, respectively, with I_{on}/I_{off} ratios of 10^3-10^4.

TH-1703_11612241

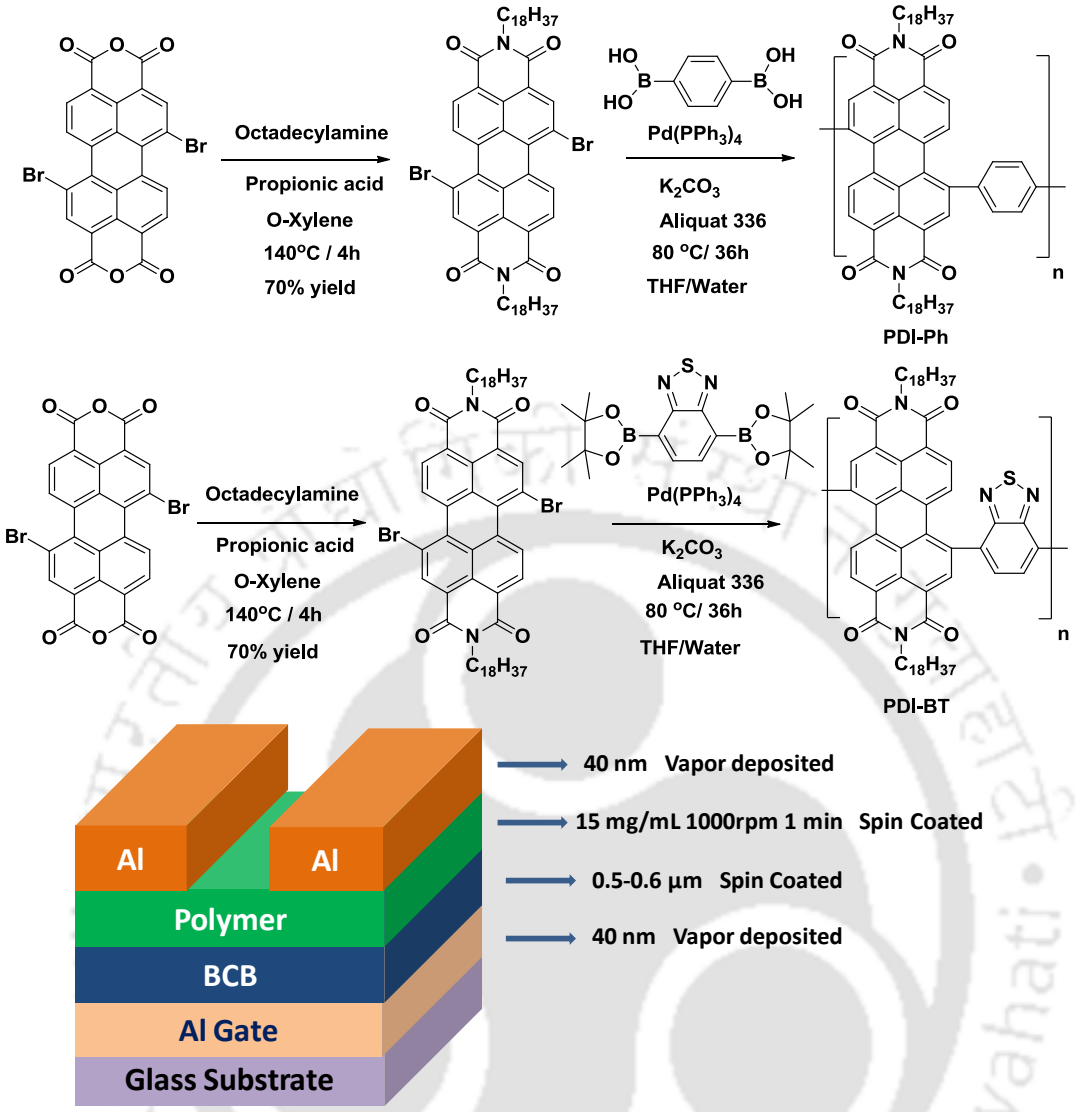

Chapter 3 demonstrates synthesis of two new n-channel naphthalene diimide (NDI) based copolymers NDI-Ph, NDI-BT, and fabrications of solution processed thin film transistor (TFT) devices are reported. These solution processable n-type copolymers were synthesized in high yields (83-86%) by Suzuki coupling reactions. As in case of PDI polymers the annealing of thin films of these polymers also results enhancement in the intermolecular interactions in the thin film state on the macro scale, facilitating improved and higher charge carrier transport in annealed devices as compared to the as-spun devices that have lesser crystalline phases. The enhancement in electron mobility (μ_e) values for all four copolymers is very large for any reported n-type copolymers. The extended conjugation in the copolymer structures, the efficient intermolecular interactions in the thin film state, and the formation of crystalline domains in the copolymers after annealing improved the device performance. These copolymers have shown electron

TH-1703_11612241

mobility enhancement of several orders and are reported to be as high as 0.8 cm^2 /Vs and 0.2 cm^2 /Vs for NDI-Ph and NDI-BT respectively, with I_{on}/I_{off} ratios of 10^3-10^4.

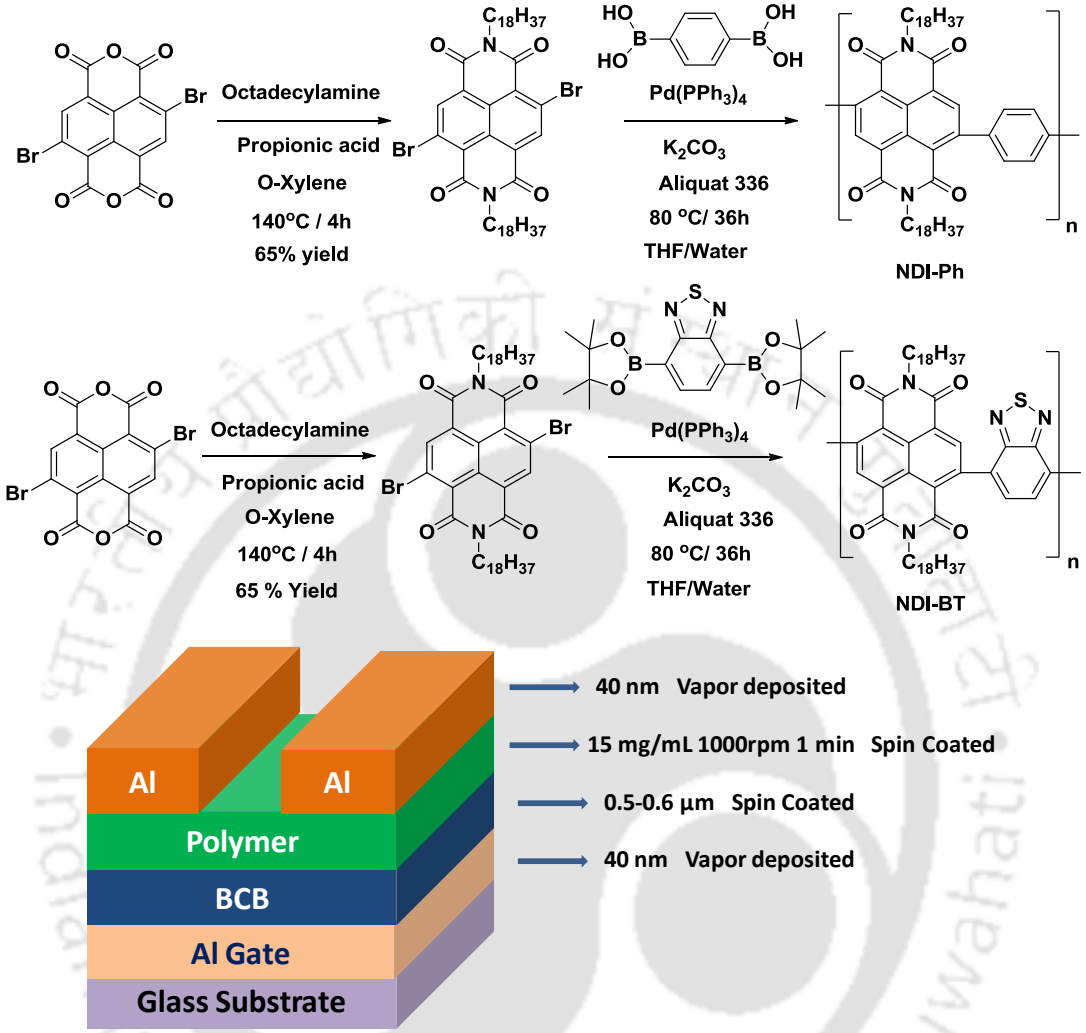

Chapter 4 provides the study of variation of the device parameters by changing the dielectric layer, modification of the dielectric layer at different channel lengths of the OFET. We fabricated the low cost OFET with a new molecule N,N´-bis(octyl)-1,7-dibromo-3,4:9,10-perylene tetracarboxylic dianhydride (Br_2PTCDI-C18) on glass substrate. In this study we used a bilayer dielectric system Al_2O_3/ PVA and Al_2O_3/PMMA. The effect of HMDS as SAM was also studied. The devices were fabricated at 25µm, 50µm, 100µm, 190µm channel lengths with all the combinations of different dielectric systems Al_2O_3/PVA, Al_2O_3/PMMA, Al_2O_3/PVA/HMDS,

TH-1703_11612241

Al_2O_3/PMMA/HMDS. It was observed that as the channel length decreases the I_{DS} increases and the HMDS layer increases the I_{on}/I_{off} ratios of the device.

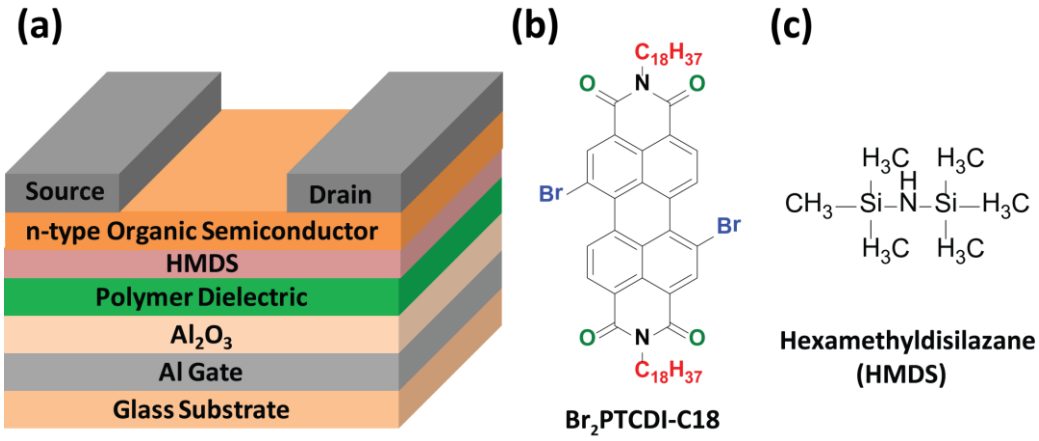

Dielectric Materials Used	Channel Length
Al_2O_3/PVA	25µm
Al_2O_3/PVA/HMDS	50µm
Al_2O_3/PMMA	100µm
Al_2O_3/PMMA/HMDS	190µm

Chapter 5 presents the fabrication of low cost, flexible, ambient stable, low operating voltage and balanced ambipolar organic field-effect transistors on plastic over-head projecter (OHP) sheets as transparent substrates using laminated Al foil as gate electrode without any mechanical or electro polishing for the first time. Br_2PTCDI-C18 is used as n-channel and copper phthalocyanine (CuPc) as p-channel semiconductors. In the first device PMMA/PVA used as the dielectric layer and achieved electron and hole mobilities as high as 1.2×10^{-2} cm^2/Vs and 5.5×10^{-3} cm^2/Vs, respectively, with the operating voltages ± 10 V. Then in the second device we used C-PVA (Crosslinked PVA) as the dielectric material and the operating voltages are further reduced to ± 3V. The electrical, ambient and long-term stabilities of the devices were studied. These results demonstrate very easy fabrication of ambipolar device on low cost substrate and gate with good ambient and electrical stability, which are highly desirable for practical applications.

TH-1703_11612241

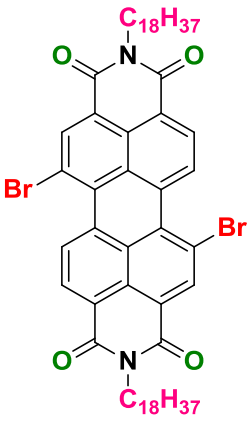

n-type

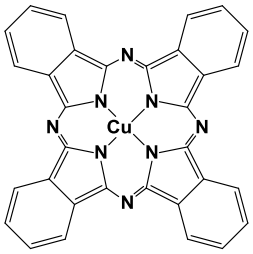

p-type

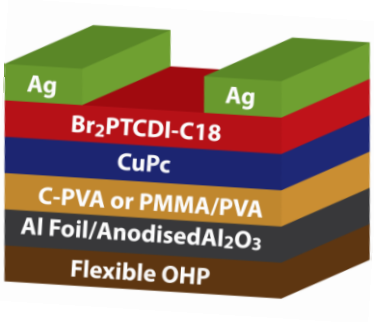

Bare substrate with Al foil Gate

Final device

TH-1703_11612241

Contents

TH-1703_11612241

TH-1703_11612241

TH-1703_11612241

TH-1703_11612241

Chapter 1

Introduction

1.1. Organic Semiconductors

In 1977, Alan J. Heeger, Alan G. MacDiarmid and Hideki Shirakawa discovered the conductivity in polyacetylene. They were awarded the Nobel Prize in Chemistry (2000) jointly for their discovery and development of conductive polymers.[1]

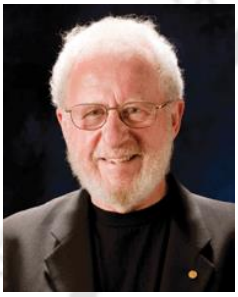

Alan J. Heager

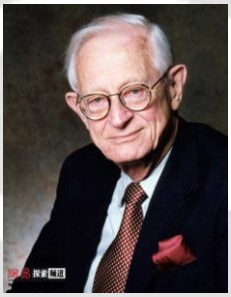

Alan G. MacDiarmid

Hideki Shirakawa

(Images taken from www.materials.ucsb.edu, www.utdallas.edu, www.goto-ikuei.ac.jp/50press/2013/2013-1128-1541-15.html)

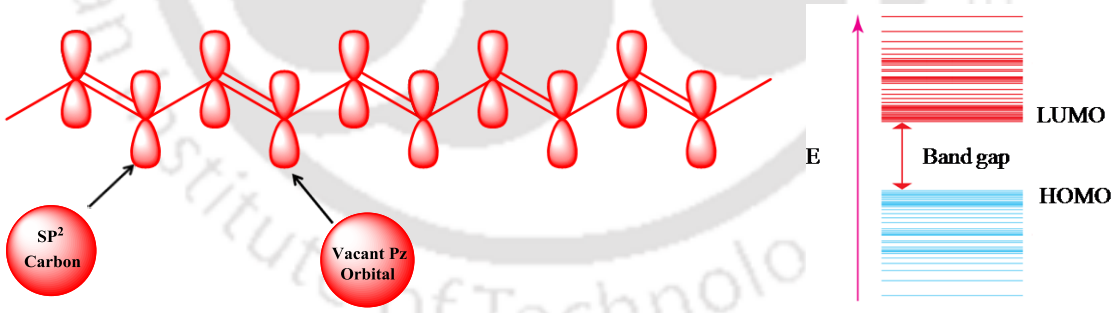

Carbon atom (Z=6) has electronic configuration of $1S^2 2S^2 2P^2$. In conjugated materials 2s, 2px and 2py orbitals of carbon are combined through sp^2 hybridization in trigonal planar form and forms covalent bond between neighboring atoms. This strong covalent bond is called a Sigma (σ) bond, which forms the backbone of the chain. Electrons in this orbital are highly localized between the atoms. The energy differences between the low energy (σ) state and the excited (σ*) state is quite large and well beyond the visible spectral range. Thus the electronic properties related with this bond are that of an insulating material. The fourth orbital (2pz) does not take part in this hybridization and is

TH-1703_11612241

perpendicular to the σ bond. Electrons in this bond are delocalized to the carbon atoms and more mobile. The coupling of two degenerate 2Pz orbitals of adjacent carbon atoms generates two new energetically different orbitals called bonding (π) which is lower in energy compare to original 2Pz orbital and anti-bonding (π*) which is higher in energy compared to the isolated 2Pz orbital. Because of the lower energy of the bonding (π) orbital both of the 2Pz electrons will occupy this orbital, leaving the anti bonding (π*) orbital empty of electrons. In this case the bonding orbital is the highest energy occupied molecular orbital (HOMO), while the anti bonding orbital is the lowest unoccupied molecular orbital (LUMO). In addition, the energy difference between the π orbital and π* orbital is much smaller compared to the energy difference of σ coupling. This band gap has absorption in the visible range and the delocalized nature of the π orbital is responsible to semiconductor properties.

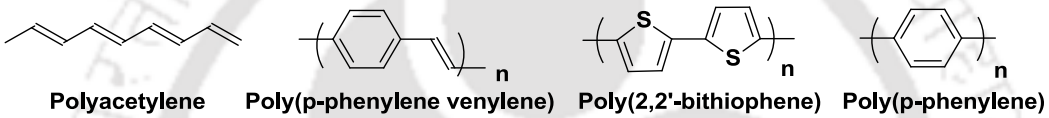

Polyacetylene Poly(p-phenylene venylene) Poly(2,2'-bithiophene) Poly(p-phenylene)

1.2. Organic electronic devices

Organic semiconducting materials have the advantages over the traditional inorganic counterparts such as structural modifications, low cost and less time for the fabrication, flexibility, and light weight. Organic semiconducting materials can be used in wide range of electronic applications such as Organic Field-effect Transistors, Organic Light Emitting Diodes and Organic Photovoltaic applications. There are certain challenges to overcome in terms of low mobility and environmental stabilities in the organic semiconductors. In the past few decades, intensive academic and commercial interest has been afforded to this subject to overcome these challenges with considerable success. There are different approaches to achieve better performance of OFETs which include developing new materials and device engineering by which the stability and all the device parameters can be improved. The structural modifications can alter the packing patterns of the molecules which affects the device performance. In the subsequent sections it was mainly discussed the development of semiconducting materials in recent years for the fabrication of high performance organic field effect transistors and some studies on the device fabrication to improve its performance.

TH-1703_11612241

1.3. Organic field-effect transistors

1.3.1 Fabrication of Organic field-effect transistors

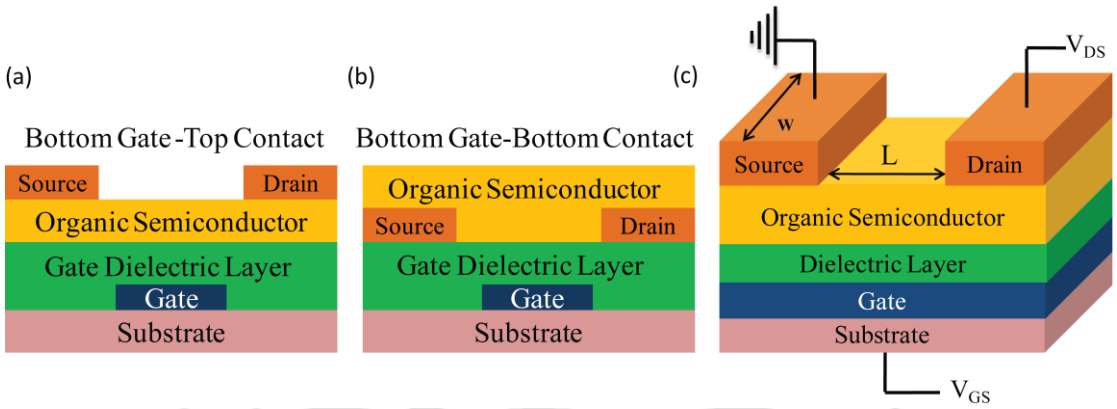

Figure 1.1. Schematic diagrams of cross sectional view of organic field-effect transistors (a) Bottom Gate-Top Contact (b) Bottom Gate-Bottom Contact and (c) Top view of the Bottom Gate-Top Contact configuration.

From the above figure, in both cases of top-contact and bottom-contact transistor configurations an organic semiconductor film is deposited on a gate/insulator substrate and is contacted with source and drain electrodes. In the top-contact case, Figure 1.1(a), the organic film is deposited first, followed by the metal electrodes. In the bottom-contact case, Figure 1.1(b), this deposition order is reversed. Usually, the gate/insulator assembly consists of a metal or doped semiconductor gate electrode coated with an insulating oxide (200-400 nm thick), though polymeric insulators are also used and might be preferable for flexible electronics. The organic semiconductor film (30-50 nm thick) can be deposited from the vapor phase or by spin or drop coated from solution. If desired, surface treatments on the insulator may be used prior to deposition of the semiconductor layer which has shown profound effects on the resulting thin film structure and electrical characteristics. The metal source and drain electrodes are often vapor-deposited through a shadow mask, but conductive inks that can be printed are also employed. Source-drain channel lengths, L, shown in Figure 1.1(c), typically range from 10 to 100 µm, and channel widths, W, are usually between 100 µm and 1 mm.

1.3.2 Working principle of Organic field-effect transistors

The voltage applied between the source and drain is referred to as the source-drain voltage, V_{DS}. For a given V_{DS}, the amount of current that flows through the

TH-1703_11612241

semiconductor film from source to drain is a function of the voltage, V_{GS}, applied to the gate electrode. The semiconductor film and the gate electrode are capacitively coupled such that application of a bias on the gate induces charge in the semiconductor film. This charge is mobile and moves from source to drain when the voltage V_{DS} is applied. When there is no gate voltage is applied, the conductivity of the semiconductor film is very low because there are no mobile charge carriers i.e., the device is "off". When the gate voltage is applied, mobile charges are induced, and the transistor is on. The origin of the gate-induced charging known as the "field effect" is described in the simplified electronic energy level diagrams shown in Figure 1.2. Figure 1.2(a) shows the positions of the HOMO and LUMO of the organic semiconductor relative to the Fermi levels of the source and drain metal electrodes. In this case, the gate bias is zero. As shown in Figure 1.2(b) when a positive gate voltage is applied (with V_{DS} = 0), a large electric field produces at the organic/insulator interface. This field causes the HOMO and LUMO levels in the semiconductor to shift down to lower in energy with respect to the Fermi levels of the metal contacts. When the gate field is large enough, the LUMO will become resonant with the Fermi levels of the contacts then electrons can flow from the contacts

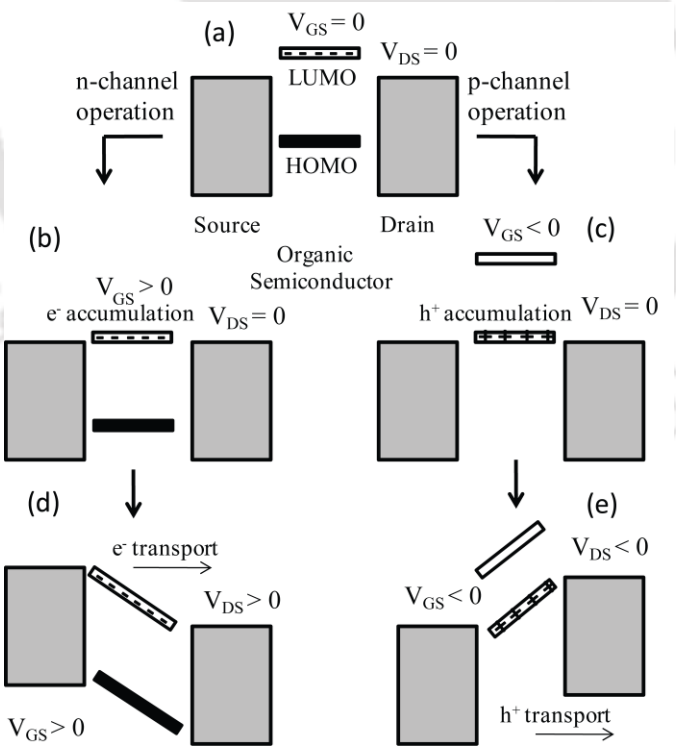

Figure 1.2. Schematic diagrams showing the working principle of Organic field-effect transistors

TH-1703_11612241

into the LUMO, Figure 1.2(b). Now there are mobile electrons at the semiconductor/insulator interface. Upon application of a drain voltage $V_{DS} > 0$, Figure 1.2 (d), results in electric current between the source and drain. This same principle applies with negative gate bias also, Figure 1.2(c), (e). Negative gate bias causes the HOMO and LUMO levels to shift up such that the HOMO becomes resonant with the contact Fermi levels and electrons spill out of the semiconductor and into the contacts, leaving positively charged holes. These holes are now the mobile charges that move in response to an applied drain voltage, (Figure 1.2(e)). In Figure 1.2(d), (e) the source electrode is always the charge-injecting contact regardless of the sign of the gate bias voltage.

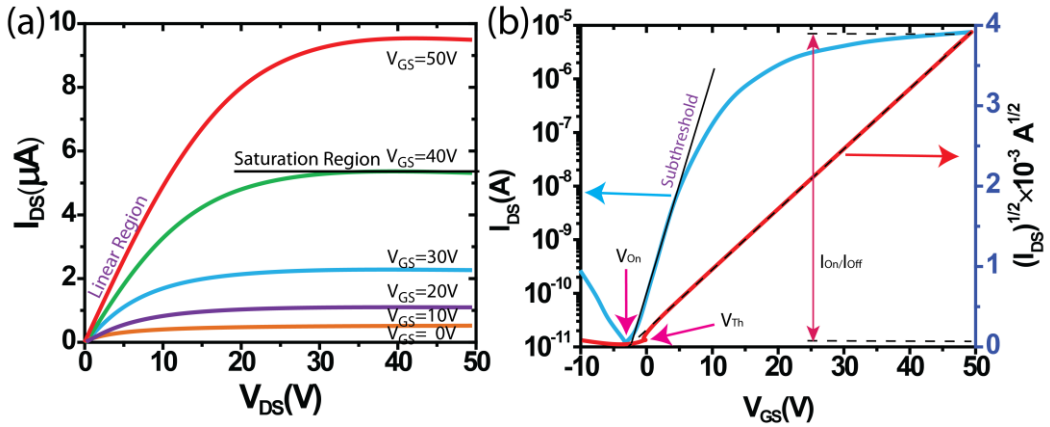

Figure 1.3. Transistor characteristics of an ideal organic field-effect transistor: (a) output characteristic, (b) saturation regime transfer characteristic.

As shown in output curve for n-type material (Figure 1.3 (a)) V_{DS} is swept while a constant V_{GS} is applied. If a positive V_{GS} is applied to an n-type OFET, I_{DS} will increase linearly as V_{DS} increases from 0 V to a positive voltage. When V_{DS} is as large as V_{GS}, the field at the drain electrode is reduced to 0 and the channel is "pinches off". As a result, I_{DS} saturates. To measure transfer characteristics V_{GS} is swept while a constant V_{DS} is applied (Figure 1.3(b)). The transfer characteristics can be measured in the linear region for lower V_{DS} and in the saturation regime for higher V_{DS}. The device parameters can be extracted from the equations derived for the drain current in the linear and saturation region.

In the linear regime $V_{GS} - V_{Th} >> V_{DS}$, the accumulation region is uniform along the channel and hence,

TH-1703_11612241

$$I_{DS} = \frac{\mu_{lin} W C_i}{L} [(V_{GS} - V_{Th}) V_{DS}]$$

In the saturation regime where pinch-off of the accumulation region occurs and $V_{DS} = V_{GS} - V_{Th}$ we have,

$$I_{DS} = \frac{\mu_{sat} W C_i}{2L} (V_{GS} - V_{Th})^2$$

Where, μ_{lin} and μ_{sat} are the field-effect mobilities in two regions for the majority charge carriers, C_i is the geometric capacitance of the dielectric, V_{Th} is the threshold voltage, V_{GS} is gate voltage, I_{DS} is drain current and W and L are channel width and channel length. Fitting a straight line to the square root of the measured I_{DS} yields the band mobility μ and the threshold voltage V_{Th}. I_{on}/I_{off} ratios can be calculated from corresponding on and off currents.

1.3.3 Different configurations of Organic field-effect transistors

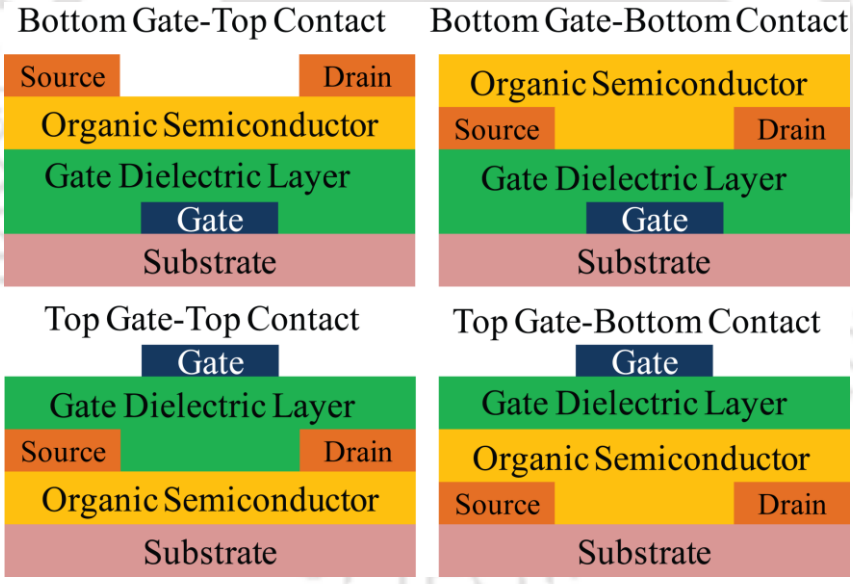

Figure 1.4. Schematic diagrams of cross sectional view of different configurations of Organic field-effect transistors

The electrode/organic layer interface has a key influence on carrier injection. In an ideal OFET, ohmic contact is assumed, such that the contact resistance is much lower than the channel resistance. However, Schottky contact is usually present in real OFETs and leads to large contact resistance. Therefore, the carrier injection barrier, which is determined by the work function of the electrodes and the energy level of the organic semiconductors, is

TH-1703_11612241

an important parameter by which to evaluate the electrode/organic layer interface. For many OFETs, especially the n-type ones, reduction of carrier injection barrier is one of the most efficient ways to improve electrode/ organic layer interface and device performance. Besides the energy barrier, the device structure also influences the contact resistance. The typical OFET device structure can be divided into Top Gate Bottom-Contact (TGBC), Top Gate-Top Contact (TGTC), Bottom Gate-Bottom Contact (BGBC), and Bottom Gate-Top Contact configurations (BGTC) (Figure 1.4). It has been well-accepted that BGTC and TGBC OFETs usually exhibit lower contact resistance than BGBC and TGTC ones. This is mainly due to the different carrier injection paths and injection areas. BGTC and TGBC devices possess large injection areas and favored injection paths compared with BGBC and TGTC devices, which leads to lower contact resistance. The contact condition of the electrode/organic interface is also dependent on the device geometry. For example the source, drain electrodes are deposited before the deposition of the organic layers for BGBC OFETs. Unfortunately, the metal electrodes usually have a negative influence on the semiconductor deposition and bring on large boundaries density at the electrodes/organic layer interface. As a result, the poor contact condition contributes in large part to the contact resistance. In fact, improvement of BGBC OFET contact conditions is an import subject since BGBC geometry is a feasible one for industrial applications, but because of the poor semiconductor morphology in the bottom contact configuration, especially at the edge of the contacts the BGTC is recognized to offer a lower contact resistance in the case of a thin film device. In a word, the energy barrier, carrier injection area, and contact condition are three major factors that determine the electrode/organic layer interface.

1.4. Types of Organic Semiconductors

Organic semiconducting materials can be classified as hole (p-type) or electron (n-type) transport materials depending on the type of majority charge carriers they can transport. Organic p-type and n-type materials differ from classical inorganic p- and n-type semiconductors. The charge carriers in inorganic semiconductor move in wide delocalized bands and have high mobility, where as in disordered organic semiconductors through phonon assisted tunneling (hopping) between localized states which gives rise to the low mobility of charge carriers. Another classes of materials, ambipolar materials having hole and electron mobilities and can act as both p-type and n-type materials,

TH-1703_11612241

depending on the dominant injection processes occurring under the experimental conditions of interest. Amongst the factors which determine the quality of an organic transistor we can mention (i) mobility of the charge carriers (ii) device stability (iii) operating voltage and (iv) on/off ratio. All these parameters, in combination with the low-cost production, drive the search for new active materials or the improvement of already existing materials. In the case of already existing materials, even if the correlation between structural properties and device performance has already been established,[2] much effort to be made to fully understand the properties of the interfaces, which are the causes of most non-ideal effects that limits the performance of the OFET devices.

Organic semiconductors must satisfy general criteria to achieve acceptable performance relating both the injection and current carrying characteristics, particularly (a) the highest occupied/lowest unoccupied molecular orbital (HOMO/LUMO) energies of the individual molecules must be at levels where holes/electrons can be induced at accessible applied electric fields (b) the crystal structure of the material must provide adequate overlap of molecular orbitals to allow efficient charge transport between adjacent molecules (c) the solid should be extremely pure because impurities may act as traps for the charge carrier (d) the molecules should be preferentially oriented the long axes approximately parallel to the substrate since the most efficient charge transport occurs along the direction of intermolecular π-π stacking. First organic thin film transistor based on Poly-thiophene (PT) was reported in 1986 with mobility of 10^{-5} cm^2/Vs.[3] After that enormous progress has been made in design and synthesis of new organic semiconductors and insulators materials, improving manufacturing techniques and in development of new OTFT structures. Here some of the p-type, n-type small molecules and polymers which have been widely used for the fabrication of Organic Field-Effect Transistors have been summarized.

1.4.1. p-type Semiconductors

Conjugated molecules which can transport holes act as p-type semiconductors. Although initial experiments on the transport properties of organic semiconductors were performed on anthracene and tetracene,[4] pentacene has become one of the most extensively studied organic semiconductors for OFETs.[5] Pentacene has a very high melting point and is virtually insoluble, even in hot aromatic solvents. Therefore, many strategies to solubilize it have been developed (**Me_2-Pentacene, Pentacene-TIPSA**). High-performance

TH-1703_11612241

pentacene devices also been fabricated using polymer dielectrics with carrier mobilities as high as 3 cm^2/Vs.[6] Recently a lot of studies have targeted on **rubrene** based transistors.[7] Another important class of molecular semiconductors is based on the thiophene ring, an electron-rich heterocycle, with sexithiophene (**6T**) and hexyl substituted thiophene oligomers (e.g. **DH-6T** and **DH-4T**) the most investigated examples[8] demonstrating relatively high mobilities. However, Hajlaoui et al have reported a field-effect mobility in a vacuum-deposited film of unsubstituted **8T** as high as 0.33 cm^2/Vs.[9] An approach to solubilize oligothiophenes has been reported by Frechet et al,[10] using an ester-terminated 6T that is converted to **Et-6T** by heating at 150 - 200°C. The performance of thiophene-based semiconductors has been further explored using benzodithiophene (**BDT**) and thienodithiophene (**TDT**) as core units.[11] Extension to the other benzo[1,2-b:4,5-b'] dichalcogenophenes (X = **Se,Te**)[12] and use of larger π-cores has resulted in new class of interesting derivatives.

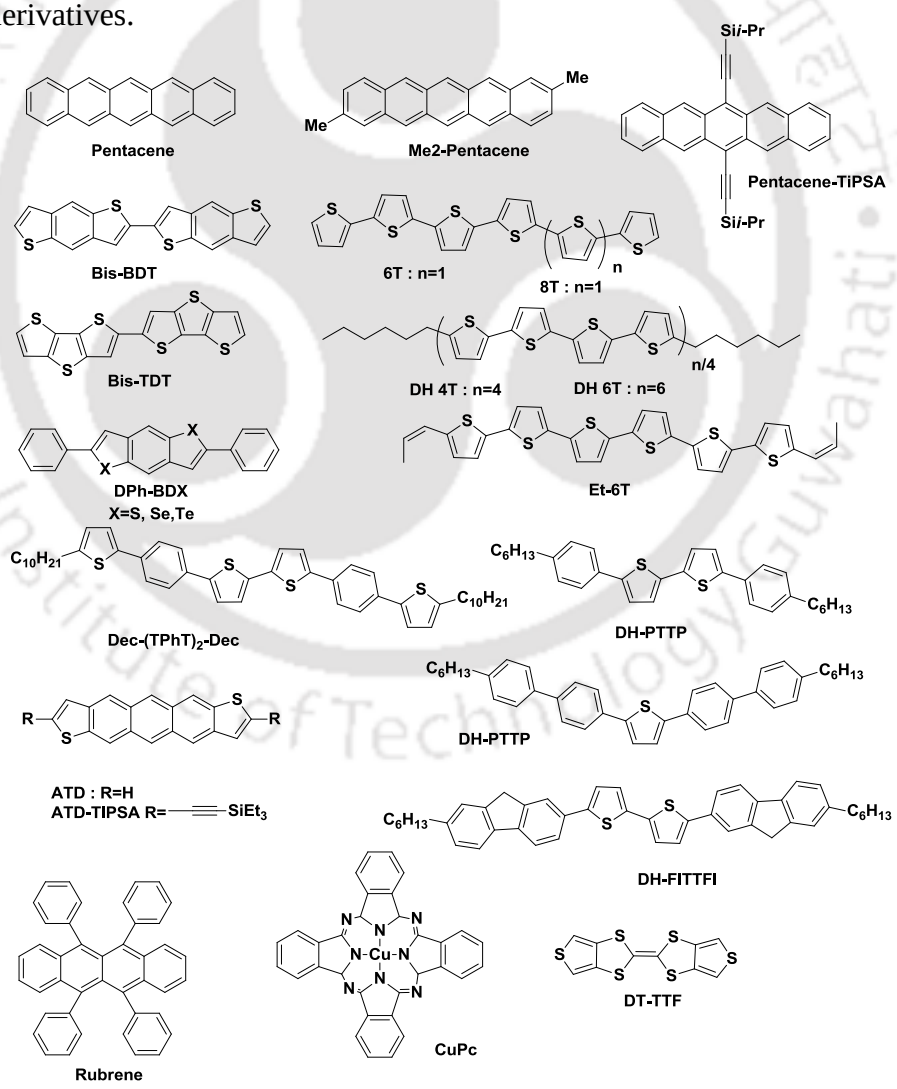

Figure 1.5. Chemical structures of some small molecule p-channel organic semiconductors

TH-1703_11612241

Mixed thiophene-phenylene oligomers (**dH-PPTPP** and **dH-PTTP**) have been synthesized by Stille coupling and display high mobilities as evaporated/solution-cast (up to 0.09/0.03 cm^2/Vs) films, as well as nonvolatile memory properties.[13] Ponomarenko et al[14] reported decyl-substituted thiophene-phenylene oligomers (e.g. **Dec-TPhT-Dec**) reaching $\mu \sim 0.4$ cm^2/Vs. Mobilities as high as 0.11 cm^2/Vs and $I_{on}/I_{off} \sim 10^5$ have been reported for thiophene fluorine oligomer **DH-FlTTFl**.[15] Anthradithiophene (**ADT**) derivatives have been prepared by combining the molecular shape of pentacene with thiophene to achieve good packing and stability and characterized for the first time by Laquindanum et al.[16] Later, a lot of research is targeting the semiconducting properties of phthalocyanines (Pcs), the most common derivative, copper Phthalocyanine (**CuPc**),[17] exhibits $\mu \sim 0.02$ cm^2/Vs and $I_{on}/I_{off} > 10^5$. OFETs fabricated with **CuPc-NiPc** composites[18] and rare earth Lu and Tm bis(phthalocyanines)[19] exhibit $\mu < 0.05$ cm^2/Vs. Another report demonstrated **CuPc** nanorods with OFET properties of $\mu \sim 0.1$ cm^2/Vs and $I_{on}/I_{off} \sim 10^2$.[20] There are numerous other p-type materials have been synthesized in recent years to fabricate high performance OFETs.[21]

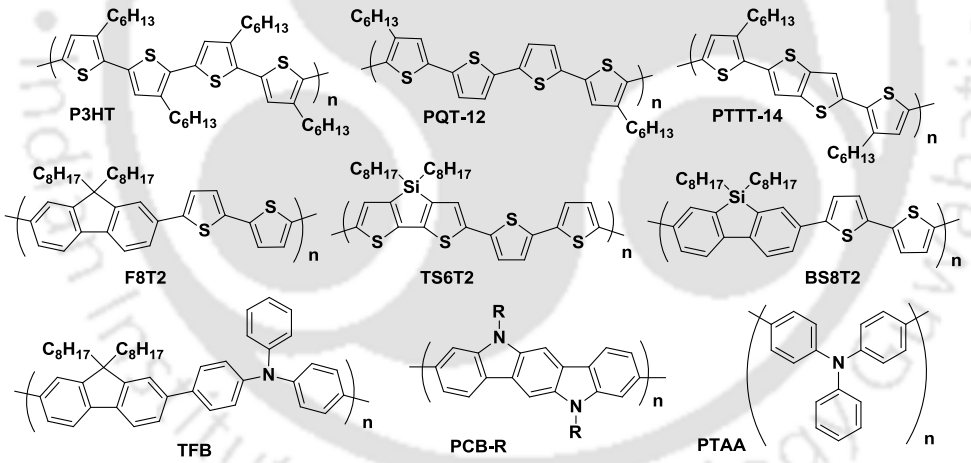

Figure 1.6. Chemical structures of some p-channel polymer organic semiconductors

In addition to the above mentioned small molecules there are many polymeric p-type semiconducting materials have been reported in the past few years. Poly 3-substituted thiophenes are one of the most studied polymers.[22] The first solution-processed polymer for OFETs ($\mu = 10^{-4}$-10^{-5} cm^2/Vs)[23] was based on a regiorandom poly(3-hexylthiophene) (**P3HT**), which exhibits FET performance comparable to electrochemically prepared, insoluble polythiophene,[24] later many P3HT based polymers were synthesized (Figure 1.6). Mc Cullogh et al[25] synthesized thieno [3,2-b] thiophene polymers that exhibit

TH-1703_11612241

liquid-crystalline behavior, highly organized morphology, and large crystal domains. Another family of solution-processable polymers for FETs is based on the fluorine ring, with poly[9,9-dioctylfluorene-co-bithiophene] (**F8T2**) being the most studied structure.[26] After that, a version of **F8T2** in which **Se** replaces **S** (**F8Se2**) has been synthesized that exhibits a hole mobility of 0.012 cm^2/Vs and a low threshold voltage of -4 V.[27] In another strategy, the carbon atom bridging the **F8T2** fluorine ring (**BS8T2**), cyclopentadithiophene (**TS6T2**) has been replaced by Si to reduce the HOMO/LUMO energies and stabilize device operation in air. Other polymeric semiconductors are based on 9,9-dialkylfluorene-alt-triarylamine (e.g. **TFB**),[28] carbazole (e.g. **PCB**),[29] and triarylamine units.[30] Polytriarylamines (**PTAA**) are amorphous semiconductors that have been used to study dielectric effects in OFETs.[31] A wide range of polymers are synthesized and used as active materials for fabrication of High performance OFETs.[32]

1.4.2. n-type Semiconductors

Despite their importance for fabricating organic photovoltaic (OPV) cells and n-channel organic field-effect transistors (OFETs), which are particularly valuable components of organic complementary logic circuits, which require both p- and n-channel transistors the development of high performance (environmentally stable, high-mobility) n-channel organic TFT materials has lagged behind that of p-channel materials. The main reason for this is the instability of these materials towards O_2 and H_2O which is attributed to their high lying LUMO levels.[33] Therefore, the area of n-channel organic semiconductors involves not only maximizing the mobility of these materials but also minimizing the deterioration of electronic properties over time. To achieve acceptable performance, n-type materials must have

i) High electron affinity (ideally greater than ~3 eV, but not exceeding ~ 5 eV) and lower LUMO levels to facilitate injection from contacting electrodes in OFETs

ii) Good intermolecular electronic orbital overlap to facilitate high mobility

iii) Good environmental stability towards O_2 and H_2O.

Early work with the rare-earth metal/ organic complexes **Pc2Lu** and **Pc2Tm** yielded devices with mobilities of 10^{-4} cm^2/Vs, and in the case of **Pc2Lu**, ambipolar (electron and hole) transport was observed after annealing.[19] **TCNQ** and **TCNNQ**, both of which have

TH-1703_11612241

received considerable attention as the acceptor half of organic/metal complexes, yielded electron mobilities of 10^{-5} and 10^{-3} cm^2/Vs, respectively, in single-component thin films.[34] In 1998, Bao et al. described that the addition of strong electron-withdrawing groups to metallophthalocyanines could result in air-stable n-channel organic semiconductors. A mobility of ~0.03 cm^2/Vs in air was reported for the perfluorinated **F16CuPc**.[35]

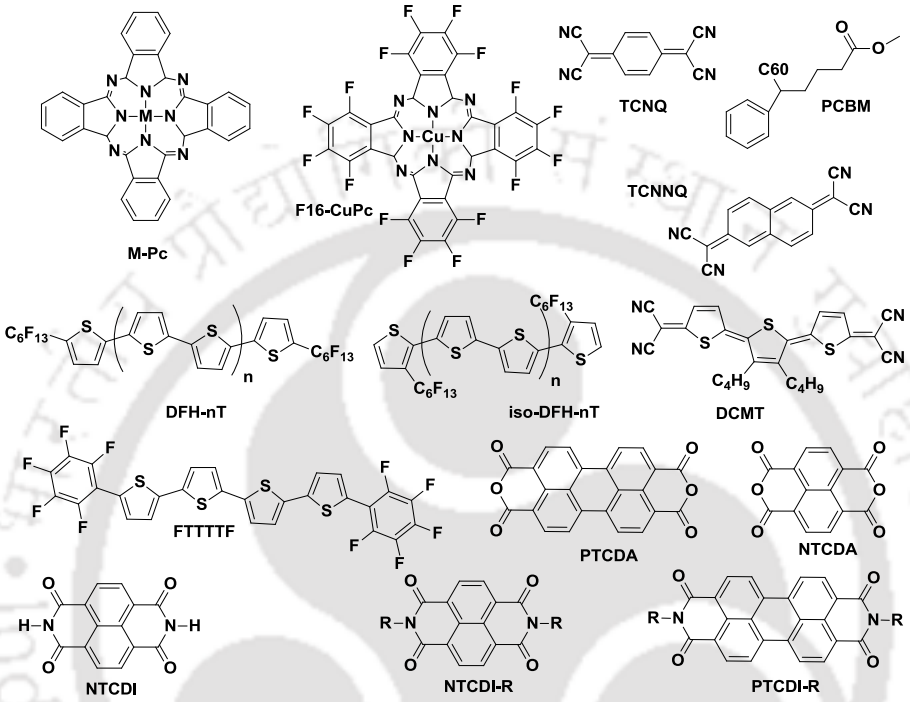

Figure 1.7. Chemical structures of some small molecule n-channel organic semiconductors

Till 2000, the highest reported electron field effect mobility in an organic thin film was for C60 on an amine modified surface (μ ~0.3 cm^2/Vs). Kobayashi et al. reported mobilities as high as 0.56 cm^2/Vs for C60 films fabricated by molecular beam deposition, but these mobilities could only be achieved by performing device fabrication and electrical characterization without breaking the vacuum.[36] Facchetti et al. have synthesized a series of n-channel semiconductors by adding perfluorohexyl groups (**C6F13**) to α, ω (**DFH-nT**) or β, β' (**iso DFH-nT**) positions of oligothiophenes, where n = 0, 0.5, 1, 1.5, or 2. The highest observed mobility in these materials is ~0.05 cm^2/Vs for thermally evaporated **DFH-4T** films.[37] This same group has also reported electron mobilities as high as 0.08 cm^2/Vs for **FTTTTF**. Chesterfield et al. have reported on the electrical characterization of the n-channel organic semiconductor **DCMT**, a quinoid terthiophene derivative with electron-withdrawing dicyanomethylene groups.[38] The most

TH-1703_11612241

extensive work thus far on n-channel molecular organic semiconductors has involved compounds formed by adding electron-withdrawing dianhydride or diimide moieties to naphthalene and perylene cores (**NTCDI-R** and **PTCDI-R** in Figure 1.7). The earliest attempts to fabricate OTFTs from these materials yielded mobilities of ~10^{-3} and 10^{-4} cm^2/Vs for **NTCDA** and **NTCDI**, respectively, and ~10^{-4} cm^2/Vs for thin films of **PTCDA**.[39] Later, Katz et al. demonstrated that the mobility and air stability of these devices could be greatly improved by incorporating various N, N' substituents on **NTCDI**. In particular, it was found that fluorinated side groups (**R**) like $\mathbf{CH_2C_6H_4CF_3}$, which may act as a kinetic barrier to the diffusion of oxidizing species, yield devices with mobilities greater than 0.1 cm^2/Vs in air.[40] Chesterfield et al. have demonstrated saturation mobilities as high as 1.7 cm^2/Vs in the **PTCDI-C8** molecule with threshold voltages of 10-15 V.[41] Apart from the small molecules many polymeric n-type materials were synthesized.[42]

1.4.3. Ambipolar Semiconductors

The fabrication of devices exhibiting ambipolar behavior that can provide both n- and p-channel performance in one device is very important due to their application in large-area manufacturing of complementary integrated circuits.[43] There are three major groups of ambipolar transport OFETs which can be classified by the semiconducting layer (i) bilayer ambipolar OFETs in which both layers forms a hetero junction,[44] (ii) by blending of both n-type and p-type semiconducting materials[45] and (iii) single component transistors in which a single active layer can transport both holes and electrons.[46] For the blend ambipolar OFETs, ambipolar charge transport and the associated carrier mobilities in blend system have a complex dependence on the blend composition and the phase separated morphology, and therefore are highly dependent on processing conditions. For OFETs with single layer that can provide both n-and p-channel performance, the semiconducting layer must be suitable for both electron and hole injection and transport. Hence the energy level of HOMO and LOMO are a key factor for the Ambipolar transporting semiconductors. The semiconductor is required to have a HOMO energy level below - 5.0 eV to achieve stable hole transport and for the stable electron transport, the LUMO level needs to be below or at least close to - 4.0 eV. Considering the single metal used as both the source and drain electrodes, the energy gap of HOMO and LUMO should not be too large to avoid charge injection barriers.

TH-1703_11612241

In 1995, in order to achieve the ambipolar device performance, Dodabalapur and co-workers tried to combine the p-type α-hexathienylene and n-type C60 semiconductors together by means of the bilayer technique, affording the first two-component active layers OTFTs with relative balanced carrier mobilities of 4×10^{-3} cm^2/Vs for holes and 5×10^{-3} cm^2/Vs for electrons, respectively, under vacuum.[14] This certainly aroused significant research interests, initiating a relatively wide range of investigations over the two-component bilayer thin film transistors with different combination of p-type and n-type organic semiconductors including polymers and in particular small molecules like **pentacene/C60**,[47] **CuPc/F16CuPc**,[48] **BP2T/F_{16}CuPc**,[49] **pentacene/PTCDI-$C_{13}H_{27}$**,[50] and **DH4T/PTCDI-$C_{13}H_{27}$**.[51]

1.5. Rylenediimide based n-type semiconductors

Widely studied electron transport materials are fullerenes, which have been used for a variety of applications, have inherently moderate to high electron affinities. The reasons such as poor photo stability in air, difficulty in synthesis, high production cost, difficulty in tuning the optical properties and electronic structures of fullerenes lead to the search in new electron transport materials. Another extensively studied materials class is that of rylene tetracarboxylic diimides. Rylenes are hydrocarbon families that can be regarded as naphthalene oligomers. The two important rylene tetracarboxylic diimides considered are naphthalene-1,8:4,5-tetracarboxylic diimide (NDIs), perylene-3,4:9,10-tetracarboxylic diimide (PDIs). More interest in these diimides stems from early observations of n-channel behavior, the ability to tune molecular electronic properties by well established organic chemistry, through either variation of substituents on the imide nitrogen atoms or on the rylene skeleton. Rylene diimides can exhibit relatively high electron affinities, high electron mobilities, and excellent chemical, thermal, and photochemical stabilities. In the subsequent sections, some of recent developments on high-mobility rylenediimide-based small molecules and polymers for high-performance OFETs have been discussed.

1.5.1. Perylenediimide based Small molecules

Perylene 3,4,9,10- tetracarboxylic acid diimides (**PDI**s) have rapidly become one of the most widely investigated n-type materials. This is due to relatively inexpensive starting material, perylene 3,4,9,10-tetracarboxylic acid dianhydride (**PTCDA**), can be chemically modified to suit particular solubility, photo physical, or electron bearing demands. PDIs

TH-1703_11612241

were used as one of the n-type OSCs from 1996 by Horowitz et al.[52] Compounds 1a alkylated with $\mathbf{C_8H_{17}}$ and 1b with $\mathbf{C_{13}H_{27}}$ are most famous among the n-type N-substituted **PDI**s.[53]

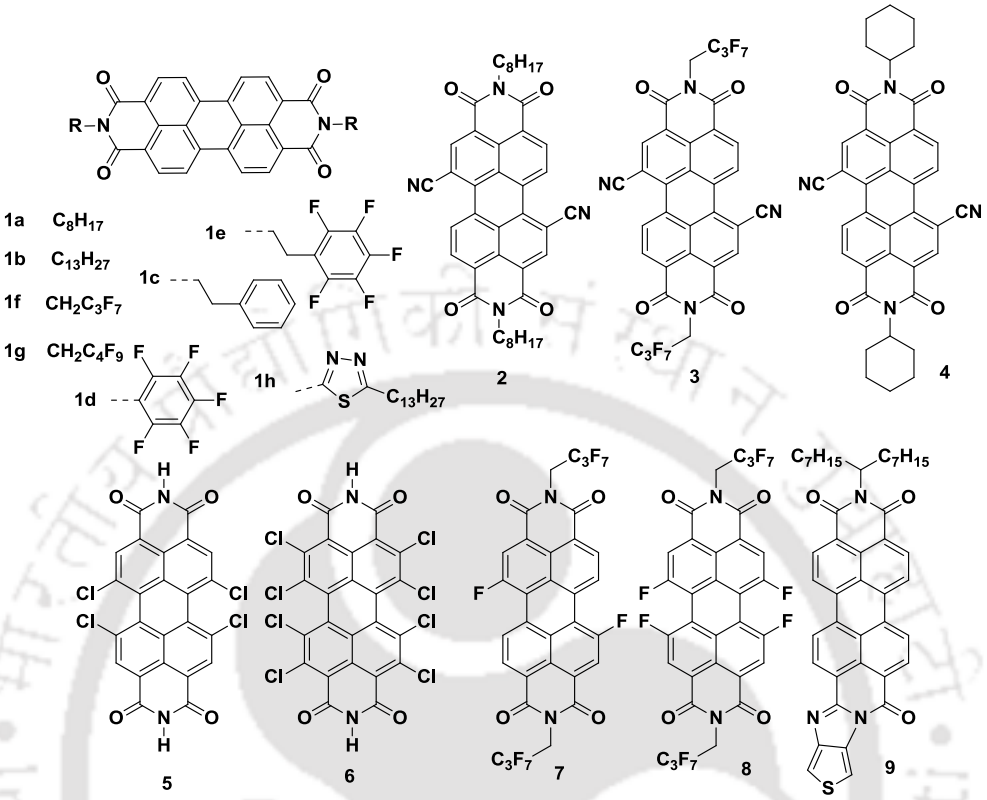

Figure 1.8. Chemical structures of some PDI based small molecule n-channel organic semiconductors

The highest μ_{FET} with **1a** as active layer is 1.7 cm^2/Vs when tested under a partial pressure of H_2 (10^{-4} Torr). **PDI**s with phenylethyl substituent (1c) is an air stable OSCs with thin film mobility of 1.4 cm^2/Vs with individual wires of **1c**.[54] In 2007 Chen et al were designed and synthesized , a series of air stable n-type OSCs based on fluorinated derivatives of PDIs [55] Compared with **1c** and **1d**, compound **1e** with perfluorinated phenyl substituent showed higher mobilities of 0.62 cm^2/Vs tested in vacuum and 0.37 cm^2/Vs in air. One more partial fluorinated alkyl substituted PDIs **1g** was used to investigate the effects of the interplay between energetic and kinetic factors on the air stability of n-channel OFET.[56] Another **PDI** OSCs of **4** (LUMO -4.33 eV) showed air stable mobility of 0.86 cm^2/Vs, the same with tested in vacuum. Some other substituents were also introduced to PDIs, such as **1h**. 1,7-Dicyano **PDI**s **3** is one of the most successful **PDI** based n-type semiconductors with high mobility of 6 cm^2/Vs in vacuum and **3** cm^2/Vs in ambient air[57] with excellent stability. With the same molecule high electron mobility of 5.1 cm^2/Vs was obtained with a vacuum-gap single-crystal **3** OFET. And the mobility

TH-1703_11612241

increased from 5.1 cm^2/Vs at T = 290 K to 10.8 cm^2/Vs at T = 230 K, showing a band-like electron transport for first time.[58] A solution-processed **2** OFET was reported by Facchetti et al. with mobility of ~ 0.08 cm^2/Vs.[59] The tetrachloro-substituted **5** , with LUMO level of -3.9 eV shown mobility of 0.18 cm^2/Vs. Octachlorosubstituted PDIs **6** showed much lower LUMO of -4.23 eV compared with the core unsubstituted (-3.7 eV) and tetrachloro substituted PDIs (-3.9 eV) which is clearly in the range of air stable n-channel semiconductors.[60] Mobilities of 0.91 cm^2/Vs and 0.82 cm^2/Vs were obtained in vacuum and in ambient air. The air-stability of these n-channel transistors is probably due to the energetically low-lying LUMO and the high packing density of **6**. Compounds **7** and **8** are two fluoro-substituted PDIs with same N-substituted alkyl chains with **1f** which showed the better stability due to the lower LUMO levels (for **1f**, -3.85 eV for **7**, -3.88 eV, for **8,** -3.93 eV).[61]

1.5.2. Perylenediimide based Polymers

Many researchers have tried to design and synthesize new n-type polymers that have suitable functionalities and a sufficient solubility in selective organic solvents, because the constituent materials for printed electronics need to be processed in solution for low-cost fabrication. The solubility issue seems to have been resolved easily by the controlled addition of side chains to the polymer backbone.[62] While a more critical challenge was to design molecules with a desired electron-transporting property, donor-acceptor architecture became one of interesting strategies to tune the properties of polymers by design.[63] Polymers with a small band gap are generally obtained by this approach because of intramolecular charge transfer between the donor and acceptor units. In 2007, another breakthrough in n-type polymer semiconductors was reported by taking the donor-acceptor approach based on fused thiophenes and a **PDI** unit. Poly[N,N′-bis(2-decyltetradecyl)-3,4,9,10-perylenediimide-1,7-diyl]-alt-(dithieno[3,2-b:2′,3′-d] thiophene-2,6-diyl) **PPDI-1** has an electron mobility of 0.013 cm^2/Vs when tested in inert conditions.[64] The LUMO energy level of PPDI-1 is -3.9 eV, which is suitable for electron transport. Copolymerization of **PDI** and bithiophene units resulted in a polymer, poly N,N′-bis(2-octyldodecyl)-3,4,9,10-perylenedicarboximide-(1,7&1,6)-diyl]-alt-5,5′-(2,2′-bithiophene) **P(PDI2OD-T2)**, further abbreviated here as **PPDI-T2**, with an electron mobility of 2×10^{-3} cm^2/Vs in vacuum.[65] Although its LUMO level is close to -4.0 eV, operation of **PPDI-T2** in air is reported to be unstable. Another noticeable **PDI**-based

TH-1703_11612241

polymer for field effect transistors is synthesized by coupling of brominated **PDI** with diethynylbenzene.[66] This polymer **PDIC8-EB** has a LUMO level of -3.9 eV and a HOMO level of -6.1 eV. **PDIC8-EB** is known to self assemble into nanowires in solution shown electron mobility as high as 0.1 cm^2/Vs when tested under a nitrogen environment (Figure 1.9). Zhan. et al. Synthesized **PPDI-PTZ** shown the mobility 0.05 cm^2/Vs.[67] Many other polymers based on **PDI** with comonomer units dithienothiophene,[68] fluorenone (**PPDI-FLN**),[69]Phenylene (**PDI-Ph**), Benzothiadiazole (**PDI-BT**),[70] dithienopyrrole (**PDI-DTP**)[71]and **DTP** with acetylene bond (**PDI-Ac-DTP**)[72] were synthesized for the fabrication of high performance OFETs.

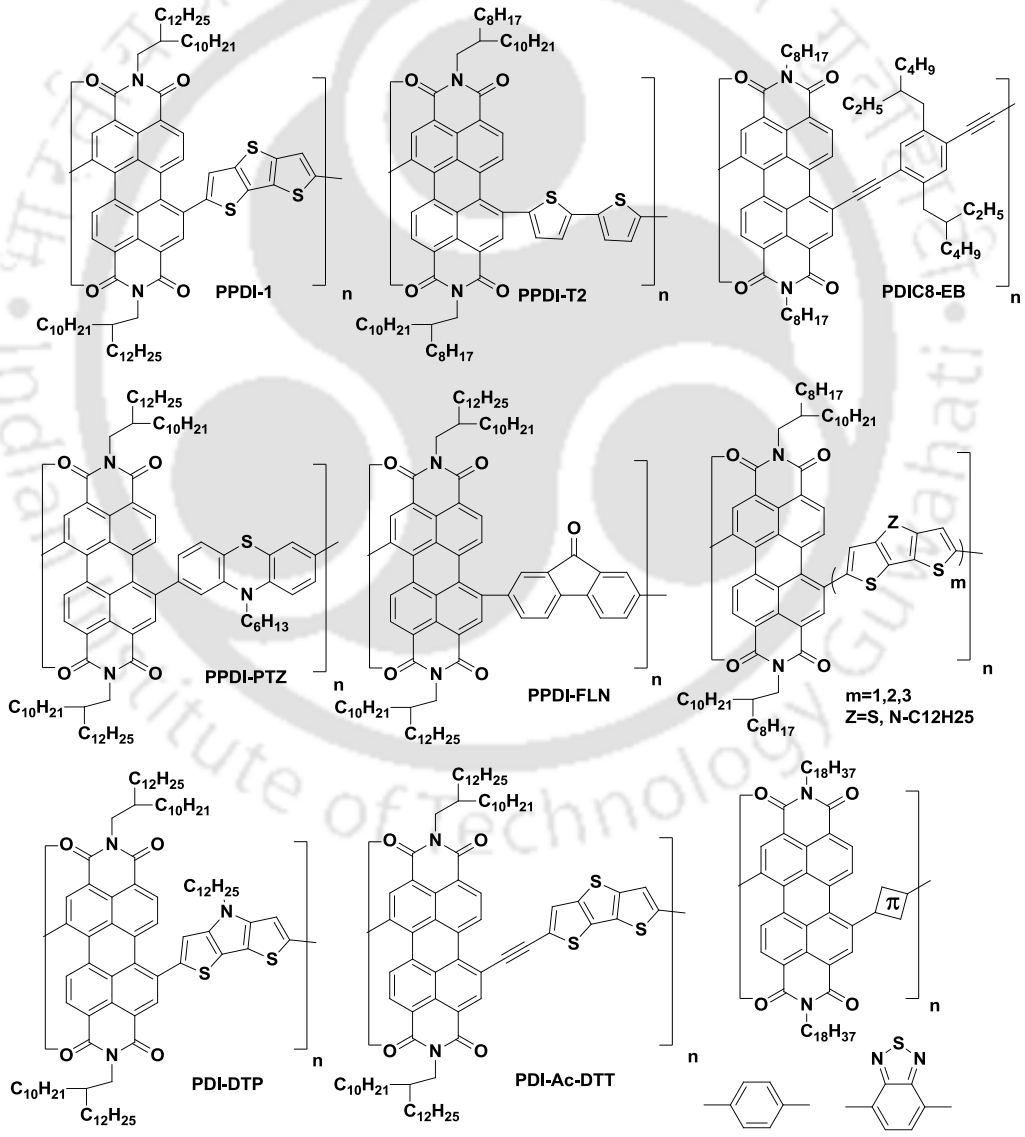

Figure 1.9. Chemical structures of some PDI based polymer n-channel organic semiconductors

TH-1703_11612241

1.5.3. Naphthalenediimide based Small molecules

Naphthalenediimide based n-channel OFETs were first observed in 1996 with the electron mobility on the order of 10^{-4} cm^2/Vs.[34] For the aliphatic alkyls or other groups substituted at the nitrogen positions of diimides, the compound **10a** is one of the most successful n-type OSCs. **10a** based OFETs with high electron mobility of 6.2 cm^2/Vs and current on/off ratio of 6×10^8 was reported by D. Shukla and coworkers when measured under a continuous stream argon.[73] The compound **10b** with alkyl substituents on the nitrogen atoms in the same work exhibits a lower FET mobility of 0.7 cm^2/Vs. Zone cast method and parylene C dielectric layer was used to fabricate **10c** OFETs, which showed mobility of 0.18 cm^2/Vs.[74] Besides alkyl and alkyl phenyls, some other groups were also introduced to substitute at the nitrogen positions of diimides like compound **10d** with alkyl thienyl group.[75] B. J. Jung et al reported **NDI** OSCs with fluorinated substituents at the nitrogen positions like compound **10e** showing electron mobility of 0.7 cm^2/Vs in air.[76] Another fluoroalkyl substituted **NDI** OSCs **10f** with a shorter fluoroalkyl side-chain showed lower mobility of 0.34 cm^2/Vs when tested in N_2 and 0.27 cm^2/Vs in air.[77] With OSC layer thermally grown on bare and **OTS-18** treated Si/SiO_2 surface, **10g** OFETs showed mobilities of 0.39 cm^2/Vs and 0.57 cm^2/Vs respectively.[78] Compound 10h with perfluorophenyl substituents showed higher mobility of 0.87 cm^2/Vs was obtained using bottom gate top contact (TC) configuration.[79] Compounds **11a** and **11b** with chlorine substituted at the naphthalene core were synthesized and showed excellent electron transport properties in ambient air with mobilities of 0.91 cm^2/Vs for **11a**, 1.43 cm^2/Vs for **11b**. Compounds **12** and **13** are two **NDI**s derivatives with backbone catenation. With **12** , OFET mobility of 0.35 cm^2/Vs was obtained when tested in vacuum and 0.1 cm^2/Vs in air based on the thermal evaporated **12** layer.[80] Core-expanded **NDI**s is also another kind of **NDI**s based n-type OSCs with high performance and stability (**14a-14d**). For compound **14a**, OFETs with spin coated **14a** film exhibit mobility up to 1.2 cm^2/Vs , current on/off ratio of 10^8.[81]Three similar compounds (**14b-14d**) were synthesized and all show air stable electron transporting properties. The obtained mobility of 3.5 cm^2/Vs based on **14c** is one of the highest mobility for solution processed air stable n-type OFETs.[82] Core-expanded **NDI**s with different functional groups (**15**) was also reported and showed promising performance.[83] Compound **16** with two NDIs linked by a π - bridge was synthesized and OFETs with **CYTOP** and Al_2O_3 as dielectric layer were fabricated with various semiconductor processing techniques and the highest mobility

TH-1703_11612241

obtained in N_2 was 0.17 cm^2/Vs.[84] **17** is another molecule with two NDIs linked by a π -bridge. High electron mobility up to 1.5 cm^2/Vs was observed in N_2 with low hole mobility of 0.01 cm^2/Vs.[85]

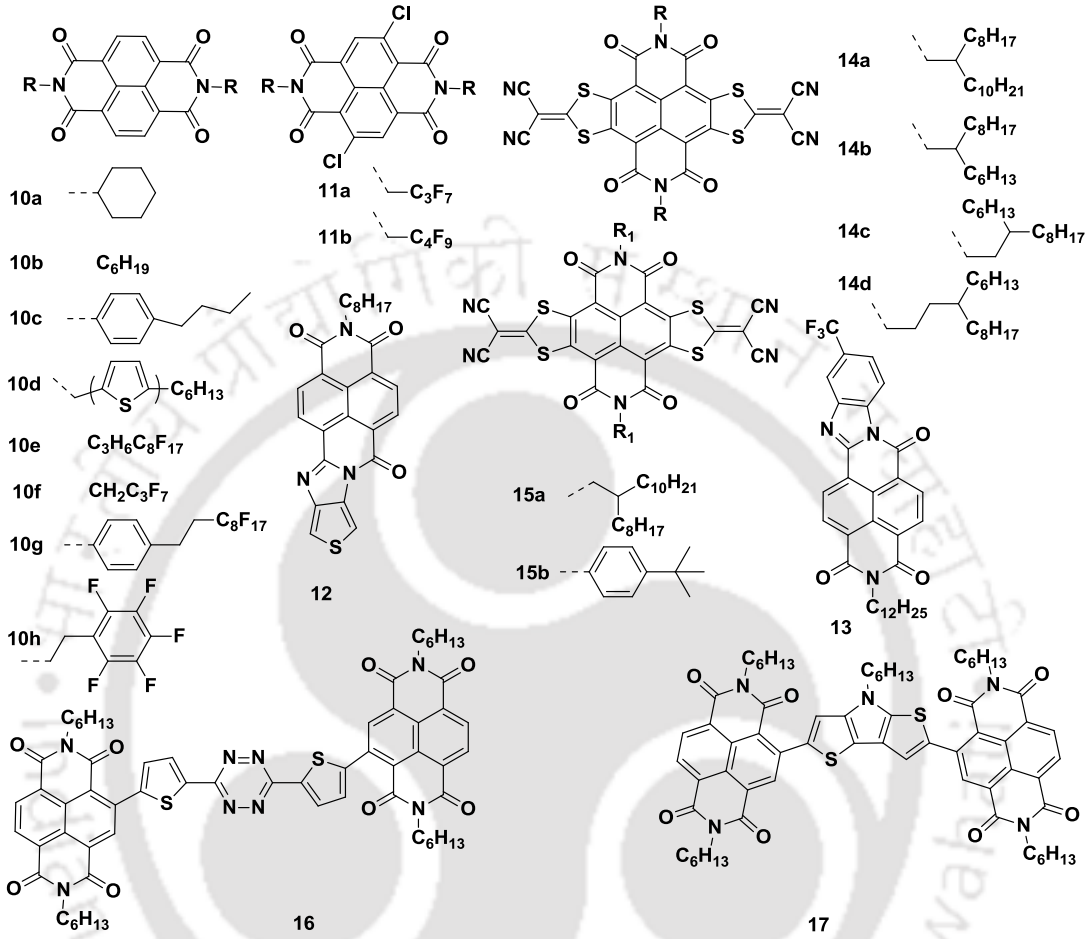

Figure 1.10. Chemical structures of some NDI based small molecule n-channel organic semiconductors

1.5.4. Naphthalenediimide based Polymers

One class of polymer semiconductors which has received much attention is a series of donor–acceptor copolymers generally named **PNDI**s, based on an electron-accepting unit of **NDI** and various electron-donating units of thiophene derivatives. Because the constituent **NDI** has been known as an excellent electron-transporting moiety, polymers with **NDI** as a main building block have been intensively investigated. In a study comparing **PNDI** with **PPDI**,[86] it was found that an **NDI** based polymer, poly[N,N′-bis(2-octyldodecyl)-1,4,5,8-naphthalenedicarboximide-2,6-diyl]-alt-5,5′-(2,2′-bithiophene)], **PNDI-T2** showed much higher electron mobility of 0.06 cm^2/Vs in vacuum. In addition, **PNDI-T2** also showed better air stability under 20-40% relative humidity than the **PDI**

TH-1703_11612241

analog **PPDI-T2**, despite their similar structures and LUMO energy levels lower than -3.9 eV. Excellent performance and processability of **PNDI-T2** have resulted in printed polymer field-effect transistors with an electron mobility as high as 0.8 cm^2/Vs.[87] From a systematic study on a series of **PNDI**s, it has been shown that the detailed structure of the polymers significantly affects their charge-transport properties.[88] From the same study, it was also found that the strength of the donor moiety in **PNDI**s can significantly affect the electronic energy levels and the charge-transport properties of the polymers. The LUMO levels of **PNDI**s are consistently low lying at around -3.9 eV because of the strong electron acceptor **NDI**. However, the HOMO level of the polymer becomes higher lying as a stronger donor is copolymerized, yielding a smaller band gap. Other **NDI** based polymers with different electron-donor units have also been studied. A series of polymers that are containing **NDI** and selenophene derivatives are among them. For example, poly [N,N′-bis(2-decyl tetradecyl) - naphthalene-1,4,5,8-bis(dicarboximide)-2,6-diyl]-alt- 5,5′-(2,2′-biselenophene)] (**PNDIBS**) has been synthesized to have an electron mobility as high as 0.07 cm^2/Vs, which is higher than the mobility of 0.04 cm^2/Vs from the bithiophene analog with the same alkyl side chains (**PNDIBT**).[89] Other selenophene based **NDI** copolymers, including poly[N,N′-bis(2-decyltetradecyl)-naphthalene-1,4,5,8-bis(dicarboximide)-2,6-diyl]-alt-2,5-(3,6-dimethyl selenoloselenophene)] (PNDISS) and poly [N, N′-bis(2-decyl tetradecyl)-naphthalene-1,4,5,8-bis(dicarboximide)-2,6-diyl]-alt-2,6-(benzo[1,2-b:4,5-b′]diselenophene)] (PNDIBDS), have also shown a very good electron mobility around ~0.01 cm^2/Vs.[90] Poly [N,N′-bis(2-octyldodecyl)-1,4,5,8-naphthalenedicarboximide-2,6-diyl]-alt-5,5′-(E)-1,2-diethoxy-1,2di(thiophen-2-yl)ethane] (PNDITaV) has an electron mobility as high as 0.5 cm^2/Vs in devices with bottom-contact and top-gate geometry.[91] Poly[(E)-2,7-bis(2-decyltetradecyl)-4-methyl-9-(5-(2-(5-methylthiophen-2-yl)vinyl)thiophen-2-yl)benzo[lmn][3,8]phenanthroline-1,3,6,8(2H,7H)-tetraone] (PNDI-TVT), a copolymer of NDI and bithienylene vinylene without alkoxy-functionalization, showed excellent electron transporting properties with a mobility as high as 1.8 cm^2/Vs. Extended structures of NDIs have also been synthesized for polymer semiconductors to tune their charge-transport properties. Alkyl-substituted poly(benzoquinolino phenanthrolinedione), also known as PNDI-2BocL, is an imine bridged ladder-type polymer synthesized by a sequential process of coupling polymerization and intramolecular cyclization.[92] The electron mobility of PNDI-2BocL is 2.6×10^{-3} cm^2/Vs, which is four orders of magnitude higher than the single-stranded

TH-1703_11612241

analog of this polymer. Another form of extended NDI, naphthobisthiazole diimide (NBTDI), has been reported.[93] Many conjugated polymers of NDI with Phenylene (NDI-Ph), Benzothiadiazole (NDI-BT),[70]thiophene, alkylated bithiophene, alkoxy bithiophene,[88]Phenylene, Naphthalene, Tetracene[94] were synthesized and used for the fabrication of high performance n-type OFETs.

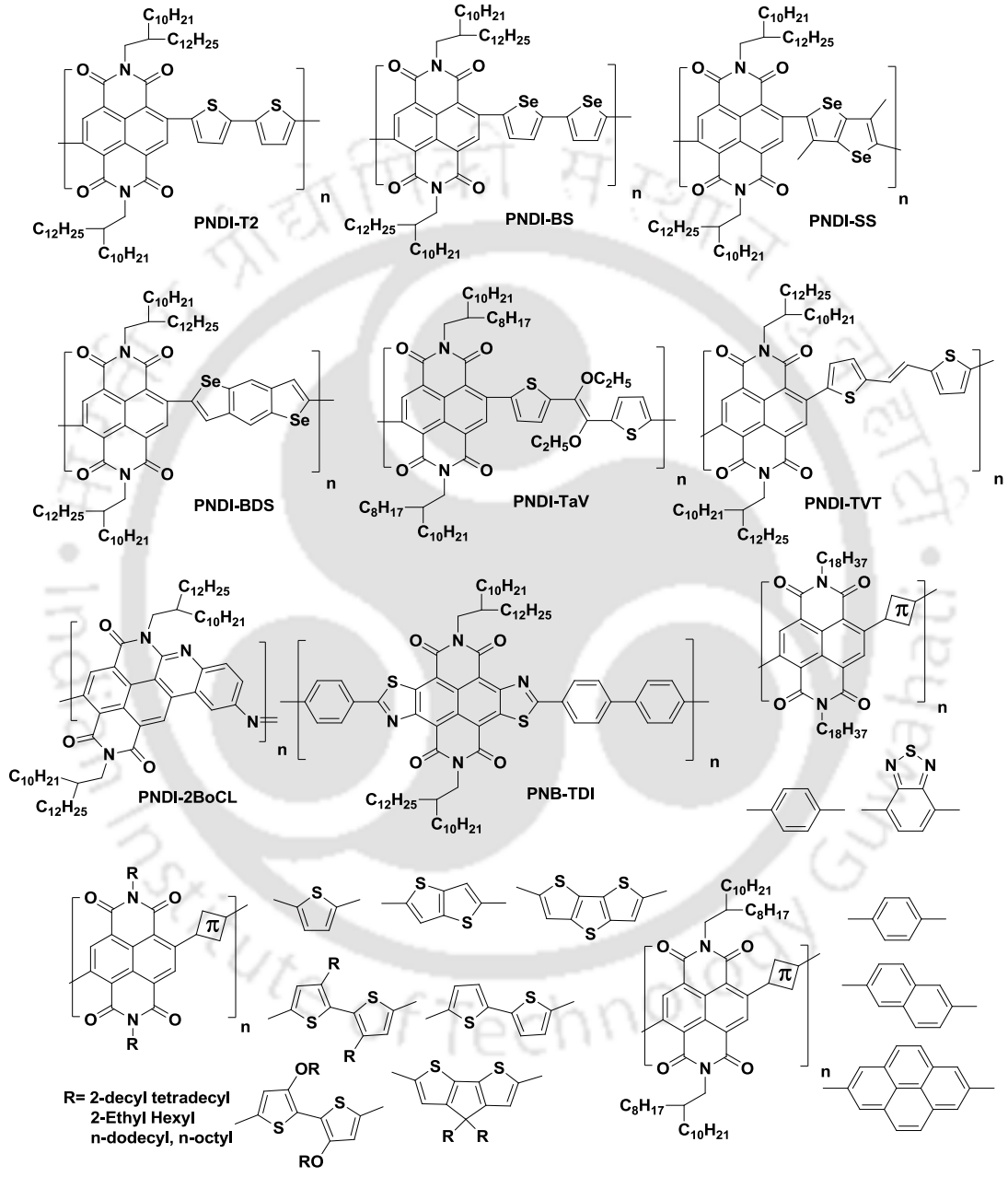

Figure 1.11. Chemical structures of some NDI based polymer n-channel organic semiconductors

1.6. Different types of Substrates

Most of the OFETs reported in the literature are fabricated on the Si substrates. This

TH-1703_11612241

material allows to manufacture a highly complicated electronic circuits used in high-tech systems. However, a lot of applications can be found which requires cheap products used commonly. It does not pay off to produce them from silicon because of a high unit cost. Their price can be decreased through applying of flexible electronics[95] which is an alternative for traditional production process of electronic circuits. Flexible, organic or plastic[96] electronics is one of the most important emerging technologies. This technique makes possible to produce electronic components on flexible substrates such as plastics,[97] foils, paper[98] or fabrics. In the consequence, printed items can be bent repeatedly or even rolled. This causes no changes in their properties. It is not possible in the traditional products made from silicon which are rigid and their bending or rolling leads to irreparable damages whereas the devices fabricated on plastic or paper substrates are bendable and stretchable.[99] Moreover, used substrate materials are cheap. In the connection with it, a unit price of printed flexible components can be decreased comparing to traditional one.

1.7. Role of the Gate dielectric

In the early times of OFETs, the attention was essentially focused on the active layer. The large majority of the devices were made on silicon oxide thermally grown on single-crystal silicon wafers. Nowadays, it is recognized that the physical properties of the organic semiconductor are not the only parameters to be taken into account for the final performance of an OFET. So even if the well-known properties and well-mastered technology of silicon microelectronics still provides a sound basis for the search of organic semiconductors with high mobility and stability, great interest is given to other insulating materials, for example, polymeric dielectrics, that offer the possibility of obtaining large area devices through simple and inexpensive solution processes. On that particular point, there are many reviews published by Veres et al.[31] and Facchetti et al.[100,101] A critical issue that limits the performance of organic transistors is the large operating voltage that arises from poor capacitive coupling as a result of the thickness and the low dielectric constant of the insulating layer. This is especially true in the case of organic insulators, which in many cases are preferred to the higher dielectric materials because of the lower mobility registered in the latter case. An interesting way to get around this problem is to use low-thickness insulating layers formed by high-density self assembled mono layers (SAMs). Using a trichlosilane SAM with an aromatic end group

TH-1703_11612241

and pentacene as the active layer, a high mobility of 1 cm^2/Vs and low operating voltage of 2V could be reached, thus avoiding molecular penetration and leakages through the dielectric.[102] More recently, the same group also obtained a high-performance low-power complementary circuit using a similar approach with phosphonic acid-based SAMs.[103] Another way to improve the performance of OFETs is the use of a high dielectric constant (high-k) nano composite dielectric, with which low sub-threshold and leakage currents are achieved.[104] One fundamental task is to understand in what way the presence of the insulator influences the motion of the mobile charge carriers in the conduction channel. It is in fact nowadays clear that the accumulation and flow of carriers in an operating field-effect device are surface processes, and that charge transport only occurs in the first few layers of the semiconductor next to the dielectric.[105] The mobility rapidly increases with increasing coverage of the dielectric until the second monolayer is completed,[106] and a further increase in the thickness of the film does not change the performance of the device. The insulator plays a leading role in the characteristics of the device and the motion of carriers is critically determined by the intrinsic properties of the semiconductor-insulator couple, by directly affecting the semiconductor structural order.[107] It has an effect on the flow of carriers in both polymeric and more ordered small-molecule-based, semiconductors. A high-performance transistor comprises a surface-smooth dielectric layer in which charge injection from the gate does not occur, and which is free of static charges, for example, as a result of interfaced trapped carriers, that might disturb the threshold voltage of the device. Details on the nature of the insulator semiconductor interface have been reviewed by Sirringhaus.[108]

1.8. Modification of dielectric by Surface assembled monolayers

Since the earlier attempt to increase the mobility of a Pentacene transistor by modifying the surface of the dielectric layer,[109] it has been widely shown that a powerful way to do so is the use of a SAM. Much effort has been carried out to control the insulator surface using SAMs[110] and many works have shown the direct influence of the dielectric surface disorder and roughness on thin films[111] and single crystals. Although they are only a few nanometer in thickness, SAM dielectrics are composed of densely packed organic molecular monolayers that suppress carrier tunneling via highly ordered aliphatic chains.[112] In addition, by tuning the surface terminal group of the SAM, it is possible to modify the interface between the organic semiconductor and dielectric by exploiting

TH-1703_11612241

compatible organic-organic interactions resulting in improved device performances. The use of SAM gate dielectrics for organic TFTs was pioneered by the Vuillaume group.[112] SAMs allow a direct control of the key parameter surface energy, and mobility as high as 3 cm^2/Vs can be reached with pentacene thin films.[6] Again, using a SAM in the case of a single-crystal transistor, the highest reported mobility for an organic device to date (a four-point mobility of 40 cm^2/Vs) was reported by Takeya and coworkers.[113] It is important to remember that a high-performance transistor is not only that with a high mobility. The control of the threshold voltage and the reduction of the sub-threshold current are other important factors to assure a low-voltage operative transistor. These two parameters heavily depend on the insulator layer because both are affected by the static charge on top of the dielectric or by the interface trap states. It has been shown that SAMs are also important for the control of these two kinds of charge.[114] Besides morphological effects the terminal group of the organosilanes induces a dipole moment at the surface of the dielectric that has an effect on the surface potential, which in turn acts as an additional gate bias that modulates the threshold. For electron-rich terminal groups, the threshold shifts towards positive voltages, so that mobile charges are already induced in the conducting channel at a zero applied gate voltage. On the other hand, an electron withdrawing group leads to a negative shift of the threshold, so that an additional applied gate voltage is needed to cause the charging of the channel. SAMs also reduces the charge carrier injection barrier.[115] The more explanation about the application of SAMs in different organic electronic devices at various interfaces was reviewed by A. K.Y. Jen et al.[116]

1.9. Contact Resistance and channel length

Besides increasing the performance of the active layer, great attention has also been paid to the interface between the electrodes and the semiconductor, especially when it comes to reducing the size of the device, because in that case the available current is no longer limited by the resistance of the conducting channel, but rather by that related to the contacts. The requirement for an ohmic contact is the basis for the downscaling of an organic device in which the charge carriers are essentially supplied by the injecting electrodes.[117] The contact resistance can be measured by single transistor method, transmission line method in which the devices with different channel length can be fabricated and from the extrapolation of resistance at zero channel length gives contact

TH-1703_11612241

resistance.[118,119] Contact resistance is a non-linear contribution that influences the correct characterization of a device. The value of contact resistance decreases with increasing gate voltage, and for this reason the mobility estimated in the linear regime may be substantially smaller than that extracted from the saturation region. Interesting theoretical works[120] have been carried out to explore this effect in a staggered device and important considerations on the dependence of the resistance on the applied voltage have been provided. The contact resistance also depends on the channel length. Many groups have studied the effect of channel length on the contact resistance and proposed different mechanisms for the relation between the contact resistance and channel length.[121] In a study of OFET fabricated with N,N´-bis(octyl)-1,7-dicyano-3,4:9,10-perylene tetracarboxylic dianhydride (PDI8-CN2), it was shown that the contact resistance also depends on the thickness of the organic semiconducting material.[122] Gate dielectric interface also influences the contact resistance. At the organic semiconductor/insulator interface, traps induced by polar groups strongly alter the gate-field dependency of contact resistance.[123] Variation in channel length is shown to influence charge carrier mobility and threshold voltage and the performance of OFETs by some of the earlier studies[124] which deal mostly with bottom contact devices. Negligible reports are available on effect of channel length for top contact OFETs. A few reports on top contact OFETs show either constant mobility or reduction in same with increase in channel length while a few others show increase in mobility with channel length.[125,126]

1.10. Stability of the OFETs

The stability of the FET devices can be classified into two types (i) Operational stability (ii) environmental stability. OFETs are layered structures consisting of a semiconductor, dielectric, gate electrode, and source/drain electrodes, so each layer as well as the interfaces between the layers plays an important role in the stability. The electrical performance and operational stability of the OFETs are correlated closely with the dielectric surface properties and microstructural order of the organic semiconducting layer as well as with the density of interface traps. The semiconductor, dielectric, and semiconductor/dielectric interface are the most vulnerable sites for charge trapping. The understanding of nature and origin of these traps is significant. The operational stability related to the stability under bias stress. The ambient stability related to the device stability under ambient humidity conditions. Hysteresis is the main cause for the bias

TH-1703_11612241

stress and device degradation. In the subsequent sections, hysteresis and bias-stress of the devices were discussed.

1.10.1. Hysteresis

OFETs often exhibit a current hysteresis (difference between the forward and the reverse sweeps). The hysteresis effects are very well observed in OFETs and causes instability in the device operation. Hysteresis is essentially the difference in the I_{DS} curves observed during forward and backward sweeping of V_{GS} of transfer characteristic curves. It could be useful in non-volatile memory devices, but it has to be avoided in standard integrated circuits particularly for display applications. The detailed investigations of hysteresis effects are rare and a complete picture of the physical background that may cause hysteresis in OFETs is still unexplored. Some of the mechanisms causing hysteresis in OFETs are already quite well described in the literature. They are (1) *Interface trapped charges* (also called interface state) are defects or impurities at the interface that can be charged or discharged (2) *Fixed charges in oxide* is a positive charge due to structural defects close to the channel (2 nm), which does not communicate with the substrate. (3) *Trapped charges in dielectric* are electrons or holes trapped in the bulk of the dielectric layer. These traps can be introduced during device fabrication and the charges (electrons or holes) are injected during device operation. (4*) Mobile charges in dielectric* are mainly small alkali metal cations and H^+, but can also be larger cations or anions.[127]

Depending on the microscopic effect the "hysteresis" can be classified in to two: (1) Clockwise hysteresis (CH) arises is due to the charge trapping at the interface of dielectric and semiconductor. (2) Anti-clockwise hysteresis (ACH) (Figure 1.12(a), (b)) arises due to (a) Effects of mobile charges close to or in the semiconductor channel near the semiconductor/ dielectric interface. They are (i) Trapped majority or minority charges in the channel close to the semiconductor/dielectric interface (ii) Charge injection from the semiconductor into the dielectric. (iii) Slow reactions (e.g. bipolaron formation) of mobile charge carriers in the polymeric semiconductor. (iv) Mobile ions in the semiconductor. (b) Effects resulting in a bulk polarization of the gate dielectric. They are (i) Polarization of the dielectric (ferroelectrics as dielectric or meta-stable "quasi-ferroelectric" polarization in the dielectric) (ii) Mobile ions in the dielectric (iii) Charge injection from the gate electrode into the dielectric.

TH-1703_11612241

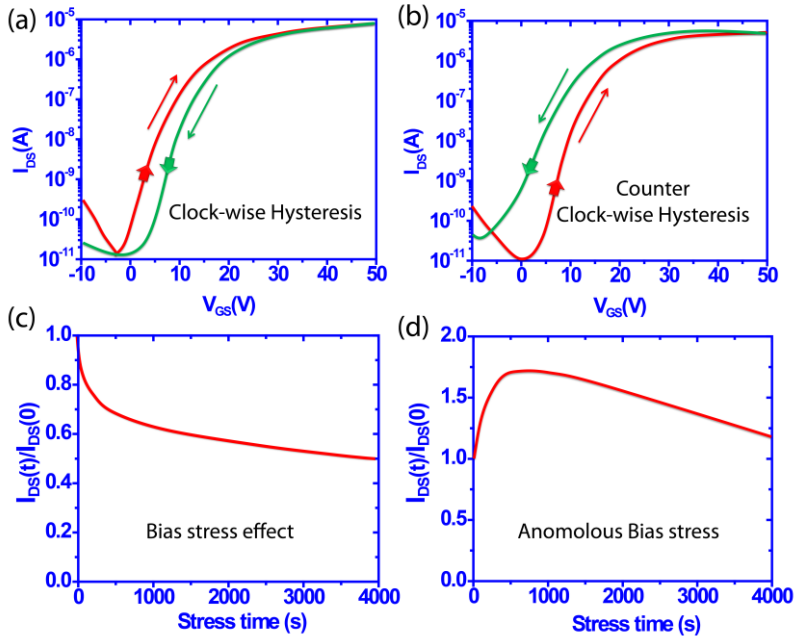

Figure 1.12. Schematic representation of hysteresis (a) Clockwise hysteresis (b) Anti-clockwise hysteresis (c) Bias-stress effect and (d) Anomalous bias-stress effect.

1.10.2. Bias-stress effect

Bias-stress is the application of constant V_{DS} and V_{GS} for an extended period of time. Moreover, we often have a persistent shift of the transfer characteristic when a gate bias is applied for a prolonged time. These phenomena are known as electrical instability or bias-stress effects. Electrical instability is most likely caused by the trapping of charge in long-lived trap states in the device layers. The term "long-lived" refers to a trapping and release time, which is long compared to the time needed to measure a transfer characteristic. Hysteresis and bias-stress I_{DS} degradation might have the same physical origin.[128]

Depending on the variation of I_{DS} with time, bias-stress effects are classified in to two types. They are (1) bias-stress effect and (2) anomalous bias-stress effect. These are shown in the Figure 1.12 (c) and (d). The bias-stress effect is due to the charge trapping at the interface and anomalous bias stress is due to the slow polarization of the gate dielectric or charge injection from the gate electrode. Under bias-stress the direction of the threshold voltage shift is such that a fully turned on OFET slowly turns itself off and vice versa under bias-stress. Investigating the bias-stress in an OFET can also cause a

TH-1703_11612241

change in effective field-effect mobility, which is attributed to an irreversible structural change in the semiconductor due to the electro-strictive effect.[129]

Based on the above literature in this thesis the second, third chapters gives the detailed study of the structure property relationship in n-type semiconducting materials based on Perylenediimide and Naphthalenediimide by fabricating the bottom gate top contact organic field-effect transistors. Fourth chapter describes the effect of dielectric material, surface assembled monolayer and channel length on the performance of OFET based on perylene diimide molecule. Finally, an ambipolar organic field effect transistor fabricated on low cost Al foil gate substrate which operates at a very low voltage is presented in the last chapter.

1.11. References

1. Chiang, C. K.; Fincher, C. R.; Park, Y. W.; Heeger, A. J.; Shirakawa, H.; Louis, E. J.; Gau, S. C.; Macdiarmid, A. G. *Phys. Rev. Lett.* **1977,** *39* (17), 1098-1101.
2. Sirringhaus, H. *Adv. Mater.* **2014,** *26* (9), 1319-1335.
3. Tsumura, A.; Koezuka, H.; Ando, T. *Appl. Phys. Lett.* **1986,** *49* (18), 1210-1212.
4. Carswell, D. J.; Ferguson, J.; Lyons, L. E. *Nature*, **1954,** *173* (4407), 736.
5. Rang, Z.; Haraldsson, A.; Kim, D. M.; Ruden, P. P.; Nathan, M. I.; Chesterfield, R. J.; Frisbie, C. D. *Appl. Phys. Lett.* **2001,** *79* (17), 2731-2733.
6. Klauk, H.; Halik, M.; Zschieschang, U.; Schmid, G.; Radlik, W.; Weber, W. *J. Appl. Phys.* **2002,** *92* (9), 5259-5263.
7. Stingelin Stutzmann, N.; Smits, E.; Wondergem, H.; Tanase, C.; Blom, P.; Smith, P.; De Leeuw, D. *Nat. Mater.* **2005,** *4* (8), 601-606.
8. Garnier, F.; Yassar, A.; Hajlaoui, R.; Horowitz, G.; Deloffre, F.; Servet, B.; Ries, S.; Alnot, P. *J. Am. Chem. Soc.* **1993,** *115* (19), 8716-8721.
9. Hajlaoui, M. E.; Garnier, F.; Hassine, L.; Kouki, F.; Bouchriha, H. *Syn. Met.* **2002,** *129* (3), 215-220.
10. Murphy, A. R.; Frechet, J. M. J.; Chang, P.; Lee, J.; Subramanian, V. *J. Am. Chem. Soc.* **2004,** *126* (37), 11750-11750.
11. Laquindanum, J. G.; Katz, H. E.; Lovinger, A. J.; Dodabalapur, A. *Adv. Mater.* **1997,** *9* (1), 36-39.
12. Takimiya, K.; Kunugi, Y.; Konda, Y.; Niihara, N.; Otsubo, T. *J. Am. Chem. Soc.* **2004,** *126* (16), 5084-5085.
13. Mushrush, M.; Facchetti, A.; Lefenfeld, M.; Katz, H. E.; Marks, T. J. *J. Am. Chem. Soc.* **2003,** *125* (31), 9414-9423.
14. Ponomarenko, S. A.; Kirchmeyer, S.; Elschner, A.; Alpatova, N. M.; Halik, M.; Klauk, H.; Zschieschang, U.; Schmid, G. *Chem. Mater.* **2006,** *18* (7), 2004-2004.
15. Meng, H.; Bao, Z. N.; Lovinger, A. J.; Wang, B. C.; Mujsce, A. M. *J. Am. Chem. Soc.* **2001,** *123* (37), 9214-9215.

TH-1703_11612241

16. Laquindanum, J. G.; Katz, H. E.; Lovinger, A. J. *J. Am. Chem. Soc.* **1998,** *120* (4), 664-672.
17. Bao, Z. N.; Lovinger, A. J.; Dodabalapur, A. *Adv. Mater.* **1997,** *9* (1), 42-44.
18. Zhang, J.; Wang, H.; Yan, X. J.; Wang, J.; Shi, J. W.; Yan, D. H. *Adv. Mater.* **2005,** *17* (9), 1191-1193.
19. Guillaud, G.; Alsadoun, M.; Maitrot, M.; Simon, J.; Bouvet, M. *Chem. Phys. Lett.* **1990,** *167* (6), 503-506.
20. Tang, Q. X.; Li, H. X.; He, M.; Hu, W. P.; Liu, C. M.; Chen, K. Q.; Wang, C.; Liu, Y. Q.; Zhu, D. B. *Adv. Mater.* **2006,** *18* (1), 65-68.
21. Abanoz, O.; Dimitrakopoulos, C. *Turkish Journal of Physics* **2014,** *38*, 497-508.
22. Pron, A.; Rannou, P. *Prog. Polym. Sci.* **2002,** *27* (1), 135-190.
23. Assadi, A.; Svensson, C.; Willander, M.; Inganas, O. *Appl. Phys. Lett.* **1988,** *53* (3), 195-197.
24. Tsumura, A.; Fuchigami, H.; Koezuka, H. *Synthetic Met.* **1991,** *41* (3), 1181-1184.
25. I, M.; Heeney, M.; Bailey, C.; Genevicius, K.; I, M.; Shkunov, M.; Sparrowe, D.; Tierney, S.; Wagner, R.; Zhang, W. M.; Chabinyc, M. L.; Kline, R. J.; Mcgehee, M. D.; Toney, M. F. *Nat. Mater.* **2006,** *5* (4), 328-333.
26. Lim, E.; Kim, Y. M.; Lee, J. I.; Jung, B. J.; Cho, N. S.; Lee, J.; Do, L. M.; Shim, H. K. *J. Polym. Sci. Pol. Chem.* **2006,** *44* (16), 4709-4721.
27. Kim, Y. M.; Lim, E.; Kang, I. N.; Jung, B. J.; Lee, J.; Koo, B. W.; Do, L. M.; Shim, H. K. *Macromolecules* **2006,** *39* (12), 4081-4085.
28. Chua, L. L.; Ho, P. K. H.; Sirringhaus, H.; Friend, R. H. *Adv. Mater.* **2004,** *16* (18), 1609-1615.
29. Drolet, N.; Morin, J. F.; Leclerc, N.; Wakim, S.; Tao, Y.; Leclerc, M. *Adv. Funct. Mater.* **2005,** *15* (10), 1671-1682.
30. Majewski, L. A.; Schroeder, R.; Grell, M. *Adv. Funct. Mater.* **2005,** *15* (6), 1017-1022.
31. Veres, J.; Ogier, S.; Lloyd, G.; de Leeuw, D. *Chem. Mater.* **2004,** *16* (23), 4543-4555.
32. Xia, X.; Lei, T.; Pei, J.; Liu, C. J. *Chinese J. Org. Chem.* **2014,** *34* (9), 1905-1915.
33. DeLeeuw, D. M.; Simenon, M. M. J.; Brown, A. R.; Einerhand, R. E. F. *Syn. Met.* **1997,** *87* (1), 53-59.
34. Laquindanum, J. G.; Katz, H. E.; Dodabalapur, A.; Lovinger, A. J. *J. Am. Chem. Soc.* **1996,** *118* (45), 11331-11332.
35. Bao, Z. A.; Lovinger, A. J.; Brown, J. *J. Am. Chem. Soc.* **1998,** *120* (1), 207-208.
36. Kobayashi, S.; Takenobu, T.; Mori, S.; Fujiwara, A.; Iwasa, Y. *Appl. Phys. Lett.* **2003,** *82* (25), 4581-4583.
37. Facchetti, A.; Mushrush, M.; Katz, H. E.; Marks, T. J. *Adv. Mater.* **2003,** *15* (1), 33-38.
38. Pappenfus, T. M.; Chesterfield, R. J.; Frisbie, C. D.; Mann, K. R.; Casado, J.; Raff, J. D.; Miller, L. L. *J. Am. Chem. Soc.* **2002,** *124* (16), 4184-4185.
39. Ostrick, J. R.; Dodabalapur, A.; Torsi, L.; Lovinger, A. J.; Kwock, E. W.; Miller, T. M.; Galvin, M.; Berggren, M.; Katz, H. E. *J. Appl. Phys.* **1997,** *81* (10), 6804-6808.
40. Katz, H. E.; Johnson, J.; Lovinger, A. J.; Li, W. J. *J. Am. Chem. Soc.* **2000,** *122* (32), 7787-7792.

TH-1703_11612241

41. Chesterfield, R. J.; McKeen, J. C.; Newman, C. R.; Ewbank, P. C.; da Silva, D. A.; Bredas, J. L.; Miller, L. L.; Mann, K. R.; Frisbie, C. D. *J. Phys. Chem. B.* **2004,** *108* (50), 19281-19292.
42. Choi, J.; Song, H.; Kim, N.; Kim, F. S. *Semicond. Sci. Tech.* **2015,** *30* (6), 064002.
43. (a) Bisri, S. Z.; Piliego, C.; Gao, J.; Loi, M. A. *Adv. Mater.* **2014,** *26* (8), 1176-1199; (b) Zhao, Y.; Guo, Y. L.; Liu, Y. Q. *Adv. Mater.* **2013,** *25* (38), 5372-5391.
44. Kim, F. S.; Ahmed, E.; Subramaniyan, S.; Jenekhe, S. A. *Acs Appl. Mater. Inter.* **2010,** *2* (11), 2974-2977.
45. Xu, X. M.; Xiao, T.; Gu, X.; Yang, X. J.; Kershaw, S. V.; Zhao, N.; Xu, J. B.; Miao, Q. *ACS. Appl. Mater. Inter.* **2015,** *7* (51), 28019-28026.
46. Lee, J.; Han, A. R.; Kim, J.; Kim, Y.; Oh, J. H.; Yang, C. *J. Am. Chem. Soc.* **2012,** *134* (51), 20713-20721.
47. Wang, S. D.; Kanai, K.; Ouchi, Y.; Seki, K. *Org. Electron.* **2006,** *7* (6), 457-464.
48. Wang, J.; Wang, H. B.; Yan, X. J.; Huang, H. C.; Yan, D. H. *Chem. Phys. Lett.* **2005,** *407* (1-3), 87-90.
49. Shi, J. W.; Wang, H. B.; Song, D.; Tian, H.; Geng, Y. H.; Yan, D. H. *Adv. Funct. Mater.* **2007,** *17* (3), 397-400.
50. Unni, K. N. N.; Pandey, A. K.; Alem, S.; Nunzi, J. M. *Chem. Phys. Lett.* **2006,** *421* (4-6), 554-557.
51. Dinelli, F.; Capelli, R.; Loi, M. A.; Murgia, M.; Muccini, M.; Facchetti, A.; Marks, T. J. *Adv. Mater.* **2006,** *18* (11), 1416-1420.
52. Horowitz, G.; Kouki, F.; Spearman, P.; Fichou, D.; Nogues, C.; Pan, X.; Garnier, F. *Adv. Mater.* **1996,** *8* (3), 242-245.
53. Lutsyk, P.; Janus, K.; Sworakowski, J.; Generali, G.; Capelli, R.; Muccini, M. *J. Phys. Chem. C.* **2011,** *115* (7), 3106-3114.
54. Oh, J. H.; Lee, H. W.; Mannsfeld, S.; Stoltenberg, R. M.; Jung, E.; Jin, Y. W.; Kim, J. M.; Yoo, J. B.; Bao, Z. N. *P. Natl. Acad. Sci. USA.* **2009,** *106* (15), 6065-6070.
55. Chen, H. Z.; Ling, M. M.; Mo, X.; Shi, M. M.; Wang, M.; Bao, Z. *Chem. Mater.* **2007,** *19* (4), 816-824.
56. Oh, J. H.; Sun, Y. S.; Schmidt, R.; Toney, M. F.; Nordlund, D.; Konemann, M.; Wurthner, F.; Bao, Z. A. *Chem. Mater.* **2009,** *21* (22), 5508-5518.
57. Molinari, A. S.; Alves, H.; Chen, Z.; Facchetti, A.; Morpurgo, A. F. *J. Am. Chem. Soc.* **2009,** *131* (7), 2462-2463.
58. Minder, N. A.; Ono, S.; Chen, Z. H.; Facchetti, A.; Morpurgo, A. F. *Adv. Mater.* **2012,** *24* (4), 503-508.
59. Noro, S.; Takenobu, T.; Iwasa, Y.; Chang, H. C.; Kitagawa, S.; Akutagawa, T.; Nakamura, T. *Adv. Mater.* **2008,** *20* (18), 33993403.
60. Gsanger, M.; Oh, J. H.; Konemann, M.; Hoffken, H. W.; Krause, A. M.; Bao, Z. N.; Wurthner, F. *Angew. Chem. Int. Edn.* **2010,** *49* (4), 740-743.
61. Schmidt, R.; Oh, J. H.; Sun, Y. S.; Deppisch, M.; Krause, A. M.; Radacki, K.; Braunschweig, H.; Konemann, M.; Erk, P.; Bao, Z. A.; Wurthner, F. *J. Am. Chem. Soc.* **2009,** *131* (17), 6215-6228.
62. Chen, T. A.; Rieke, R. D. *J. Am. Chem. Soc.* **1992,** *114* (25), 10087-10088.

TH-1703_11612241

63. Beaujuge, P. M.; Amb, C. M.; Reynolds, J. R. *Acc. Chem. Res.* **2010,** *43* (11), 1396-1407.
64. Zhan, X. W.; Tan, Z. A.; Domercq, B.; An, Z. S.; Zhang, X.; Barlow, S.; Li, Y. F.; Zhu, D. B.; Kippelen, B.; Marder, S. R. *J. Am. Chem. Soc.* **2007,** *129* (23), 7246-7247.
65. Chen, Z. H.; Zheng, Y.; Yan, H.; Facchetti, A. *J. Am. Chem. Soc.* **2009,** *131* (1), 8-9.
66. Hahm, S. G.; Rho, Y.; Jung, J.; Kim, S. H.; Sajoto, T.; Kim, F. S.; Barlow, S.; Park, C. E.; Jenekhe, S. A.; Marder, S. R.; Ree, M. *Adv. Funct. Mater.* **2013,** *23* (16), 2060-2071.
67. Zhou, W. Y.; Wen, Y. G.; Ma, L. C.; Liu, Y. Q.; Zhan, X. W. *Macromolecules* **2012,** *45* (10), 4115-4121.
68. Zhan, X. W.; Tan, Z. A.; Zhou, E. J.; Li, Y. F.; Misra, R.; Grant, A.; Domercq, B.; Zhang, X. H.; An, Z. S.; Zhang, X.; Barlow, S.; Kippelen, B.; Marder, S. R. *J. Mater. Chem.* **2009,** *19* (32), 5794-5803.
69. Zhao, X. G.; Wen, Y. G.; Ren, L. B.; Ma, L. C.; Liu, Y. Q.; Zhan, X. W. *J. Polym. Sci. Pol. Chem.* **2012,** *50* (20), 4266-4271.
70. Vasimalla, S.; Senanayak, S. P.; Sharma, M.; Narayan, K. S.; Iyer, P. K. *Chem. Mater.* **2014,** *26* (13), 4030-4037.
71. Zhang, S. M.; Wen, Y. G.; Zhou, W. Y.; Guo, Y. L.; Ma, L. C.; Zhao, X. G.; Zhao, Z.; Barlow, S.; Marder, S. R.; Liu, Y. Q.; Zhan, X. W. *J. Polym. Sci. Pol. Chem.* **2013,** *51* (7), 1550-1558.
72. Zhao, X. G.; Ma, L. C.; Zhang, L.; Wen, Y. G.; Chen, J. M.; Shuai, Z. G.; Liu, Y. Q.; Zhan, X. W. *Macromolecules* **2013,** *46* (6), 2152-2158.
73. Shukla, D.; Nelson, S. F.; Freeman, D. C.; Rajeswaran, M.; Ahearn, W. G.; Meyer, D. M.; Carey, J. T. *Chem. Mater.* **2008,** *20* (24), 7486-7491.
74. Tszydel, I.; Kucinska, M.; Marszalek, T.; Rybakiewicz, R.; Nosal, A.; Jung, J.; Gazicki-Lipman, M.; Pitsalidis, C.; Gravalidis, C.; Logothetidis, S.; Zagorska, M.; Ulanski, J. *Adv. Funct. Mater.* **2012,** *22* (18), 3840-3844.
75. Gawrys, P.; Boudinet, D.; Kornet, A.; Djurado, D.; Pouget, S.; Verilhac, J. M.; Zagorska, M.; Pron, A. *J. Mater. Chem.* **2010,** *20* (10), 1913-1920.
76. Jung, B. J.; Lee, K.; Sun, J.; Andreou, A. G.; Katz, H. E. *Adv. Funct. Mater.* **2010,** *20* (17), 2930-2944.
77. Oh, J. H.; Suraru, S. L.; Lee, W. Y.; Konemann, M.; Hoffken, H. W.; Roger, C.; Schmidt, R.; Chung, Y.; Chen, W. C.; Wurthner, F.; Bao, Z. N. *Adv. Funct. Mater.* **2010,** *20* (13), 2148-2156.
78. See, K. C.; Landis, C.; Sarjeant, A.; Katz, H. E. *Chem. Mater.* **2008,** *20* (11), 3609-3616.
79. Sun, J.; Devine, R.; Dhar, B. M.; Jung, B. J.; See, K. C.; Katz, H. E. *ACS. Appl. Mater. Inter.* **2009,** *1* (8), 1763-1769.
80. Deng, P.; Yan, Y.; Wang, S. D.; Zhang, Q. *Chem. Commun.* **2012,** *48* (20), 2591-2593.
81. Zhao, Y.; Di, C. A.; Gao, X. K.; Hu, Y. B.; Guo, Y. L.; Zhang, L.; Liu, Y. Q.; Wang, J. Z.; Hu, W. P.; Zhu, D. B. *Adv. Mater.* **2011,** *23* (21), 2448-2453.

TH-1703_11612241

82. Zhang, F. J.; Hu, Y. B.; Schuettfort, T.; Di, C. A.; Gao, X. K.; McNeill, C. R.; Thomsen, L.; Mannsfeld, S. C. B.; Yuan, W.; Sirringhaus, H.; Zhu, D. B. *J. Am. Chem. Soc.* **2013,** *135* (6), 2338-2349.
83. Hu, Y. B.; Qin, Y. K.; Gao, X. K.; Zhang, F. J.; Di, C. A.; Zhao, Z.; Li, H. X.; Zhu, D. B. *Org. Lett.* **2012,** *14* (1), 292-295.
84. Hwang, D. K.; Dasari, R. R.; Fenoll, M.; Alain-Rizzo, V.; Dindar, A.; Shim, J. W.; Deb, N.; Fuentes-Hernandez, C.; Barlow, S.; Bucknall, D. G.; Audebert, P.; Marder, S. R.; Kippelen, B. *Adv. Mater.* **2012,** *24* (32), 4445-4450.
85. Tiwari, S. P.; Kim, J.; Knauer, K. A.; Hwang, D. K.; Polander, L. E.; Barlow, S.; Marder, S. R.; Kippelen, B. *Org. Electron.* **2012,** *13* (7), 1166-1170.
86. Katz, H. E.; Lovinger, A. J.; Johnson, J.; Kloc, C.; Siegrist, T.; Li, W.; Lin, Y. Y.; Dodabalapur, A. *Nature* **2000,** *404* (6777), 478-481.
87. Yan, H.; Chen, Z. H.; Zheng, Y.; Newman, C.; Quinn, J. R.; Dotz, F.; Kastler, M.; Facchetti, A. *Nature* **2009,** *457* (7230), 679-687.
88. Guo, X. G.; Kim, F. S.; Seger, M. J.; Jenekhe, S. A.; Watson, M. D. *Chem. Mater.* **2012,** *24* (8), 1434-1442.
89. Hwang, Y. J.; Ren, G. Q.; Murari, N. M.; Jenekhe, S. A. *Macromolecules* **2012,** *45* (22), 9056-9062.
90. Hwang, Y. J.; Murari, N. M.; Jenekhe, S. A. *Polym. Chem.* **2013,** *4* (11), 3187-3195.
91. Huang, H.; Chen, Z. H.; Ortiz, R. P.; Newman, C.; Usta, H.; Lou, S.; Youn, J.; Noh, Y. Y.; Baeg, K. J.; Chen, L. X.; Facchetti, A.; Marks, T. J. *J. Am. Chem. Soc.* **2012,** *134* (26), 10966-10973.
92. Durban, M. M.; Kazarinoff, P. D.; Segawa, Y.; Luscombe, C. K. *Macromolecules* **2011,** *44* (12), 4721-4728.
93. Subramaniyan, S.; Earmme, T.; Murari, N. M.; Jenekhe, S. A. *Polym. Chem.* **2014,** *5* (19), 5707-5715.
94. Kim, Y.; Hong, J.; Oh, J. H.; Yang, C. *Chem. Mater.* **2013,** *25* (15), 3251-3259.
95. Yan, Y.; Huang, L. B.; Zhou, Y.; Han, S. T.; Zhou, L.; Zhuang, J. Q.; Xu, Z. X.; Roy, V. A. L. *Sci. Rep.* **2015,** *5*, 1-8.
96. Yadav, S.; Ghosh, S. *Acs. Appl. Mater. Inter.* **2016,** *8* (16), 10436-10442.
97. Higgins, S. G.; Muir, B. V. O.; Dell'Erba, G.; Perinot, A.; Caironi, M.; Campbell, A. J. *Appl. Phys. Lett.* **2016,** *108* (2), 023302 (1-5).
98. Tobjork, D.; Osterbacka, R. *Adv. Mater.* **2011,** *23* (17), 1935-1961.
99. Loi, A.; Basirico, L.; Cosseddu, P.; Lai, S.; Barbaro, M.; Bonfiglio, A.; Maiolino, P.; Baglini, E.; Denei, S.; Mastrogiovanni, F.; Cannata, G. *IEEE Sens. J.* **2013,** *13* (12), 4764-4772.
100. Facchetti, A.; Yoon, M. H.; Marks, T. J. *Adv. Mater.* **2005,** *17* (14), 1705-1725.
101. Ortiz, R. P.; Facchetti, A.; Marks, T. J. *Chem. Rev.* **2010,** *110* (1), 205-239.
102. Halik, M.; Klauk, H.; Zschieschang, U.; Schmid, G.; Dehm, C.; Schutz, M.; Maisch, S.; Effenberger, F.; Brunnbauer, M.; Stellacci, F. *Nature* **2004,** *431* (7011), 963-966.
103. Klauk, H.; Zschieschang, U.; Pflaum, J.; Halik, M. *Nature* **2007,** *445* (7129), 745-748.

TH-1703_11612241

104. Zirkl, M.; Haase, A.; Fian, A.; Schon, H.; Sommer, C.; Jakopic, G.; Leising, G.; Stadlober, B.; Graz, I.; Gaar, N.; Schwodiauer, R.; Bauer-Gogonea, S.; Bauer, S. *Adv. Mater.* **2007,** *19* (17), 2241-2245.
105. Daraktchiev, M.; von Muhlenen, A.; Nuesch, F.; Schaer, M.; Brinkmann, M.; Bussac, M. N.; Zuppiroli, L. *New. J. Phys.* **2005,** *7*(133), 1-8.
106. Dinelli, F.; Murgia, M.; Levy, P.; Cavallini, M.; Biscarini, F.; de Leeuw, D. M. *Phys. Rev. Lett.* **2004,** *92* (11), 116802.
107. Shtein, M.; Mapel, J.; Benziger, J. B.; Forrest, S. R. *Appl. Phys. Lett.* **2002,** *81* (2), 268-270.
108. Sirringhaus, H. *Adv. Mater.* **2005,** *17* (20), 2411-2425.
109. Lin, Y. Y.; Gundlach, D. J.; Nelson, S. F.; Jackson, T. N. *IEEE. T. Electron. Dev.* **1997,** *44* (8), 1325-1331.
110. Park, Y. D.; Lim, J. A.; Lee, H. S.; Cho, K. *Mater. Today* **2007,** *10* (3), 46-54.
111. Steudel, S.; De Vusser, S.; De Jonge, S.; Janssen, D.; Verlaak, S.; Genoe, J.; Heremans, P. *Appl. Phys. Lett.* **2004,** *85* (19), 4400-4402.
112. Boulas, C.; Davidovits, J. V.; Rondelez, F.; Vuillaume, D. *Phys. Rev. Lett.* **1996,** *76* (25), 4797-4800.
113. Takeya, J.; Yamagishi, M.; Tominari, Y.; Hirahara, R.; Nakazawa, Y.; Nishikawa, T.; Kawase, T.; Shimoda, T.; Ogawa, S. *Appl. Phys. Lett.* **2007,** *90* (10), 102120.
114. Pernstich, K. P.; Haas, S.; Oberhoff, D.; Goldmann, C.; Gundlach, D. J.; Batlogg, B.; Rashid, A. N.; Schitter, G. *J. Appl. Phys.* **2004,** *96* (11), 6431-6438.
115. Jesper, M.; Alt, M.; Schinke, J.; Hillebrandt, S.; Angelova, I.; Rohnacher, V.; Pucci, A.; Lemmer, U.; Jaegermann, W.; Kowalsky, W.; Glaser, T.; Mankel, E.; Lovrincic, R.; Golling, F.; Hamburger, M.; Bunz, U. H. F. *Langmuir* **2015,** *31* (37), 10303-10309.
116. Ma, H.; Yip, H. L.; Huang, F.; Jen, A. K. Y. *Adv. Funct. Mater.* **2010,** *20* (9), 1371-1388.
117. Shen, Y. L.; Hosseini, A. R.; Wong, M. H.; Malliaras, G. G. *Chem. Phys. Chem.* **2004,** *5* (1), 16-25.
118. (a) Torricelli, F.; Ghittorelli, M.; Colalongo, L.; Kovacs-Vajna, Z. M. *Appl. Phys. Lett.* **2014,** *104* (9); (b) Takagaki, S.; Yamada, H.; Noda, K. *Jpn. J. Appl. Phys.* **2016,** *55* (3).
119. Matsumoto, T.; Ou-Yang, W.; Miyake, K.; Uemura, T.; Takeya, J. *Org. Electron.* **2013,** *14* (10), 2590-2595.
120. Richards, T. J.; Sirringhaus, H. *J. Appl. Phys.* **2007,** *102* (9), 094510.
121. Weis, M.; Lee, K.; Taguchi, D.; Manaka, T.; Iwamoto, M. *Jpn. J. Appl. Phys.* **2012,** *51* (10).
122. Chiarella, F.; Barra, M.; Carella, A.; Parlato, L.; Sarnelli, E.; Cassinese, A. *Org. Electron.* **2016,** *28*, 299-305.
123. Liu, C.; Xu, Y.; Li, Y.; Scheideler, W.; Minari, T. *J. Phys. Chem. C.* **2013,** *117* (23), 12337-12345.
124. (a) Mittal, P.; Kumar, B.; Negi, Y. S.; Kaushik, B. K.; Singh, R. K. *Microelectron. J.* **2012,** *43* (12), 985-994; (b) Reese, C.; Bao, Z. *Adv. Funct. Mater.* **2009,** *19* (5), 763-771.
125. Meric, I.; Dean, C. R.; Young, A. F.; Baklitskaya, N.; Tremblay, N. J.; Nuckolls, C.; Kim, P.; Shepard, K. L. *Nano. Lett.* **2011,** *11* (3), 1093-1097.

TH-1703_11612241

126. Rodel, R.; Letzkus, F.; Zaki, T.; Burghartz, J. N.; Kraft, U.; Zschieschang, U.; Kern, K.; Klauk, H. *Appl. Phys. Lett.* **2013,** *102* (23), 233303.
127. Sharma, A.; Mathijssen, S. G. J.; Smits, E. C. P.; Kemerink, M.; de Leeuw, D. M.; Bobbert, P. A. *Phys. Rev. B.* **2010,** *82* (7), 075322.
128. (a) Nouchi, R.; Kubozono, Y. *Org. Electron.* **2010,** *11* (6), 1025-1030; (b) Egginger, M.; Irimia-Vladu, M.; Schwodiauer, R.; Tanda, A.; Frischauf, I.; Bauer, S.; Sariciftci, N. S. *Adv. Mater.* **2008,** *20* (5), 1018-1022.
129. Street, R. A. *Phys. Rev. B.* **2008,** *77* (16), 165311.

TH-1703_11612241

Chapter 2

Synthesis of Perylenediimide based polymers and fabrication of Organic Field-Effect transistors

2.1. Introduction

Organic field effect transistors (OFETs) have been extensively studied during the past several years since they have played important role in the fabrication of low cost organic optoelectronic devices such as p-n junctions,[1,2] photovoltaic cells,[3,4] complementary circuits[5] and organic light emitting diodes (OLED) for flexible display.[6,7] These applications require both hole transporting (p-type) and electron transporting (n-type) materials with suitable physical, chemical, electrical and photochemical properties. The development of n-type materials has lagged behind the p-type materials for many years since majority of the reported molecules are p-type semiconductors because of the instability of n-type materials to the environment.[8,9] In recent years, few reports on the development of ambipolar[10,11] and n-type semiconductors with encouraging performances have appeared.[12,13] For the electronics industries that are working on organic materials, development of low-cost solution processable n-type semiconducting materials with high performance is an immediate goal. One of the major drawbacks with n-type materials is their instability at ambient conditions. In this regard, n-type PFETs were demonstrated with electron mobilities ~0.5 cm^2/Vs which are relatively stable under ambient conditions and could be aligned to improve the transport properties by several orders.

There are numerous building blocks being developed to fabricate air stable n-channel semiconducting materials, while rylene based polymers, especially naphthalene,[14,15] perylene,[16,17] pyromellitic tetracarboxylic diimides[18,19] are the most important. Perylene diimides (PDI) possess aromatic planar conjugated structure and are favorable for good charge transport with performances comparable to p-type semiconducting materials. These classes of materials have excellent thermal, optical, redox and electrical properties

TH-1703_11612241

and also very high moisture and oxygen resistance which is essential for n-type materials.[20] In organic materials perylene imides (Figure 2.1) are among the most stable compounds.[21] They have been known for nearly 100 years, when Kardos found a way to synthesize perylenedimides in the beginning of 1910s. Several decades later, perylene derivatives have been applied for the coloration of automotive paint and for the mass coloration of synthetic fiber and engineering resins. The perylene core has twelve functionalizable positions -the 3,4,9,10 positions, which are known as the peri- the 1,6,7,12, known as the bay- and the 2,5,8,11 known as the ortho-positions. According to the functionalizing positions, there are three important stages for the development of perylene imides (Figure 2.1). In the 1st generation, the 3,4,9,10-diimides substitutions were intensively developed. In 2nd generation, additional or exclusive bay-decoration as well as the asymmetric perylene monoimides or monoanhydrides are being investigated. The recent discovery of the ortho-functionalization finally rounds out the synthesis options of perylene and will become an interesting direction for research in the future as the 3rd generation of perylene derivatives.[22]

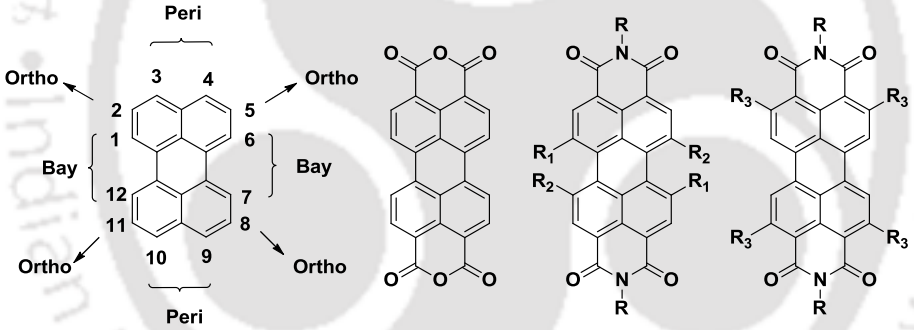

Figure 2.1. Perylene, Perylene dianhydride and Perylene diimides

The functionalization at the diimide position with aliphatic alkyl chain, either branched or long chain provides good solubility in common organic solvents enhancing their processability.[23] Additionally, the possibility to obtain inter-digitated structures limits the percolation of moisture to the conjugated core, thereby, making it stable for ambient performance.[24] Many PDI based small molecules[22] and oligomers[25] have been reported with self-assembling properties and good charge transporting ability. Few newly developed materials showing high electron mobility include: ladder type perylene diimide,[26] and D-A type copolymers of PDI with thiophene,[27] bithiophene[28] dithienothiophene,[29] phenothiazine,[30] dithienopyrrole[31] and phenylene. High electron mobility of up to ~0.5 cm^2/Vs were reported with PDI derivative and bithiophene

TH-1703_11612241

copolymers.[32] In PDI based copolymers, electron mobilities up to 0.075 cm^2/Vs have been possible with dithienothiophene unit,[33] with liquid crystalline copolymers.[34,35]

Although there are many n-type polymers reported, it is still unclear why D-A based PDI copolymers have shown better μ_{FET}. For obtaining high-performance OFETs, the role of anisotropic properties and improving the structural order in solution-processed n-type polymers and the enhanced film morphology on macroscopic scale is very crucial. As there are very few thiophene free polymers, in this work two copolymers based on phenylene and benzothiadiazole as copolymerizing units with linear C18 substituted PDI derivatives were synthesized in order to understand the roles and features of different D-A and A-A structures and carefully studied the transport behavior in these polymers. It was also demonstrated that annealing at appropriate temperatures enhanced the polymer anisotropic properties by significantly improving the intermolecular interactions as well as the formation of crystalline domains on macroscopic scale facilitating large enhancement in charge carrier transport. Since conjugated polymers inherently possess anisotropic characteristics, they can be realized in device applications only when these conjugated chains are aligned in such a manner that the crystallites do not remain entrenched within the amorphous polymer phases. Tuning the thin film structures of the polymers by annealing facilitates the conjugated chain alignment over larger macro domains and enhances the structure-property relationships by exhibiting highly improved charged transport behavior here. Hence, developing processing strategies in these materials to overcome the amorphous domains and recognizing the importance of conjugated backbone macrostructure chain alignment are, in principle, extremely crucial for device improvements.

2.2. Experimental Section

2.2.1. Materials and Instruments

Perylene tetracarboxylic dianhydride, 1,4-benzene diboronic acid, 2,1,3-Benzothiadiazole-4,7-bis(boronic acid pinacol ester), were purchased from Sigma Aldrich and were used without further purification. The dielectric material hydroxyl free divinyltetramethylsiloxanebis-benzocyclobutene (BCB) was obtained from Dow Chemicals. 1,7-dibromo-3,4:9,10-perylene teracarboxylic dianhydride (PTCDA-Br_2), N,N´-bis(octadecyl)-1,7-dibromo-3,4:9,10-perylene tetracarboxylic dianhydride, were

TH-1703_11612241

synthesized following the published literature procedure (Scheme 1).[31] Both the polymers PDI-Ph, PDI-BT were synthesized by Suzuki coupling reaction. ^{1}H NMR, ^{13}C NMR were recorded on Varian AS 400MHz and Bruker 600MHz NMR spectrometers. MALDI-TOF-MS experiments were done on AB SCIEX, USA instrument with a 4800 plus MALDI TOF/TOF Analyzer. Elemental analysis was done on CHNS Analyzer, Perkin Elmer, 2400 (USA). UV-Vis spectra were recorded on a Perkin-Elmer Model Lambda-25 spectrophotometer. Photoluminescence spectra were recorded on Varian Cary Eclipse spectrophotometer. Electrochemical measurements were carried out under argon on a deoxygenated solution of tetra n-butyl ammonium perchlorate (0.1 M) in Acetonitrile using a CH instruments Model 700D series Electrochemical workstation. A glassy carbon as working electrode, platinum wire as counter electrode, Ag/Ag^{+} as reference electrodes were used. Thermo gravimetric analysis (TGA) was performed on METTLER TOLEDO, Model TG/SDTA 851 e Thermo Gravimetric analyzer under a nitrogen flow at a heating rate of 10°C/min. Differential scanning calorimeter were done on METTLER TOLEDO, Model DSC 1, Stare system. The gel permeation chromatography measurements were performed on a waters 515 chromatograph connected to waters 2414 refractive index detector using THF as eluent and polystyrene standards as calibrants. AFM images were taken by Agilent 5500-STM instrument and FESEM images were recorded in a Sigma Carl ZEISS scanning electron microscope. XRD analyses were done by Bruker D8 Discover Diffractometer. Leica polarizable optical microscope was used to study the anisotropic morphology of the copolymer films.

2.2.2. Preparation of films for AFM, FESEM, XRD and POM

The copolymers were spin coated on glass substrates at 500 rpm for two minutes and then heated for 30 min at 50 °C to evaporate the solvent. The films were prepared under the same conditions to record the FESEM images. Similarly, AFM images of the films were recorded for as spun and annealed films. For XRD measurement the films were prepared under the same conditions as followed for the device fabrication. For POM studies, the copolymers were dissolved in chloroform and drop casted on glass slide, heated for 2h at 50°C to remove residual solvent. During the POM annealing experiments the films were heated from 50-180°C at a rate of 5°C/min and then cooled to 50°C at the same rate and the images were recorded at 50X resolution.

TH-1703_11612241

2.2.3. Synthesis of Monomers and Polymers

Two new conjugated copolymers were synthesized in good yields 83% and 86%. (Scheme 2.1). The synthesis details of the monomers and copolymers are explained in detail in subsequent sections. The Suzuki coupling reaction of dibrominated PDI derivatives with benzene-1,4-diboronic acid and 2,1,3-benzothiadiazole bisboronic ester resulted in the formation of PDI-Ph and PDI-BT copolymers.

(a) Synthesis of Br_2-PDIOD: A mixture of PTCDA-Br_2 (0.4 g, 0.72 mmol) (Precaution: The dibromination of PTCDA by bromine in concentrated H_2SO_4 and must be handled with great care), octadecylamine (0.58 g, 2.18 mmol), O-xylene (3 mL), and propionic acid (1 mL) were stirred at 140 °C for 6h. After cooling to room temperature the solvents were removed in vacuo and the product was purified by column chromatography on silica gel, using a mixture of chloroform: hexane (1:2, v/v) as eluent, yielding red color solid as product (0.49 g, yield 65%). ^{1}HNMR (600MHz, $CDCl_3$, δ ppm): 9.47 (d, J = 8.0 Hz, 2H), 8.90 (s, 2H), 8.69 (d, J = 8.0 Hz, 2H), 4.184 (t, 4H), 1.729 (m, 4H), 1.25-1.42 (m, 60H), 0.853 (t, 6H); ^{13}C NMR ($CDCl_3$, 150MHz, δ ppm): 163.08, 162.57, 138.20, 133.18, 133.02, 130.21, 129.47, 128.71, 127.16, 123.43, 123.00, 120.99, 41.05-14.32 (Aliphatic Carbons); MALDI-TOF: m/z calcd. 1053.44, found, $[M+2H]^+$: 1055.47; Elemental Analysis Calcd. C, 68.43; H, 7.66; N, 2.66; found, C, 68.33; H, 7.19; N, 1.84;

(b) Synthesis of PDI-Ph: To a three neck round bottom flask Br_2-PDIOD (0.1 g, 0.095 mmol), benzene-1,4-diboronic acid (15.7mg, 0.0949 mmol), were added and degassed thrice by freeze thaw cycles. Aqueous solution of K_2CO_3 (0.131 g, 0.949 mmol) in 2 mL deoxygenated water were added under nitrogen. $Pd(PPh_3)_4$ (0.0054 g, 0.004 mmol), two drops of aliquat and 6 mL THF were added under nitrogen atmosphere, degassed thrice by freeze thaw cycles. The dark red solution was stirred at 80°C for 36h. Phenyl boronic acid was added under nitrogen and the reaction was continued for other 12h. The brown sticky mixture was cooled to room temperature. The mixture was extracted with $CHCl_3$, washed with 100 mL water thrice and dried over anh. $MgSO_4$. The solution was concentrated to 5 mL and dropped in 50 mL methanol. The precipitate was filtered and washed with methanol twice to get black color solid. (0.076 g, Yield 83%) ^{1}HNMR (600MHz, $CDCl_3$, δ ppm): 8.57 (br, m, 2H), 8.30 (br, m, 4H), 7.69 (br, m, 2H), 4.1-4.4 (br, m, 4H), 1.67 (br, m, 4H), 1.2 (br, m, 60H), 0.86 (br, m, 6H); ^{13}C NMR

TH-1703_11612241

($CDCl_3$, 150MHz, δ ppm): 163.49, 163.18, 136.50, 135.50, 134.61, 133.88, 132.30, 131.45, 129.14, 128.70, 126.45, 124.50, 123.46, 123.22, 40.97-14.16 (Aliphatic Carbons); GPC: M_n: 16082; M_w: 24657; PDI: 1.53.

(c) Synthesis of PDI-BT: To a three neck round bottom flask Br_2-PDIOD (0.1 g, 0.095 mmol), 2,1,3-benzothiadiazole bisboronic ester (0.037 g, 0.0949 mmol), were added and degassed thrice by freeze thaw cycles. Aqueous solution of K_2CO_3 (0.131 g, 0.949 mmol) in 2 mL deoxygenated water were added under nitrogen. $Pd(PPh_3)_4$ (0.0054 g, 0.004 mmol), two drops of aliquat and 6 mL THF were added under nitrogen atmosphere, degassed thrice by freeze thaw cycles. The dark red solution was stirred at 80°C for 36h. Phenyl boronic acid was added under nitrogen and the reaction was continued for other 12h. The brown sticky mixture was cooled to room temperature. The mixture was extracted with $CHCl_3$, washed with 100 mL water thrice and dried over anh. $MgSO_4$. The solution was concentrated to 5 mL and added drop by drop in 50 mL methanol .The precipitate was filtered and washed with methanol twice to get black color solid. (0.084 g,Yield 86%). ^{1}HNMR (600MHz, $CDCl_3$, δ ppm): 8.76 (br, m, 2H), 8.10 (br, m, 4H), 7.83 (br, m, 2H), 4.1-4.4 (br, m, 4H), 1.67 (br, m, 4H), 1.2 (br, m, 60H), 0.86 (br, m, 6H); ^{13}C NMR ($CDCl_3$, 150MHz, δ ppm): 163.46, 163.23, 136.19, 134.54, 133.04, 132.31, 132.00, 131.80, 131.43, 129.07, 128.52, 127.79, 124.19, 123.24, 40.99-14.31 (Aliphatic Carbons); GPC: M_n: 30619 Da; M_w: 35739 Da; PDI: 1.16.

2.2.4. Device fabrication and characterization

Bottom gate top contact FETs, were fabricated in order to understand the detailed transport behavior of the PDI copolymers. For device fabrication, Al metal is coated as the gate electrode by physical vapor deposition (10^{-6} mbar, 40 nm thick) on RCA cleaned glass substrate. Dielectric layer hydroxyl free divinyl tetramethyl siloxane bisbenzocyclobutene (BCB) is then coated at 1000 rpm for 1 min and annealed in N2 filled glove box atmosphere at 290°C. The resultant dielectric layer had a C_i ~4 nF/cm^2 measured directly using the C-V meter inbuilt in Keithley 4200 semiconductor parameter analyzer. Typical dielectric thickness is estimated to be around 0.5 - 0.6 µm as measured using Filmetrics (F20-EXR) thickness measurement set up. The surface of the dielectric was coated (1500 rpm for 30 s) with a thin monolayer of hexamethyldisilazane (HMDS) and annealed at 110°C for 2 h. Copolymer layer is then introduced from solution phase (15 mg/mL in THF) by spin coating at 1000 rpm for 1 minute and annealed at different

TH-1703_11612241

temperatures 110°C - 150°C for 30 min to optimize the performance. In order to facilitate electron injection Al source-drain electrodes were then coated (10^{-6} mbar, 40 nm thick) to complete the device fabrication. An injection limited response with lower OFET for Au S-D electrodes was observed. The device characterizations were performed using standard Keithley 4200 Semiconductor characterization systems and cross-checked with measurement using Keithley 2400 Source meters and High-impedance Keithley 6514 Electrometer. Typical FET performance is estimated from average characteristics of five to seven devices.

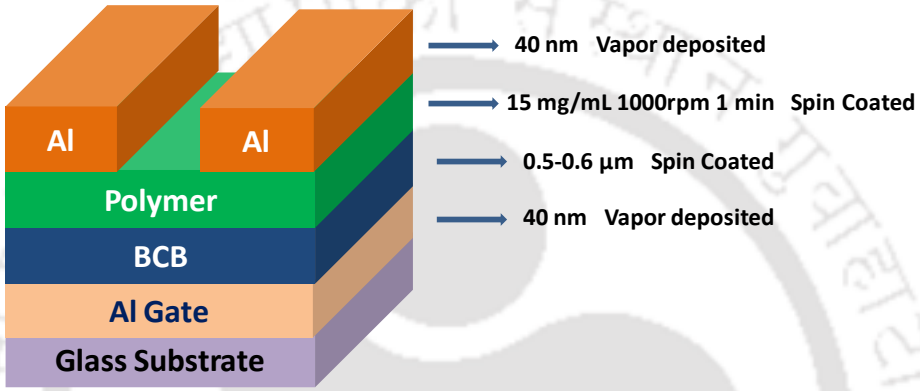

2.3. Results and discussion

2.3.1. Characterizations

All the monomers and polymers were well characterized by NMR, (Figure 2.10-2.11, 2.13-2.16), MALDI (Figure 2.12)/gel permeation chromatography (GPC), elemental analysis, DSC, TGA, PL, UV-Vis and cyclic voltammetry and their morphology studied by AFM, FESEM, POM (Figures 2.6, 2.7, 2.8) and XRD (Figures 2.4, 2.5) techniques. The TGA analysis reveals that the copolymers are stable up to 350 °C. These polymers were fabricated and tested for solution processable polymer field effect transistors (PFETs). It was observed that these PDI derivatives exhibit field effect electron mobilities (OFET) that are as high as 0.04 cm^2/Vs (PDI-Ph) and 0.032 cm^2/Vs (PDI-BT) with a current modulation in the range of 10^4-10^5. High OFET can be attributed to the enhanced π-π stacking originating from the intermolecular overlap of the D-A orbitals. Table 2.2 represents their molecular weight and poly dispersity index (*PDI*) as obtained from GPC in THF (Polystyrene standard). Due to the presence of alkyl chains both the copolymers were readily soluble in common organic solvents such as toluene, THF, chloroform,

TH-1703_11612241

dichloromethane, chlorobenzene, xylenes and could be solution processed onto desired substrates for achieving smooth films.

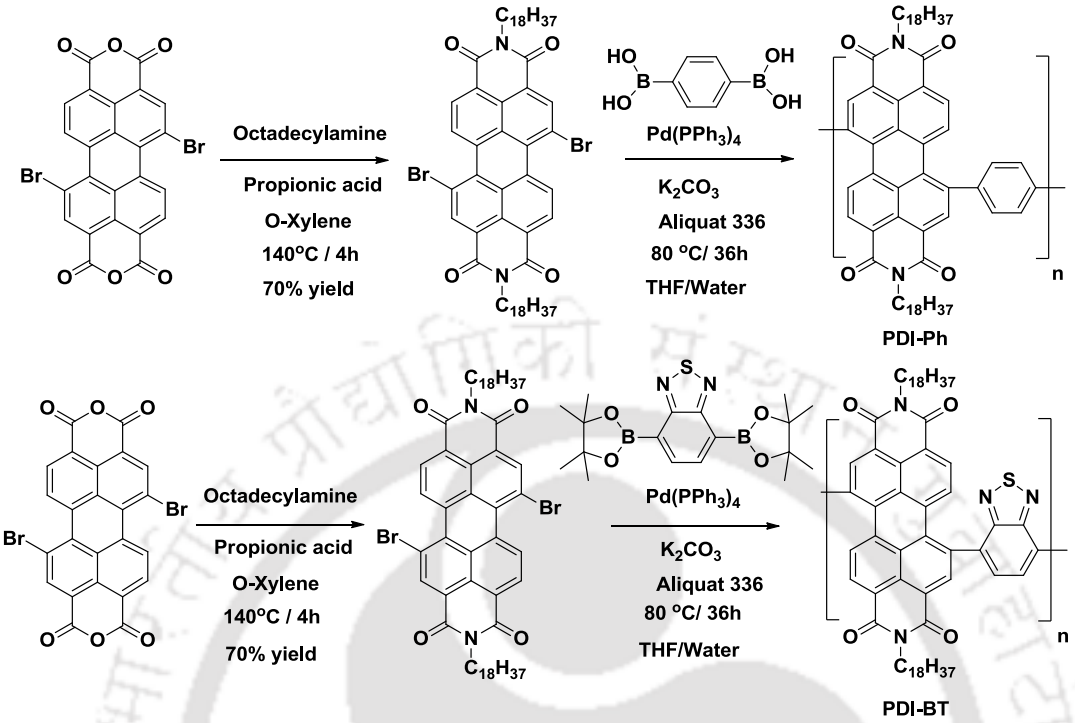

Scheme 2.1. Synthesis of monomers and copolymers

2.3.2. Photophysical Properties

In order to study the aggregation mechanism the UV-visible spectra of the copolymers were studied in THF at a concentration of 10^{-5} M. PDI-Ph shows absorption peaks at 548 nm, 513 nm and 485 nm, which are assigned to the general PDI based (S_o-S_o, S_o-S_1, S_o-S_2) transitions and a peak of polymer aggregation at 540 nm (Figure 2.2(a)).[36] Similarly, PDI-BT shows peaks at 550 nm, 525 nm and 489 nm. The absorption spectra of the spin coated polymer films on glass (Figure 2.2(b)) show red shift in the peaks for all the copolymers as compared to the solution state absorption peaks. The shoulders at 660 nm in PDI-Ph and 675 nm in PDI-BT which are assigned to π-π polymer interactions are observed to be shifted to 721 nm and 739 nm respectively in thin films indicating the general polymer aggregation in solid state. All other peaks of PDI-Ph and PDI-BT are found to be red shifted. The optical band gaps calculated from the absorption edge for PDI-BT, PDI-Ph copolymers were found to be 1.57 eV and 1.59 eV respectively (Table 2.1). PL spectroscopy measurements of polymers were performed in dilute 10^{-5} M THF solutions. The PDI-Ph copolymer shows emission peak at 538 nm and 575 nm which corresponds to the main absorption peak at 513 nm and 548 nm. Similarly, PDI-BT

TH-1703_11612241

polymer showed emission peaks at 537 nm, 577 nm corresponding to 525 nm, 550 nm peaks in UV (Figure 2.2(c)) in THF.

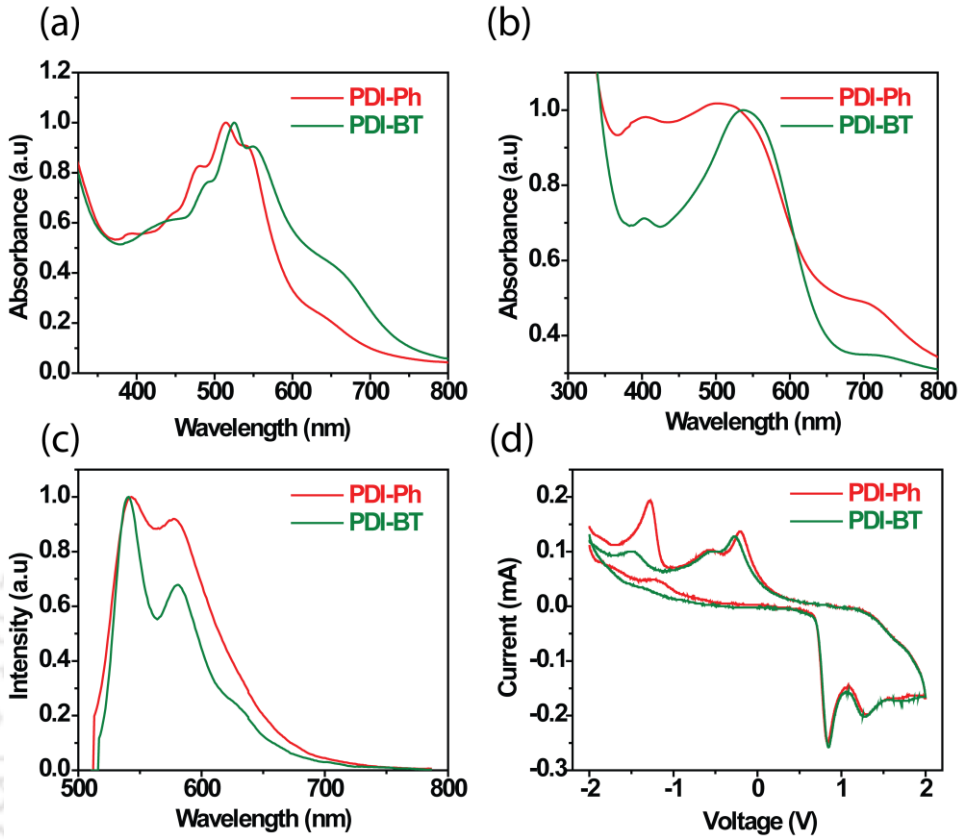

Figure 2.2. (a) UV-Vis spectra of polymers in THF (10^{-5} M) (b) UV-Vis spectra of polymers in thin films (~ 50 - 60 nm) (c) PL spectra in THF (10^{-5} M) of polymers (d) Cyclic voltagramms of the drop casted polymer films (~ 100 nm) on carbon working electrode performed at a scan rate of 0.5 mV/s in 0.1 M TBAP in acetonitrile under argon atmosphere.

Table 2.1. UV-vis absorption values in [a] solution and [b] thin film, emission values in solution, [c]optical band gaps and yields of the polymers.

Polymer	$\lambda_{max}{}^{a}$ (nm)	$\lambda_{max}{}^{b}$ (nm)	Emission (nm)	$E_g{}^{c}$ (eV)	Yield (%)
PDI-Ph	548, 513, 485	532	538, 575	1.59	83
PDI-BT	550, 525, 489	537	537, 577	1.57	86

TH-1703_11612241

2.3.3. Electrochemical Properties

HOMO and LUMO energy levels of the copolymers were estimated by cyclic voltammetry (CV) experiment. The copolymers were drop casted on the carbon working electrode. Silver as reference electrode and platinum wire as counter electrode were used in these experiments. The HOMO and LUMO levels were estimated by the onset oxidation and onset reduction peaks assuming the absolute energy level of the ferrocene/ferrocenium couple to be -4.8 eV below vacuum. 0.1 M tetra butyl ammonium perchlorate (TBAP) as electrolyte in deoxygenated acetonitrile and ferrocene as standard were used in argon atmosphere. The HOMO/LUMO were calculated by substituting the onset reduction and onset oxidation peak values in E_{LUMO} = - [(E_{red} - $E_{1/2}$(ferrocene)) + 4.8] eV, E_{HOMO} = - [(E_{ox} - $E_{1/2}$(ferrocene)) + 4.8] eV. The LUMO levels of PDI-BT, PDI-Ph are -3.49 eV and -3.08 eV respectively. Similarly HOMO levels of the copolymers PDI-BT, PDI-Ph calculated from CV are -5.89 eV, -5.49 eV respectively (Figure 2.2(d). The energy levels, band gaps calculated from cyclic voltammetry of thin films are represented in Table 2.2.

Table 2.2. Cyclic Voltammetry, TGA and GPC data

Polymer	[a]HOMO (eV)	[a]LUMO (eV)	[b]E_g(eV)	[c]T_d(^{o}C)	M_n(Da)	M_w(Da)	*PDI*
PDI-Ph	-5.89	-3.49	2.40	363	16000	24657	1.53
PDI-BT	-5.49	-3.08	2.41	385	30000	35739	1.16

M_n, M_w - number average and weight average molecular weights, *PDI* - polydispersity index are obtained from GPC. [a]HOMO and LUMO estimated from the onset oxidation and reduction potentials, respectively, assuming the absolute energy level of ferrocene/ferrocenium couple to be -4.8 eV below vacuum. [b]HOMO-LUMO gap estimated by electrochemistry. [c]T_d - degradation temperature calculated by TGA.

2.3.4. Thermal Properties

The thermal properties of the polymers were studied by thermo gravimetric analysis (TGA) and differential scanning calorimeter (DSC). TGA analysis was done in the range 25-800°C at a rate of 5 °C/min under nitrogen flow. Both the polymers were very stable and their onset degrading temperatures were found to be in the range of 360-390°C

TH-1703_11612241

(Figure 2.3(a)). The onset thermal degradation temperatures of both the polymers are shown in Table 2.2. In DSC, the polymers were heated from 25 °C to 325 °C and then again cooled to 25 °C with a rate of 5 °C/min for three cycles under nitrogen flow. The chromatograms of second cycle are shown in Figure 2.3(b). The PDI-Ph copolymer did not undergo any change during heating or cooling process. PDI-BT copolymer shows an endothermic peak at 164 °C during heating which corresponds to melting and exothermic peak of crystallization at 110 °C, during cooling process which indicates the crystal-line behavior of the copolymer. Hence, the DSC reveals that PDI-BT copolymer possess crystalline domains within its structure. The AFM, FESEM and polarized optical microscope images confirm that PDI-Ph also possesses crystalline domains within its structure.

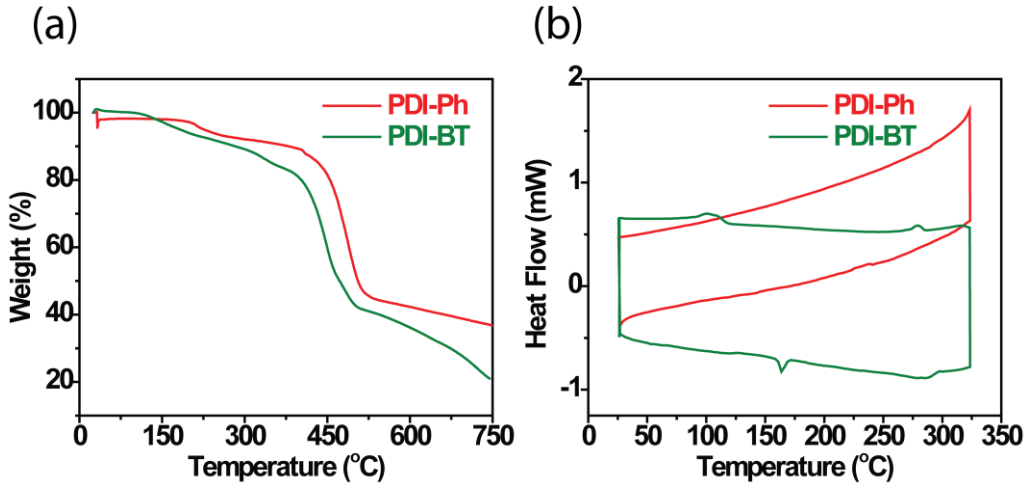

Figure 2.3. (a) TGA chromatograms carried out at a rate of 5°C/ min (b) DSC chromatograms of second cycle of the polymers carried out at a rate 5°C/ min under nitrogen atmosphere

2.3.5. Morphology Characterization

Polymer thin films were characterized by AFM, FESEM, XRD and polarized optical microscopy (POM) to obtain further information on crystallinity and morphology which is relevant for device characterization. Out-of plane XRD measurements were performed on thin films of PDI co-polymers (Figure 2.4, 2.5) to obtain information regarding the molecular re-organization. As spun polymeric films reveal π-π stacking in the range of 4.10-4.14 Å and a diffraction peak at 2θ = 6.12-6.64° corresponding to the d-spacing values of 25.91 ~28.11 Å. Annealing of the thin films reduced the d-spacing to a range of 25.81-28.02 Å and π-π stacking distance to 4.10-4.12 Å (Table 2.3). This indicates that denser inter-digitated lamellar packing is obtained by annealing of the polymer films,

TH-1703_11612241

which is an inherent anisotropic characteristic of conjugated backbone possessing polymers which gets reflected in the enhanced transport properties. In addition, annealing of the polymer film decreases the FWHM of the peaks (Table 2.4) corresponding to π-π stacking as well as the d-spacing pointing to the enhanced morphological ordering with annealing.

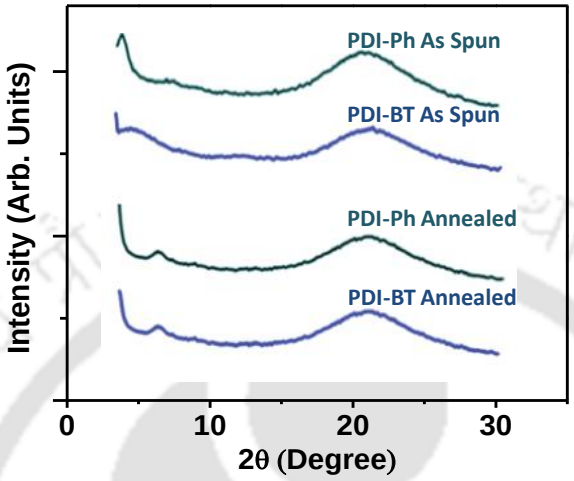

Figure 2.4. Out of plane X-ray diffraction patterns of as spun and annealed (150°C) copolymer films

Table 2.3. Summary of variation in π -π stacking and d spacing of the Polymers

		As cast films		**Annealed Films**	
Polymers	(00n)	2θ	d (00n) spacing(Å)	2θ	d (00n) spacing(Å)
PDI-Ph	(001)	-	-	-	-
	(002)	6.64	25.91	6.66	25.81
	π-π	20.84	4.14	20.97	4.12
PDI-BT	(001)	-	-	-	-
	(002)	6.12	28.11	6.14	28.02
	π-π	21.06	4.10	21.05	4.10

AFM analysis was carried out on optical quality films coated under similar condition as those used in device studies. AFM images for as spun films do not exhibit any crystallite formation (Figure 2.6a, 2.6c,). However, it was observed that annealing the thin films at 150 °C introduces crystallites in the film (Figure 2.6b, 2.6d). This trend is consistent with DSC measurement which shows crystallization at ~110 °C. It should be noted that the

TH-1703_11612241

degree of enhancement of crystallinity is more prominent for PDI films. This was substantiated from observations of larger number of crystallites obtained in case of PDI-Ph and PDI-BT. Furthermore, FESEM measurements of PDI-Ph and PDI-BT (Figure 2.7) were also performed on these copolymers to examine the thin film microstructure.

Table 2.4. Table showing the variation in the FWHM of the XRD spectra with annealing of the polymer films

		As cast film	Annealed Film
Polymer	(00n)	FWHM	FWHM
PDI-Ph	001	-	-
	002	1.0112	0.713
	π- π	7.9777	7.6657
PDI-BT	001	-	-
	002	7.1364	1.0482
	π- π	8.2268	7.9777

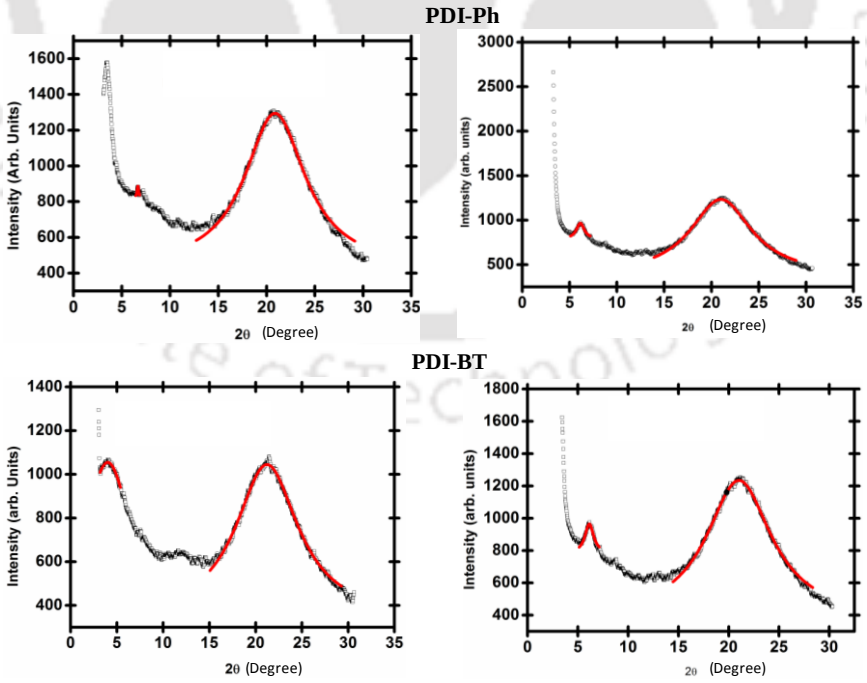

Figure 2.5. XRD spectra of the annealed (right side) and as spun (left side) polymer films fitted with Lorentzian to correctly estimate the peaks

TH-1703_11612241

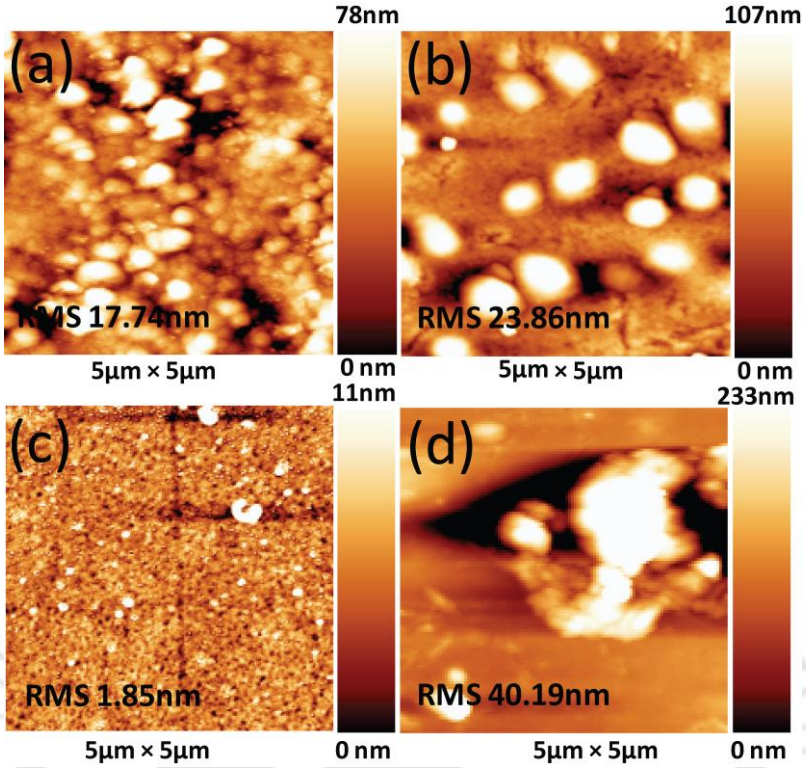

Figure 2.6. AFM topography image (5 μm × 5 μm) for the copolymer films: PDI-Ph (a) as spun (b) annealed; PDI-BT (c) as spun (d) annealed

FESEM images show interconnected crystalline fibrillar network of the copolymers which supports enhanced transport, weakly affected by defects.[37,38] In addition, POM studies performed on films of the these four copolymers confirmed the appearance of macroscale crystalline domains after annealing above 150 °C (Figure 2.8) due to their inherent structural anisotropic. These features can be directly correlated to large enhancement of OFET upon thermal annealing in PDI derivatives.

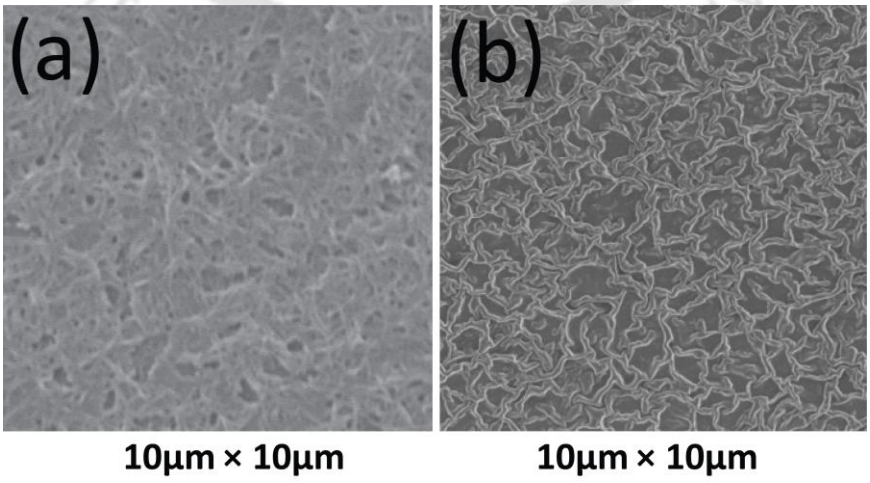

Figure 2.7. Typical FESEM images (10 μm × 10 μm) of (a) PDI-Ph (b) PDI-BT

TH-1703_11612241

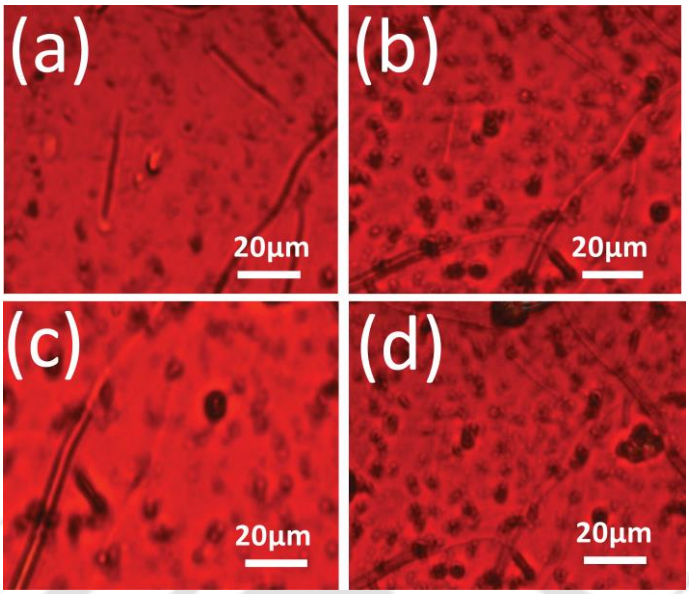

Figure 2.8. Polarizable Optical Microscope images of PDI-Ph (a) before annealing, (b) after annealing, PDI-BT (c) before annealing (d) after annealing

2.3.6. OFET Measurements

Top contact bottom gate OFETs were fabricated using newly synthesized PDI-Ph and PDI-BT copolymers as active layers. The devices demonstrated well defined linear and saturation behavior with electron only mobility and On/Off ratio exceeding 10^4 (Figure 2.9). Typical plot showing FET characteristics measured under inert condition is shown in Figure 2.9. Although molecules with phenylene substitution are of D-A type, hole transport was not observed even with Au S-D electrodes. This feature can be attributed to weaker electron donating ability of phenylene group. PDI-Ph showed the highest electron OFET~0.04 cm^2/Vs whereas FETs fabricated with PDI-BT had OFET~0.032 cm^2/Vs after annealing at 150 °C. Annealing increases the OFET by several orders, which are the high enhancement values for PDI based copolymers (Table 2.5). The observed enhancement of μ_{FET} is consistent with the occurrence of crystallites with annealing in the microscopic images and a crystalline transition temperature in DSC. In addition, XRD measurements on these thin films also indicate a decrease in d-spacing and π-π stacking distance with annealing for both the polymers. Specifically, it was also observed that with annealing the decrease in d-spacing and π-π stacking distance is higher for benzothiadiazole based molecules compared to phenylene substituted copolymers which corroborates with a larger change in the μ_{FET}.

TH-1703_11612241

The presence of linear alkyl chains in PDI-Ph and PDI-BT polymer improves the polymer packing and the π-π stacking indicating better lamellar structure and closely packed inter-digitated structure. These molecules have a higher propensity to form ordered crystallites and interconnected aggregates which support enhanced transport as observed for other high mobility polymers reported recently.[39] Another interesting observation in the transport measurement is the enhanced performance of the D-A type PDI-Ph molecules compared to A-A type PDI-BT molecule. This indicates the apparent importance of the intermolecular D-A type interaction on the charge transport compared to the geometry and microstructure of the molecule which can be a general way to achieve high mobility in PDI polymeric materials.

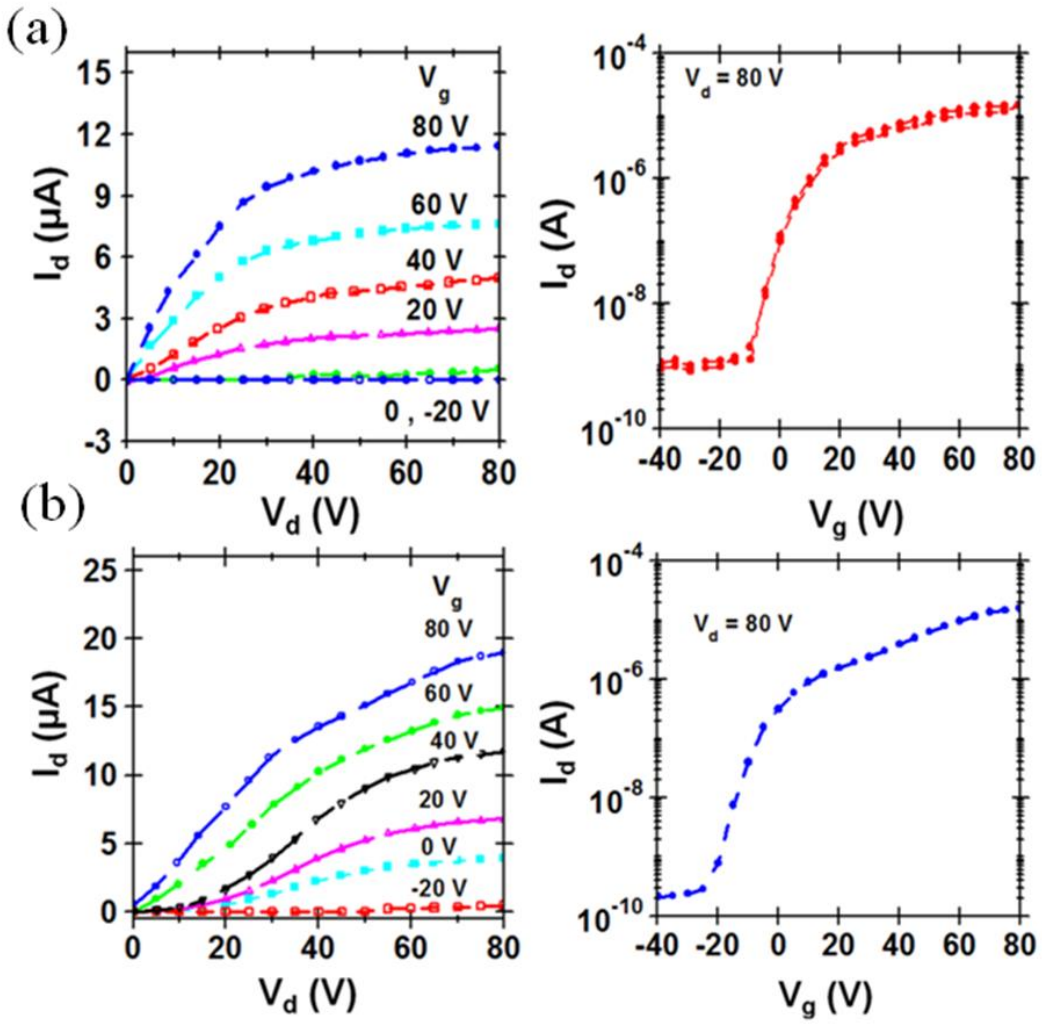

Figure 2.9. Typical output and transconductance characteristics for OFETs fabricated with (a) PDI-Ph (b) PDI-BT active layer and BCB as the dielectric (C_i ~ 4 nF/cm^2). Typical device dimensions are W ≈ 1 mm and L ≈ 60-100 μm

TH-1703_11612241

Table 2.5. Performance parameters of OFETs obtained under different annealing conditions

Polymers	Annealing temperature (°C)	Average μ_{FET} (cm^2/Vs)	Maximum μ_{FET} (cm^2/Vs)	I_{on}/I_{off}
PDI-Ph	as spun	0.005	0.04	$> 10^4$
	110	0.008		
	150	0.015		
PDI-BT	as spun	0.001	0.032	$> 10^4$
	110	0.004		
	150	0.01		

2.4. Conclusions

In summary, these solution processable n-type copolymers having PDI backbone were synthesized in high yields (83, 86%) by palladium catalyzed Suzuki coupling reactions and their excellent solubility in several organic solvents allowed their deposition in organic thin film transistor (OTFT) devices directly from solution. We demonstrated the importance of the correlation between the conjugated backbone macro structure and anisotropy behavior in spin-coated aligned thin films of perylene diimide copolymers. The thin film structures and electronic anisotropic properties in conjugated copolymers can be regulated, which resulted in efficient intermolecular interactions and the formation of crystalline domains over large area after annealing, thereby facilitating large enhancement in charge carrier transport. The optical, thermal and redox characterization of the copolymers indicate good polymeric aggregates, high thermal stability with tendency to form crystalline domains and suitable energetic which support efficient electron injection. This was further supported by the morphology patterns observed in the AFM, FESEM and POM images. The transport studies performed under different annealing conditions up to 150°C demonstrated huge enhancement in electron μFET with maximum values of 0.04 cm^2/Vs for the PDI-Ph and 0.032 cm^2/Vs for the PDI-BT polymers. The extended conjugation and efficient intermolecular interactions observed in thin films, especially in PDI copolymers along with the formation of crystalline domains as also confirmed by DSC analysis after annealing are collectively responsible for the

TH-1703_11612241

enhanced device characteristics. This study conclusively illustrates that D-A copolymers display better properties compared to A-A copolymers and demonstrates a route to develop high-performing, solution processable copolymers.

2.5. References

1. Cheng, C. H. W.; Lonergan, M. C. *J. Am. Chem. Soc.* **2004,** *126* (34), 10536-10537.
2. Robinson, S. G.; Lonergan, M. C. *J. Phys. Chem. C.* **2013,** *117* (4), 1600-1610.
3. Zhou, E. J.; Cong, J. Z.; Zhao, M. X.; Zhang, L. Z.; Hashimoto, K.; Tajima, K. *Chem. Commun.* **2012,** *48* (43), 5283-5285.
4. Zhang, Q. L.; Cirpan, A.; Russell, T. P.; Emrick, T. *Macromolecules* **2009,** *42* (4), 1079-1082.
5. Baeg, K. J.; Kim, J.; Khim, D.; Caironi, M.; Kim, D. Y.; You, I. K.; Quinn, J. R.; Facchetti, A.; Noh, Y. Y. *Acs. Appl. Mater. Inter.* **2011,** *3* (8), 3205-3214.
6. Fron, E.; Deres, A.; Rocha, S.; Zhou, G.; Mullen, K.; De Schryver, F. C.; Sliwa, M.; Uji-i, H.; Hofkens, J.; Vosch, T. *J. Phys. Chem. B.* **2010,** *114* (3), 1277-1286.
7. Strukelj, M.; Jordan, R. H.; Dodabalapur, A. *J. Am. Chem. Soc.* **1996,** *118* (5), 1213-1214.
8. Suraru, S. L.; Zschieschang, U.; Klauk, H.; Wurthner, F. *Chem. Commun.* **2011,** *47* (6), 1767-1769.
9. Lin, Y. Z.; Fan, H. J.; Li, Y. F.; Zhan, X. W. *Adv. Mater.* **2012,** *24* (23), 3087-3106.
10. Ben-Sasson, A. J.; Chen, Z. H.; Facchetti, A.; Tessler, N. *Appl. Phys. Lett.* **2012,** *100* (26), 263306.
11. Li, C. H.; Huang, C. H.; Kuo, M. Y. *Phys. Chem. Chem. Phys.* **2011,** *13* (23), 11148-11155.
12. Letizia, J. A.; Salata, M. R.; Tribout, C. M.; Facchetti, A.; Ratner, M. A.; Marks, T. J. *J. Am. Chem. Soc.* **2008,** *130* (30), 9679-9694.
13. Anthony, J. E.; Facchetti, A.; Heeney, M.; Marder, S. R.; Zhan, X. W. *Adv. Mater.* **2010,** *22* (34), 3876-3892.
14. Alvey, P. M.; Ono, R. J.; Bielawski, C. W.; Iverson, B. L. *Macromolecules* **2013,** *46* (3), 718-726.
15. Yuan, M. J.; Durban, M. M.; Kazarinoff, P. D.; Zeigler, D. F.; Rice, A. H.; Segawa, Y.; Luscombe, C. K. *J. Polym. Sci. Pol. Chem.* **2013,** *51* (19), 4061-4069.
16. De Witte, P. A. J.; Hernando, J.; Neuteboom, E. E.; van Dijk, E. M. H. P.; Meskers, S. C. J.; Janssen, R. A. J.; van Hulst, N. F.; Nolte, R. J. M.; Garcia-Parajo, M. F.; Rowan, A. E. *J. Phys. Chem. B.* **2006,** *110* (15), 7803-7812.
17. Neuteboom, E. E.; Meskers, S. C. J.; van Hal, P. A.; van Duren, J. K. J.; Meijer, E. W.; Janssen, R. A. J.; Dupin, H.; Pourtois, G.; Cornil, J.; Lazzaroni, R.; Bredas, J. L.; Beljonne, D. *J. Am. Chem. Soc.* **2003,** *125* (28), 8625-8638.
18. Kola, S.; Kim, J. H.; Ireland, R.; Yeh, M. L.; Smith, K.; Guo, W. M.; Katz, H. E. *ACS. Macro. Lett.* **2013,** *2* (8), 664-669.
19. Zheng, Q. D.; Huang, J.; Sarjeant, A.; Katz, H. E. *J. Am. Chem. Soc.* **2008,** *130* (44), 14410-14411.

TH-1703_11612241

20. Zhan, X. W.; Facchetti, A.; Barlow, S.; Marks, T. J.; Ratner, M. A.; Wasielewski, M. R.; Marder, S. R. *Adv. Mater.* **2011,** *23* (2), 268-284.
21. Herrmann, A.; Mullen, K. *Chem. Lett.* **2006,** *35* (9), 978-985.
22. Li, C.; Wonneberger, H. *Adv. Mater.* **2012,** *24* (5), 613-636.
23. Langhals, H. *Heterocycles* **1995,** *40* (1), 477-500.
24. Choi, D.; Jeong, B. S.; Ahn, B.; Chung, D. S.; Lim, K.; Kim, S. H.; Park, S. U.; Ree, M.; Ko, J.; Park, C. E. *ACS. Appl. Mater. Inter.* **2012,** *4* (2), 702-706.
25. Yan, Q. F.; Zhao, D. H. *Org. Lett.* **2009,** *11* (15), 3426-3429.
26. Yuan, Z. Y.; Xiao, Y.; Yang, Y.; Xiong, T. *Macromolecules* **2011,** *44* (7), 1788-1791.
27. Hu, X. L.; Zuo, L. J.; Pan, H. B.; Hao, F.; Pan, J. Y.; Fu, L.; Shi, M. M.; Chen, H. Z. *Sol. Energ. Mat. Sol. C.* **2012,** *103*, 157-163.
28. Chen, Z. H.; Zheng, Y.; Yan, H.; Facchetti, A. *J. Am. Chem. Soc.* **2009,** *131* (1), 8-9.
29. Zhan, X. W.; Tan, Z. A.; Domercq, B.; An, Z. S.; Zhang, X.; Barlow, S.; Li, Y. F.; Zhu, D. B.; Kippelen, B.; Marder, S. R. *J. Am. Chem. Soc.* **2007,** *129* (23), 7246-7247.
30. Zhou, W. Y.; Wen, Y. G.; Ma, L. C.; Liu, Y. Q.; Zhan, X. W. *Macromolecules* **2012,** *45* (10), 4115-4121.
31. Zhang, S. M.; Wen, Y. G.; Zhou, W. Y.; Guo, Y. L.; Ma, L. C.; Zhao, X. G.; Zhao, Z.; Barlow, S.; Marder, S. R.; Liu, Y. Q.; Zhan, X. W. *J. Polym. Sci. Pol. Chem.* **2013,** *51* (7), 1550-1558.
32. Yan, H.; Chen, Z. H.; Zheng, Y.; Newman, C.; Quinn, J. R.; Dotz, F.; Kastler, M.; Facchetti, A. *Nature* **2009,** *457* (7230), 679-687.
33. Zhao, X. G.; Ma, L. C.; Zhang, L.; Wen, Y. G.; Chen, J. M.; Shuai, Z. G.; Liu, Y. Q.; Zhan, X. W. *Macromolecules* **2013,** *46* (6), 2152-2158.
34. Kim, B. G.; Jeong, E. J.; Chung, J. W.; Seo, S.; Koo, B.; Kim, J. S. *Nat. Mater.* **2013,** *12* (7), 659-664.
35. Kolhe, N. B.; Asha, S. K.; Senanayak, S. P.; Narayan, K. S. *J. Phys. Chem. B.* **2010,** *114* (50), 16694-16704.
36. Balakrishnan, K.; Datar, A.; Oitker, R.; Chen, H.; Zuo, J. M.; Zang, L. *J. Am. Chem. Soc.* **2005,** *127* (30), 10496-10497.
37. Noriega, R.; Rivnay, J.; Vandewal, K.; Koch, F. P. V.; Stingelin, N.; Smith, P.; Toney, M. F.; Salleo, A. *Nat. Mater.* **2013,** *12* (11), 1037-1043.
38. Pati, P. B.; Senanayak, S. P.; Narayan, K. S.; Zade, S. S. *ACS. Appl. Mater. Inter.* **2013,** *5* (23), 12460-12468.
39. Li, J.; Zhao, Y.; Tan, H. S.; Guo, Y. L.; Di, C. A.; Yu, G.; Liu, Y. Q.; Lin, M.; Lim, S. H.; Zhou, Y. H.; Su, H. B.; Ong, B. S. *Sci. Rep.* **2012,** *2*, 1-9.

TH-1703_11612241

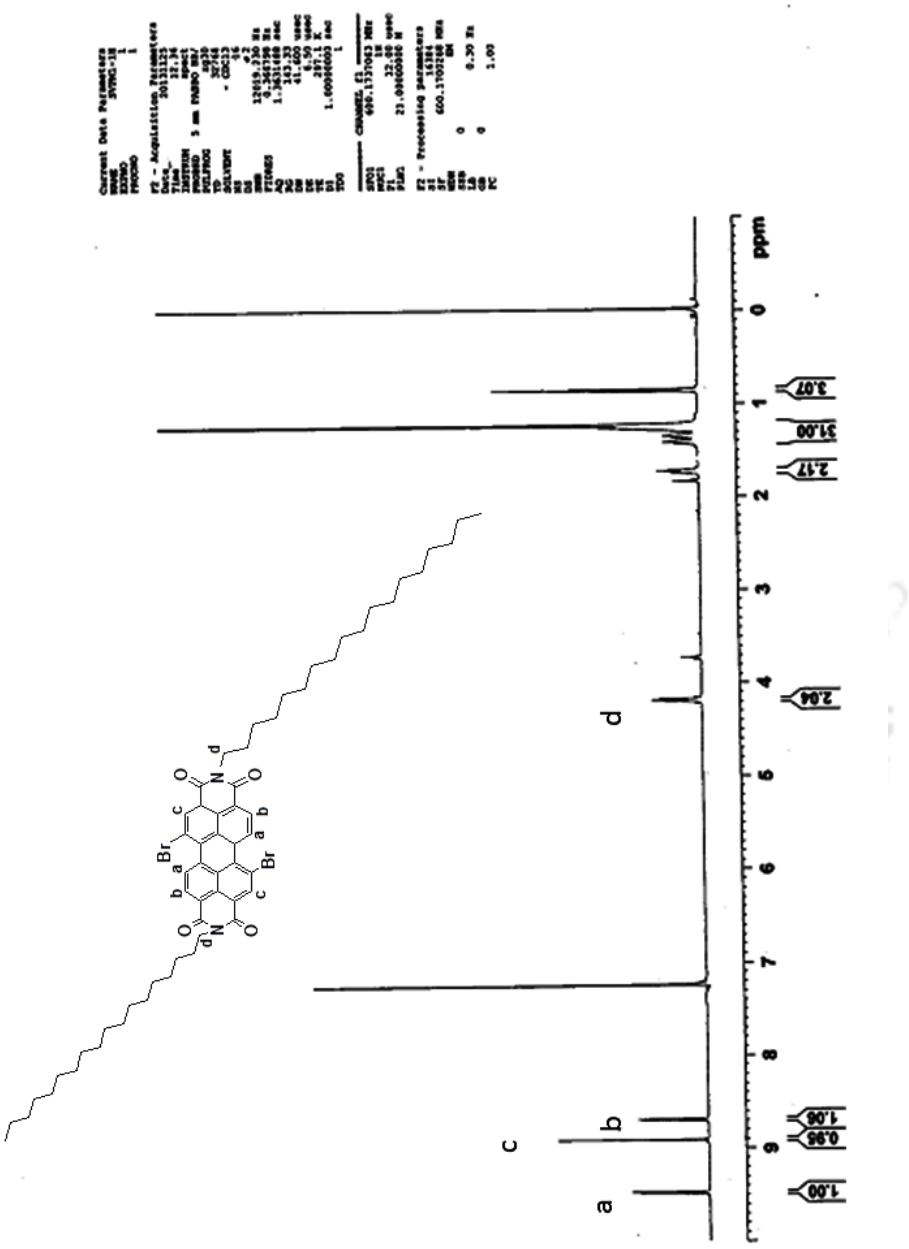

Figure 2.10. ^{1}H NMR Spectrum of Br_2-PDIOD ($CDCl_3$, 600MHz)

TH-1703_11612241

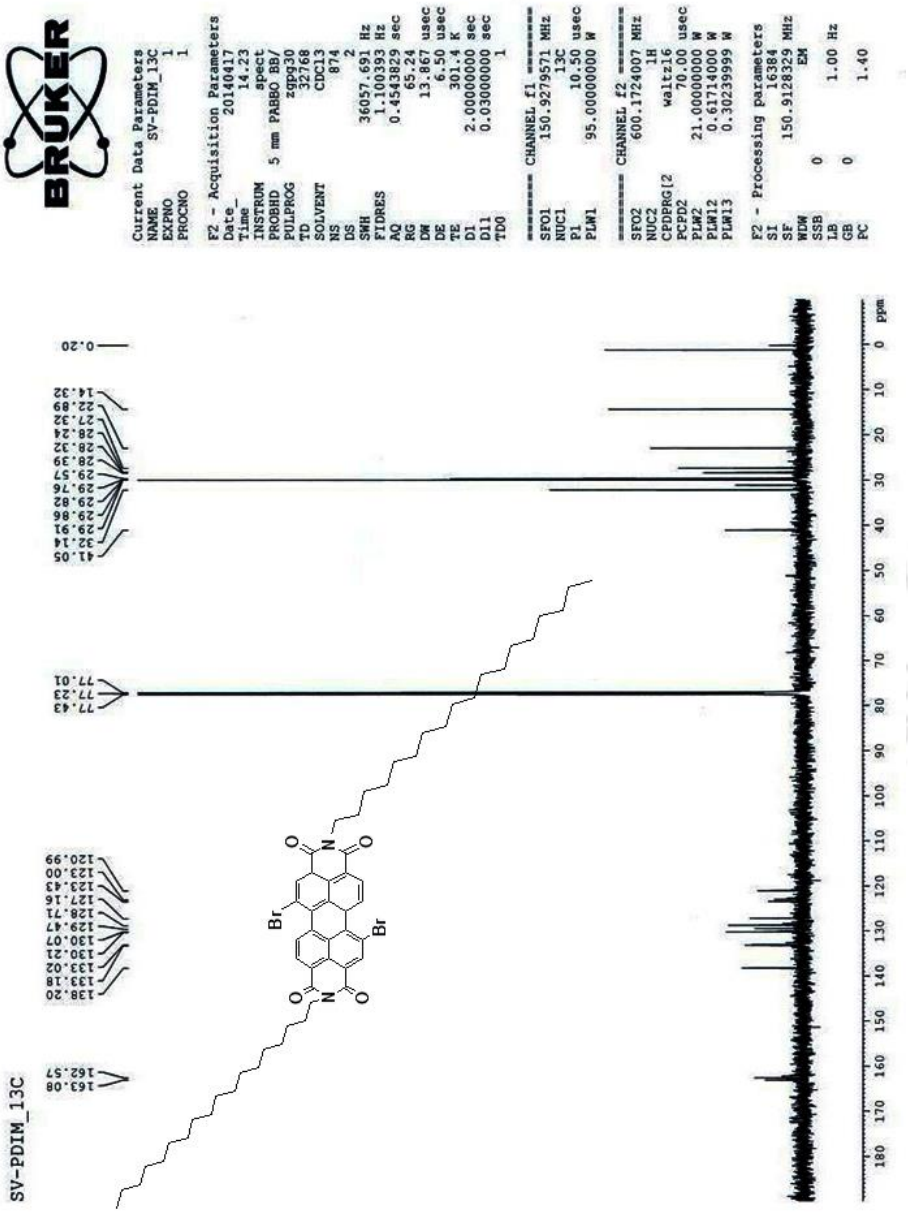

Figure 2.11. ^{13}C NMR Spectrum of Br_2-PDIOD ($CDCl_3$, 600MHz)

TH-1703_11612241

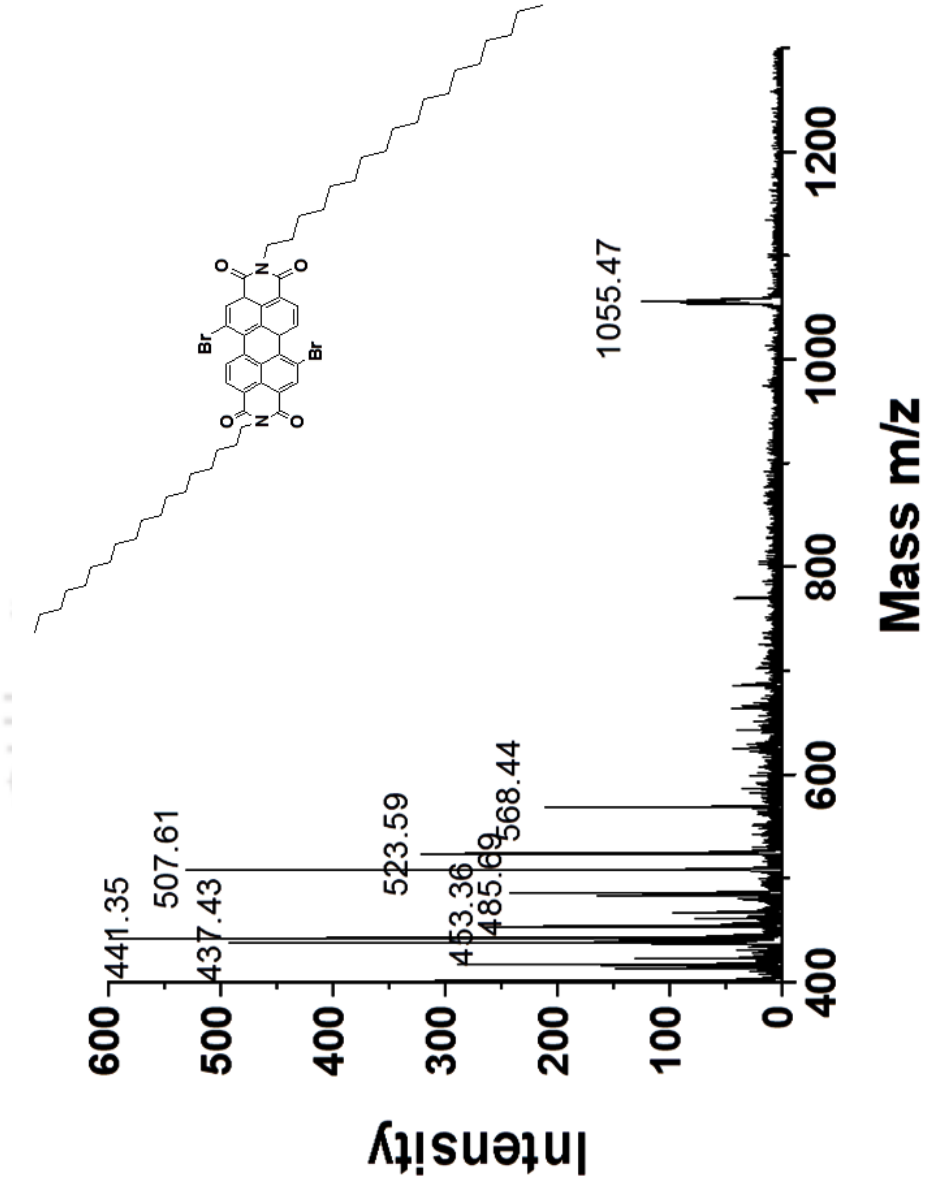

Figure 2.12. MALDI-TOF Spectrum of Br_2-PDIOD

TH-1703_11612241

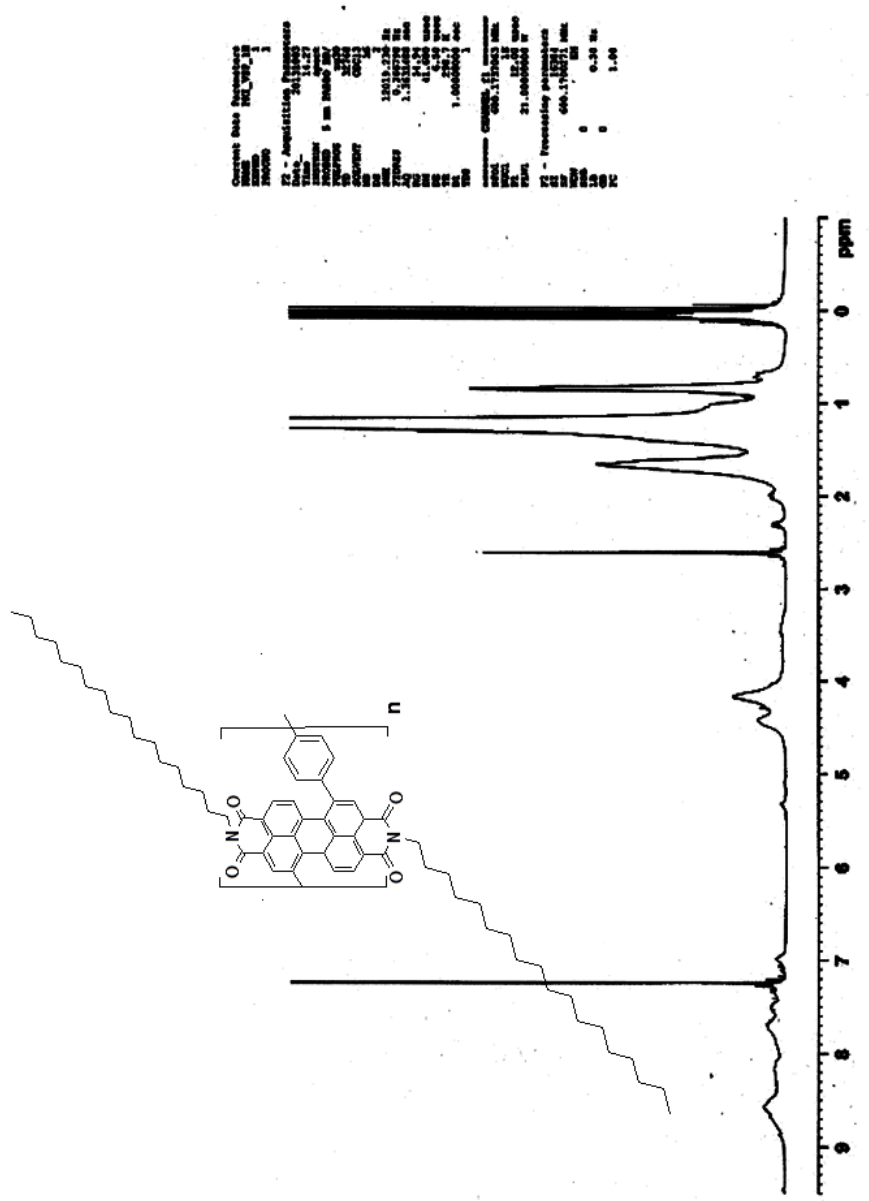

Figure 2.13. ^{1}H NMR Spectrum of PDI-Ph polymer ($CDCl_3$, 600MHz)

TH-1703_11612241

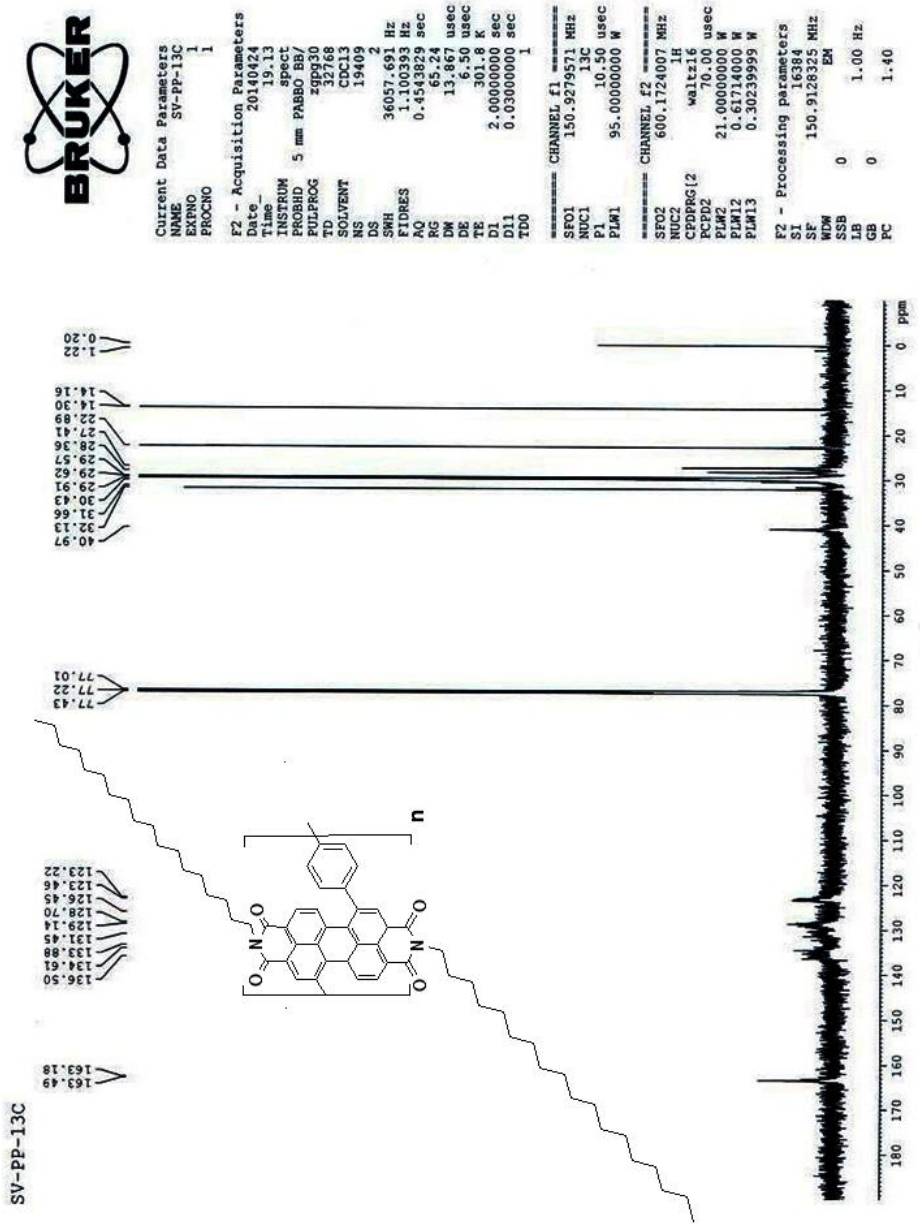

Figure 2.14. ^{13}C NMR Spectrum of PDI-Ph ($CDCl_3$, 600MHz)

TH-1703_11612241

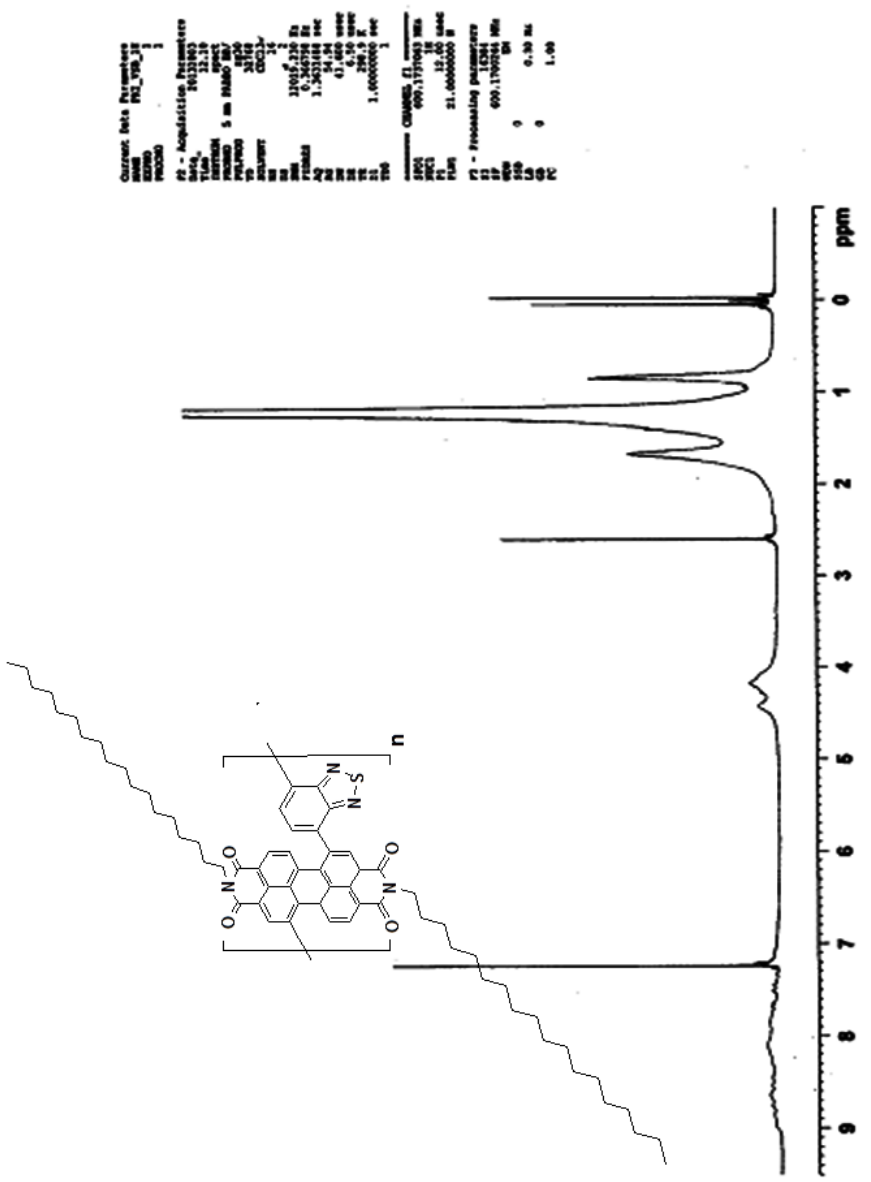

Figure 2.15. ^{1}H NMR Spectrum of PDI-BT polymer ($CDCl_3$, 600MHz)

TH-1703_11612241

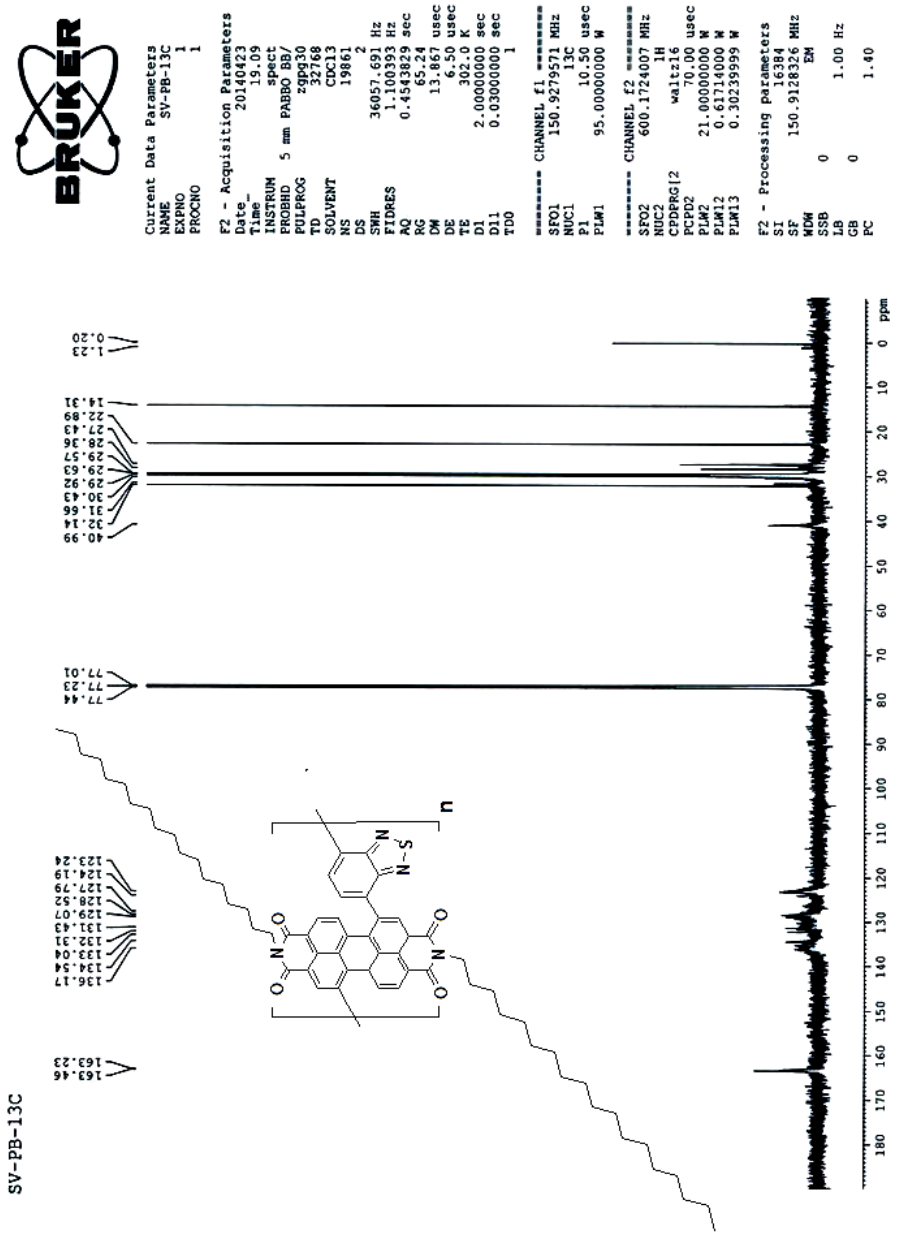

Figure 2.16. ^{13}C NMR Spectrum of PDI-BT ($CDCl_3$, 600MHz)

TH-1703_11612241

Chapter 3

Synthesis of Naphthalenediimide based polymers and fabrication of Organic Field-Effect transistors

3.1. Introduction

Polymer field effect transistors (PFETs) have attracted significant interest during the past few decades because they have been widely used in the fabrication of low cost organic optoelectronic devices such as p-n junctions,[1,2] photovoltaic cells,[3,4] complementary circuits[5] and driving organic light emitting diodes (OLED) for flexible display.[6,7] All these applications require both hole transporting (p-type) and electron transporting (n-type) materials with suitable physical, chemical, electrical and photochemical properties. The n-type materials development has lagged behind the p-type materials because of their low stability, scarcity of suitable molecules over the years and hence majority studies reported so far have focused on p-type semiconductor materials and devices.[8,9] In past years, some reports on the development of ambipolar[10,11]and n-type semiconductors with encouraging performances have reported.[12,13]

There are numerous building blocks being developed to fabricate air stable n-channel semiconducting materials, while rylene based polymers, especially naphthalene,[14,15] perylene,[16,17] pyromellitic tetracarboxylic diimides[18,19] are the most promising. Among aromatic molecules that have found utility, particularly in the design of conducting materials, the 1,4,5,8-naphthalenediimides (NDIs) (also known as naphthalene carbodiimides) have attracted much attention due to their tendency to form n-type over p-type semiconductor materials.[20] The naphthalenediimides are a compact, electron deficient class of aromatic compounds capable of self-organisation[21] and being incorporated into larger multicomponent assemblies through intercalation.[22] Functionalization through the diimide nitrogens or via core substitution (substitution on the naphthalene core) produces analogues whose absorption and emission properties are

TH-1703_11612241

variable.[23] Core substituted NDIs (cNDIs) are rapidly emerging as a class of their own in an attractive strategy to create highly colorful, conducting, functional materials with much different photophysical properties than their core unsubstituted counterparts.[23] It is with this versatility in properties that naphthalene diimides have found popularity in the latter half of the 20th century and due, in part, to the pioneering work of Vollmann et al. in the early 1930s.[24] Naphthalene diimides can act as ideal components for the creation of supramolecular functional materials (e.g. catenanes, rotaxanes and barrels)[25] as a result of their desirable electronic and spectroscopic properties over pyromellitic diimides and show better fabrication properties than the perylene diimide dyes, the latter being a result of their enhanced solubility properties.

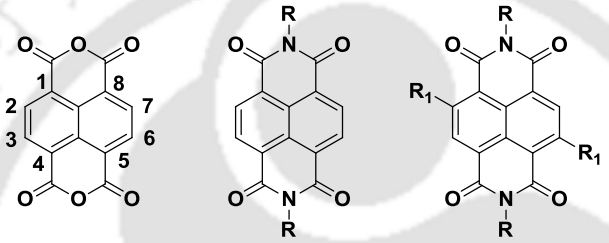

Figure 3.1. Naphthalene dianhydride and Naphthalene diimides

Naphthalene (NDI) possesses aromatic planar conjugated structure and is favorable for good charge transport with performances comparable to p-type semiconducting materials. These classes of materials have excellent combination of thermal, optical, redox and electrical properties as well as very high moisture and oxygen resistance.[26] The functionalization at the diimide position with aliphatic alkyl chain, either branched or long chain provides good solubility in common organic solvents enhancing their processability.[27] Additionally, the possibility to obtain inter-digitated structures limits the percolation of moisture to the conjugated core, thereby, making it stable for ambient performance.[28] Many NDI based small molecules[29,30] and oligomers[31,32] have been reported with self-assembling properties and good charge transporting ability. Few newly developed materials showing high electron mobility include: ladder type naphthalene[33] and D-A type copolymers of NDI with thiophene,[34,35] bithiophene[36] dithienothiophene,[37] phenothiazine,[38] dithienopyrrole[39] and phenylene.[40] High electron mobility of up to 0.45-0.85 cm^2/Vs was reported with NDI derivative and bithiophene copolymers.[5] A NDI-vinylene-thiophene copolymers which exhibited mobilities of up to 1.8 cm^2/Vs were reported.[14] For the electronics industries that rely on organic materials, development of

TH-1703_11612241

low-cost solution processable n-type semiconducting materials with high performance remains a challenge. One of the major drawbacks with n-type materials is their instability at ambient conditions. In this regard, n-type PFETs with electron mobilities ~1 cm^2/Vs which are relatively stable under ambient conditions and that can be aligned to improve the transport properties by several orders were demonstrated here.

Apart from these efforts it remains unclear why D-A based NDI copolymers have shown better OFET properties. In addition, the role of anisotropic properties and improving the structural order in solution-processed n-type polymers and the enhanced film morphology on macroscopic scale is also very essential for obtaining high-performance OFETs. In this chapter two thiophene-free copolymers based on phenylene and benzothiadiazole as copolymerizing units with linear C18 substituted NDI derivatives are developed in order to gain a relatively higher understanding on the roles and features of different D-A and A-A structures and the transport behavior in these polymers are carefully studied. It was also demonstrated that enhancing the polymer anisotropic properties by annealing at appropriate temperature significantly improves the intermolecular interactions as well as the formation of crystalline domains on macroscopic scale facilitating large enhancement in charge carrier transport. Since conjugated polymers inherently possess anisotropic characteristics, they can be realized in device applications only when these conjugated chains are aligned in such a manner that the crystallites do not remain entrenched within the amorphous polymer phases. Tuning the thin film structures of the polymers by annealing facilitates the conjugated chains alignment over larger macro domains and enhances the structure-property relationships by demonstrating highly improved charged transport behavior here. Hence, developing processing strategies in these materials to overcome the amorphous domains and recognizing the importance of conjugated backbone macrostructure chain alignment are, in principle, extremely crucial for device improvements.

3.2. Experimental Section

3.2.1. Materials and Instruments

Naphthalene tetracarboxylic dianhydride, 1,4-benzene diboronic acid, 2,1,3-Benzothiadiazole-4,7-bis(boronic acid pinacol ester), were purchased from Sigma Aldrich and were used without further purification. The dielectric material hydroxyl free

TH-1703_11612241

divinyltetramethylsiloxanebis-benzocyclobutene (BCB) is obtained from Dow Chemicals. 2-6-dibromo naphthalene tetracarboxylic dianhydride (NTCDA-Br_2) and N,N'-bis(octadecyl)-2,6-dibromo naphthalene-1,4,5,8-tetracarboxylic dianhydride were synthesized following the published literature procedure (Scheme 1).[31] Both the polymers NDI-Ph and NDI-BT were synthesized by Suzuki coupling reaction. ^{1}HNMR, ^{13}CNMR were recorded on Varian AS 400MHz and Bruker 600MHz NMR spectrometers. MALDI-TOF-MS experiments were done on AB SCIEX, USA instrument with a 4800 plus MALDI TOF/TOF Analyzer. Elemental analysis was done on CHNS Analyzer, Perkin Elmer, 2400 (USA). UV-vis spectra were recorded on a Perkin-Elmer Model Lambda-25 spectrophotometer. Photoluminescence spectra were recorded on Varian Cary Eclipse spectrophotometer. Electrochemical measurements were carried out under argon on a deoxygenated solution of tetra n-butyl ammonium perchlorate (0.1 M) in Acetonitrile using a CH instruments Model 700D series Electrochemical workstation. A glassy carbon as working electrode, platinum wire as counter electrode, Ag/Ag^{+} as reference electrodes were used. Thermo gravimetric analysis (TGA) was performed on METTLER TOLEDO, Model TG/SDTA 851 e Thermo Gravimetric analyzer under a nitrogen flow at a heating rate of 10°C/min. Differential scanning calorimeter were done on METTLER TOLEDO, Model DSC 1, Stare system. The gel permeation chromatography measurements were performed on a waters 515 chromatograph connected to waters 2414 refractive index detector using THF as eluent and polystyrene standards as calibrants. AFM images were taken by Agilent 5500-STM instrument and FESEM images were recorded in a Sigma Carl ZEISS scanning electron microscope. XRD analyses were done by Bruker D8 Discover Diffractometer. Leica polarizable optical microscope was used to study the anisotropic morphology of the copolymer films.

3.2.2. Preparation of films for AFM, FESEM, XRD and POM

The copolymers were spin coated on glass substrates at 500rpm for two minutes and then heated for 30 min at 50°C to evaporate the solvent. The films were prepared under the same conditions to record the FESEM images. Similarly, AFM images of the films were recorded for as spun and annealed films and for XRD measurement also the films were prepared under the same conditions as followed for the device fabrication. For POM studies, the copolymers were dissolved in chloroform and drop casted on glass slide, heated for 2h at 50 °C to remove residual solvent. During the POM annealing

TH-1703_11612241

experiments the films were heated from 50-180 °C at a rate of 5 °C/min and then cooled to 50 °C at the same rate and the images were recorded at 50X resolution.

3.2.3. Synthesis of Monomers and Polymers

The syntheses of two new conjugated copolymers were achieved in 84, 85% yields (Scheme 3.1). The synthesis details of the monomers and copolymers are explained in detail in subsequent sections. The Suzuki coupling reaction of dibrominated NDI derivatives with benzene-1,4-diboronic acid and 2,1,3-benzothiadiazole bisboronic ester resulted in the formation of NDI-Ph and NDI-BT copolymers.

(a) Synthesis of Br_2-NDIOD: A mixture of NTCDA-Br_2 (0.4 g, 0.93 mmol) (Precaution: The dibromination of NTCDA by dibromoisocyanuric acid has to be carried out in presence of concentrated H_2SO_4 or Oleum and must be handled with great care), 2-octyldodecylamine (0.629 g, 2.33 mmol), o-xylene (3 mL), and propionic acid (1 mL) were stirred at 140 °C for 6 h. Upon cooling to room temperature, most of solvents were removed in vacuo and the residue was purified by column chromatography on silica gel with a mixture of chloroform : hexane (1:2, v/v) as eluent, affording the slightly yellowish red color solid as product (0.61 g, yield 70%). ^{1}HNMR (600 MHz, $CDCl_3$, δ ppm): 8.75 (s, 2H), 4.18 (t, 4H), 1.73 (m, 4H), 1.25-1.15 (m, 60H), 0.87 (t, 6H); ^{13}C NMR ($CDCl_3$, 150MHz, δ ppm): 163.07, 139.28, 128.87, 128.54, 127.97, 125.60, 124.35, 41.85-14.32 (Aliphatic Carbons). MALDI-TOF: m/z calcd. 928.41, found. $[M+2H]^+$: 930.11; Elemental Analysis Calcd. C, 64.65; H, 8.25; N, 3.02; found, C, 64.16; H, 8.255; N, 1.46;

(b) Synthesis of NDI-Ph: To a three neck round bottom flask Br_2-NDIOD (0.1 g, 0.107 mmol), benzene-1,4-diboronic acid (0.0177 g, 0.107 mmol), were added and degassed thrice by freeze thaw cycles. Aqueous solution of K_2CO_3 (0.147 g, 1.07 mmol) in 2 mL deoxygenated water were added under nitrogen. $Pd(PPh_3)_4$(0.006 g, 0.004 mmol), two drops of aliquat and 6 mL THF were added under nitrogen atmosphere, degassed thrice by freeze thaw cycles (15 minutes each). The dark red solution was stirred at 80 °C for 36 h. Phenyl boronic acid was added under nitrogen and the reaction was continued for other 12 h. The brown sticky mixture was cooled to room temperature. The mixture was extracted with $CHCl_3$, washed with 100 mL water thrice and dried over anh. $MgSO_4$. The solution was concentrated to 5 mL and dropped in 50 mL methanol. The brown color precipitate was filtered and washed with methanol twice (0.076 g, Yield

TH-1703_11612241

84 %). ^{1}HNMR (400MHz, $CDCl_3$, δ ppm): 8.5-8.8 (br, m, 2H), 7.4-7.8 (br, m, 4H), 4.0 (br, m, 4H), 1.67 (br, m, 4H), 1.2 (br, m, 60H), 0.87 (br, m, 6H); 13C NMR (CDCl3, 150MHz, δ ppm): 163.06, 135.66, 132.00, 131.10, 128.76, 125.07, 124.68, 124.19, 41.14-14.32 (Aliphatic Carbons); GPC: M_n: 6811; M_w: 13579; PDI: 1.99.

(c) Synthesis of NDI-BT: To a three neck round bottom flask Br_2-NDIOD (0.1 g, 0.107 mmol), 2,1,3-benzothiadiazole bis boronic ester (0.0415 g, 0.107 mmol), were added and degassed thrice by freeze thaw cycles. Aqueous solution of K_2CO_3 (0.147 g, 1.07 mmol) in 2 mL deoxygenated water were added under nitrogen. $Pd(PPh_3)_4$(0.006 g, 0.004 mmol), two drops of aliquat and 6 mL THF were added under nitrogen atmosphere, degassed twice by freeze thaw cycles. The dark red solution was stirred at 80°C for 36h. Phenyl boronic acid was added under nitrogen and the reaction was continued for other 12h. The brown sticky mixture was cooled to room temperature. The mixture was extracted with $CHCl_3$, washed with 100 mL water thrice and dried over anh. $MgSO_4$. The solution was concentrated to 5 mL and added drop by drop in 50 mL methanol .The brown color precipitate was filtered and washed with methanol twice (0.082 g, Yield 85%) ^{1}HNMR (400MHz, $CDCl_3$, δ ppm): 8.85 (br, m, 2H), 7.6 (br, m, 2H), 4.15 (br, m, 4H), 1.7 (br, m, 4H), 1.2 (br, m, 60H), 0.85 (br, m, 6H); ^{13}C NMR ($CDCl_3$, 150MHz, δ ppm): 163.07, 135.42, 132.18, 131.10, 129.98, 129.06, 124.68, 124.19, 41.14-14.33 (Aliphatic Carbons); GPC: M_n: 5171; M_w: 6627; PDI: 1.74.

3.2.4. Device fabrication and characterization

Detailed transport study of the NDI copolymers were performed using bottom gate top contact FET geometry. For device fabrication, Al metal is coated as the gate electrode by physical vapor deposition (10^{-6} mbar, 40 nm thick) on RCA cleaned glass substrate. Dielectric layer hydroxyl free divinyltetramethylsiloxane bis-benzocyclobutene (BCB) is then coated at 1000 rpm for 1 min and annealed in N2 filled glove box atmosphere at 290 °C. The resultant dielectric layer had a Ci ~4 nF/cm^2 measured directly using the C-V meter inbuilt in Keithley 4200 semiconductor parameter analyzer. Typical dielectric thickness is estimated to be around 0.5 - 0.6 µm as measured using Filmetrics (F20-EXR) thickness measurement set up. The surface of the dielectric was coated (1500 rpm for 30 s) with a thin monolayer of hexamethyldisilazane (HMDS) and annealed at 110 °C for 2 h. Copolymer layer is then introduced from solution phase (15 mg/mL in THF) by spin coating at 1000 rpm for 1 minute and annealed at different temperatures 110 °C – 150 °C

TH-1703_11612241

for 30 min to optimize the performance. In order to facilitate electron injection, Al source-drain electrodes were then coated (10^{-6} mbar, 40 nm thick) to complete the device fabrication. An injection limited response with lower OFET for Au S-D electrodes was observed. The device characterizations were performed using standard Keithley 4200 Semiconductor characterization systems and cross-checked with measurement using Keithley 2400 Source meters and High-impedance Keithley 6514 Electrometer. Typical FET performance is estimated from average characteristics of five to seven devices.

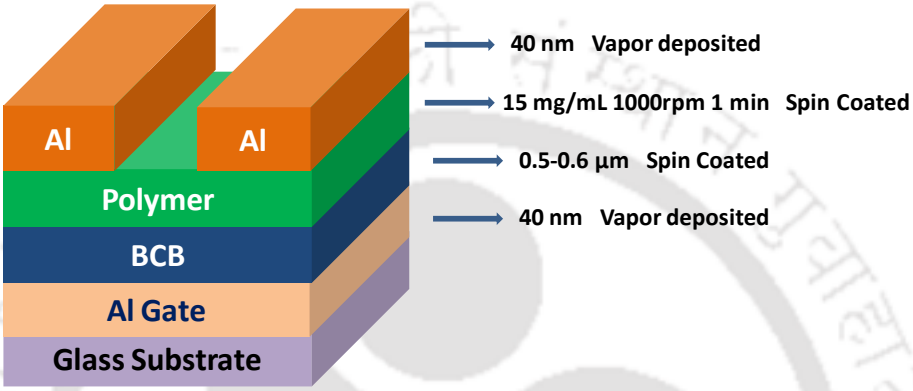

3.3. Results and discussion

3.3.1. Characterizations

All the monomers and polymers were well characterized by NMR, (Figure 3.10-3.11, 3.13-3.16), MALDI (Figure 3.12)/gel permeation chromatography (GPC), elemental analysis, DSC, TGA, PL, UV-Vis and cyclic voltammetry and their morphology studied by AFM, FESEM, POM (Figures 3.6, 3.7, 3.8) and XRD (Figures 3.4, 3.5) techniques. The TGA analysis reveals that the copolymers are stable up to 350 °C. These polymers were fabricated and tested for solution processible polymer field effect transistors (PFETs). It was observed that these NDI derivatives exhibit field effect electron mobilities (OFET) that are as high as 0.8 cm^2/Vs (NDI-Ph) and 0.2 cm^2/Vs (NDI-BT) with a current modulation in the range of 10^4-10^5. High OFET can be attributed to the enhanced π-π stacking originating from the intermolecular overlap of the D-A orbitals. Table 3.2 represents their molecular weight and poly dispersity index (*PDI*) as obtained from GPC in THF (Polystyrene standard). Due to the presence of alkyl chains all the four copolymers were readily soluble in common organic solvents such as toluene, THF, chloroform, dichloromethane, chlorobenzene, xylenes and could be solution processed onto desired substrates for achieving smooth films.

TH-1703_11612241

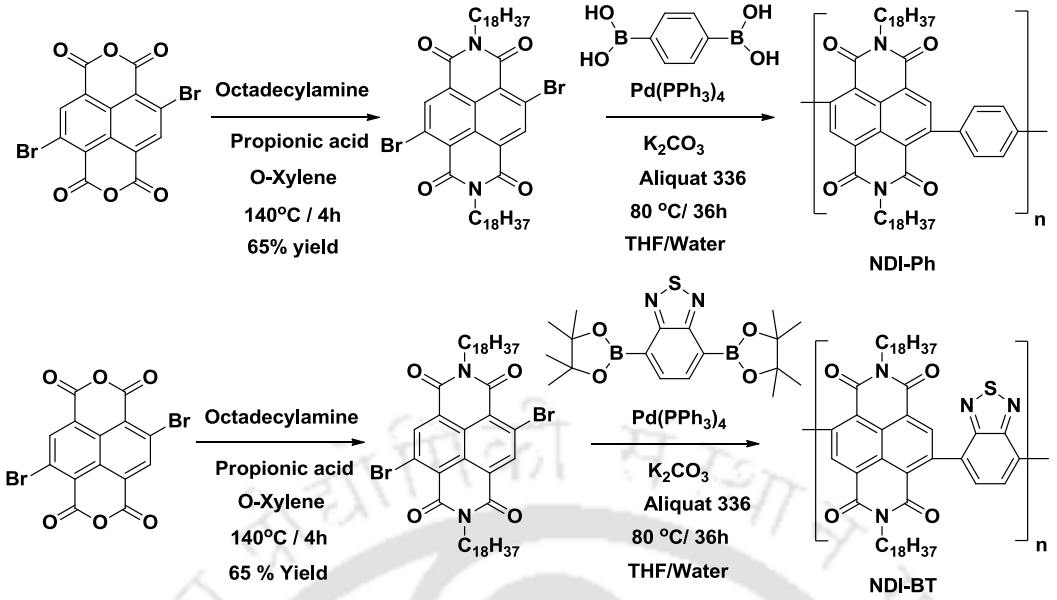

Scheme 3.1. Synthesis of monomers and copolymers

3.3.2. Photophysical Properties

To understand the aggregation mechanism the UV-visible spectra of the copolymers were studied in THF at a concentration of 10^{-5} M. NDI-BT showed absorption peaks at 360 nm, 371 nm and 449 nm, which are assigned to basic naphthalene diimide core transitions while the peak at 538 nm is due to general polymer aggregation. Another peak observed at 438 nm is generally observed for the benzothiadiazole moiety. NDI-Ph shows peaks at 360 nm, 370 nm which are assigned to the basic naphthalene core transitions and a peak of polymer aggregation at 540 nm (Figure 3.2(a)). The absorption spectra of the spin coated polymer films on glass (Figure 3.2(b)) showed red shift in the peaks for all the copolymers as compared to the solution state absorption peaks. For NDI-BT copolymer the 538 nm peak was significantly red shifted to around 625 nm with similar red shift of up to 371 nm, 391 nm and 449 nm from the initial positions of 360 nm, 371 nm and 438 nm respectively. Similarly, the 540 nm peak of the NDI-Ph copolymer was shifted to 600 nm caused by the strong polymer inter-chain interaction. The other peaks observed at 360 nm, 370 nm for NDI-Ph are also shifted to 370 nm, 390 nm in thin films as compared to the solution spectra. The optical band gaps calculated from the absorption edge for NDI-Ph, NDI-BT were found to be 1.55 eV, 1.72 eV respectively (Table 3.1). PL spectroscopy measurements of polymers were performed in dilute 10^{-5} M THF solutions. The NDI-BT copolymer shows emission peak at 480 nm which corresponds to the main absorption peak at 371 nm of the naphthalene core transition. NDI-Ph polymer exhibits an emission

TH-1703_11612241

peak at around 472 nm corresponding to that of 370 nm in absorption spectra in THF (Figure 3.2(c)).

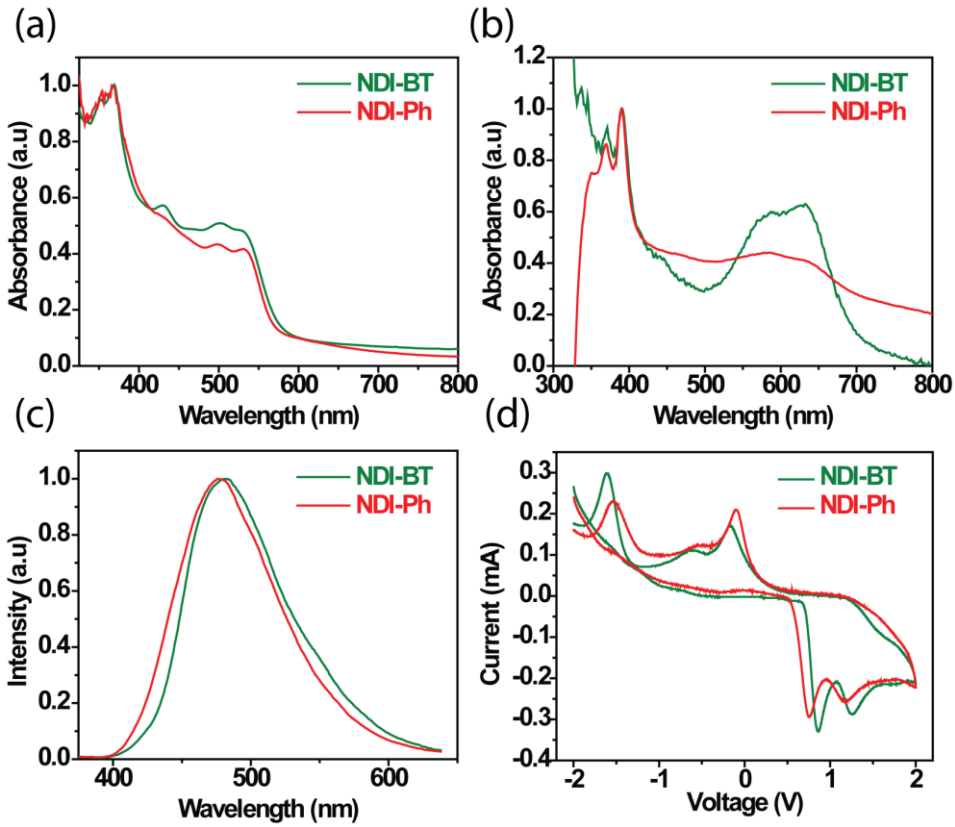

Figure 3.2. (a) UV-Vis spectra in THF (10^{-5} M) (b) UV-Vis spectra in thin films (~ 50 - 60 nm) (c) PL spectra in THF (10^{-5} M) of polymers (d) Cyclic Voltagramms of the drop casted polymer films (~ 100 nm) on carbon working electrode performed at a scan rate of 0.5 mV/s in 0.1 M TBAP in acetonitrile under argon atmosphere.

Table 3.1. UV-vis absorption values in [a] solution and [b] thin film, emission values in solution, [c]optical band gaps and yields of the polymers.

Polymer	$\lambda_{max}{}^{a}$ (nm)	$\lambda_{max}{}^{b}$ (nm)	Emission (nm)	$E_g{}^{c}$ (eV)	Yield (%)
NDI-Ph	360, 370, 540	370, 391, 600	472	1.55	84
NDI-BT	360, 371, 449	371, 391, 625	480	1.72	85

3.3.3. Electrochemical Properties

To estimate the HOMO and LUMO energy levels of the copolymers, cyclic voltammetry

TH-1703_11612241

(CV) was performed. The copolymers were drop casted on the carbon working electrode. Silver as reference electrode and platinum wire as counter electrode were used in these experiments. The HOMO and LUMO levels were estimated by the onset oxidation and onset reduction peaks assuming the absolute energy level of the ferrocene/ferrocenium couple to be -4.8 eV below vacuum. 0.1 M tetra butyl ammonium perchlorate (TBAP) as electrolyte in deoxygenated acetonitrile and ferrocene as standard were used in argon atmosphere. The HOMO/LUMO were calculated by substituting the onset reduction and onset oxidation peak values in E_{LUMO} = - [(E_{red} - $E_{1/2}$(ferrocene)) + 4.8] eV, E_{HOMO} = - [(E_{ox} - $E_{1/2}$(ferrocene)) + 4.8] eV. The LUMO levels of NDI-BT, NDI-Ph are -3.03 eV, -3.15 eV respectively. Similarly HOMO levels of the copolymers NDI-BT, NDI-Ph calculated from CV are -5.14 eV, -5.173 eV respectively (Figure 3.2(d)). The energy levels, band gaps calculated from cyclic voltammetry of thin films are represented in Table 3.2

Table 3.2. Cyclic Voltammetry, TGA and GPC data

Polymer	[a]HOMO (eV)	[a]LUMO (eV)	[b]E_g(eV)	[c]T_d(^{o}C)	M_n(Da)	M_w(Da)	*PDI*
NDI-Ph	-5.01	-3.22	1.8	341	6800	13579	1.99
NDI-BT	-5.14	-3.03	2.1	350	5100	6627	1.74

M_n, M_w - number average and weight average molecular weights, *PDI* - polydispersity index are obtained from GPC. [a]HOMO and LUMO estimated from the onset oxidation and reduction potentials, respectively, assuming the absolute energy level of ferrocene/ferrocenium couple to be -4.8 eV below vacuum. [b]HOMO-LUMO gap estimated by electrochemistry. [c]T_d - degradation temperature calculated by TGA.

3.3.4. Thermal Properties

The thermal properties of the polymers were studied by thermo gravimetric analysis (TGA) and differential scanning calorimeter (DSC). TGA analysis was done in the range 25-800 °C at a rate of 5 °C/min under nitrogen flow. All the polymers were very stable and their onset degrading temperatures were found to be in the range of 340-350 °C (Figure 3.3(a)). The onset thermal degradation temperatures of all the polymers are shown in Table 3.2. In DSC, the polymers were heated from 25 °C to 325 °C and then again cooled to 25 °C with a rate of 5 °C/min for three cycles under nitrogen flow. The

TH-1703_11612241

chromatograms of second cycle are shown in Figure 3.3(b). NDI-Ph copolymer shows an endothermic peak at 145 °C in second heating cycle and an exothermic peak at 132 °C in second cooling cycle which indicates the melting and crystalline temperatures of the polymer respectively. Similarly, NDI-BT copolymer shows an endothermic peak at 142 °C and an exothermic peak at 125 °C in second heating and cooling cycles corresponding to the melting and crystalline temperatures respectively showing that both polymers are crystalline in nature. Hence, the DSC reveals that NDI-Ph, NDI-BT copolymers possess crystalline domains within their structures.

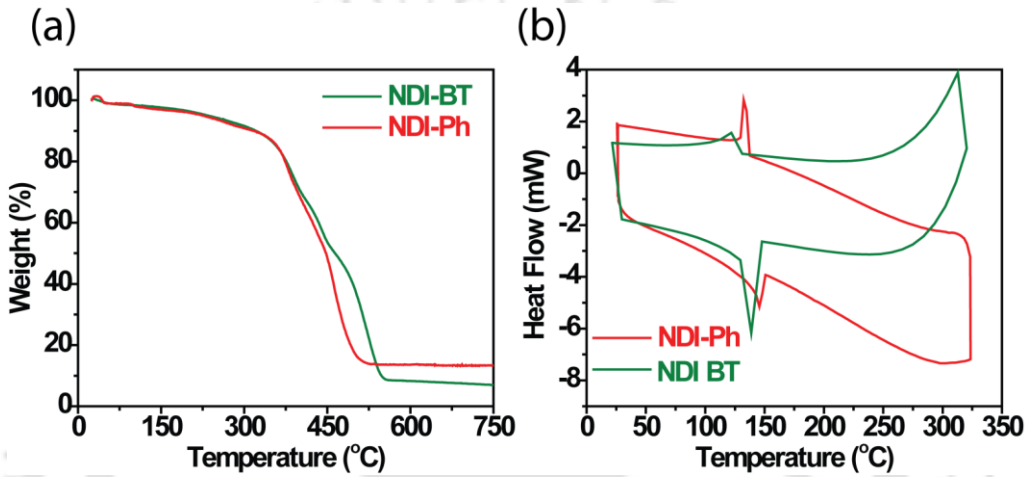

Figure 3.3. (a)TGA chromatograms carried out at a rate of 5°C/ min (b) DSC chromatograms of second cycle of the polymers carried out at a rate 5°C/ min under nitrogen atmosphere

3.3.5. Morphology Characterization

Both polymer thin films were characterized by AFM, FESEM, XRD and polarized optical microscopy (POM) to obtain further information on crystallinity and morphology which is relevant for device characterization. Out of plane XRD measurements were performed on thin films of the NDI co-polymers (Figure 3.4, 3.5) to obtain information regarding the molecular re-organization. As-spun polymeric films reveal π-π stacking in the range of 4.02-4.07 Å and a broad primary diffraction peak at 2θ = 4.33° and 4.65° corresponding to the d-spacing values of 18.51 and 19.85 Å. Annealing of the thin films reduced the d-spacing to a range of 18.26 and 19.82 Å and π-π stacking distance to 4.0-4.06 Å (Table 3.3). This indicates that denser inter-digitated lamellar packing is obtained by annealing of the polymer films, which is an inherent anisotropic characteristic of conjugated backbone possessing polymers. It should be noted that these magnitudes of d-spacing and π-π stacking obtained in these polymers are relatively lower than other non-thiophene

TH-1703_11612241

based NDI polymer reported[35] which gets reflected in the enhanced transport properties. In addition, annealing of the polymer films decreases the FWHM of the peaks (Table 3.4) corresponding to π-π stacking as well as the d-spacing pointing to the enhanced morphological ordering with annealing.

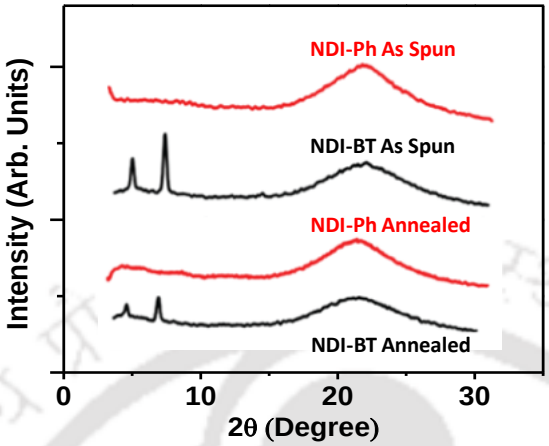

Figure 3.4. Out of plane X-ray diffraction patterns of as spun and annealed (150°C) copolymer films

Table 3.3. Summary of variation in π -π stacking and d spacing of the Polymers

		As cast films		Annealed Films	
Polymers	(00n)	2θ	d (00n) spacing(Å)	2θ	d (00n) spacing(Å)
NDI-Ph	(001)	4.33	19.85	4.34	19.82
	(002)	-	-	-	-
	π-π	21.25	4.07	21.27	4.06
NDI-BT	(001)	4.65	18.51	4.71	18.26
	(002)	-	-	-	-
	π-π	21.48	4.02	21.58	4.00

AFM imaging was carried out on thin films coated under similar condition as those used in device studies. AFM images for as spun films do not exhibit any crystallite formation (Figure 3.6a, 3.6c). However, it was observed that annealing the thin films at 150°C introduces crystallites in the film (Figure 3.6b, 3.6d). This trend is consistent with DSC measurement which shows crystallization at ~150 °C. It should be noted that the degree of enhancement of crystallinity is more prominent for NDI copolymer films. This was substantiated from observations of larger number of crystallites obtained in case of NDI-Ph and NDI-BT. Furthermore, FESEM measurements were also performed on these

TH-1703_11612241

copolymers to examine the thin film microstructure (Figure 3.7). FESEM images show interconnected crystalline fibrillar network of the copolymers which supports enhanced transport, weakly affected by defects.[43,44] In addition, POM studies performed on films of the these four copolymers confirmed the appearance of macroscale crystalline domains after annealing above 150°C (Figure 3.8) due to their inherent structural anisotropic. These features can be directly correlated to large enhancement of OFET upon thermal annealing in the NDI derivatives.

Table 3.4. Table showing the variation in the FWHM of the XRD spectra with annealing of the polymer

		As cast film	Annealed Film
Polymer	(00n)	FWHM	FWHM
NDI-Ph	(001)	0.3326	0.5331
	π- π	7.1387	6.8727
NDI-BT	(001)	0.2542	0.2526
	(002)	-	-
	π- π	8.0554	7.9907

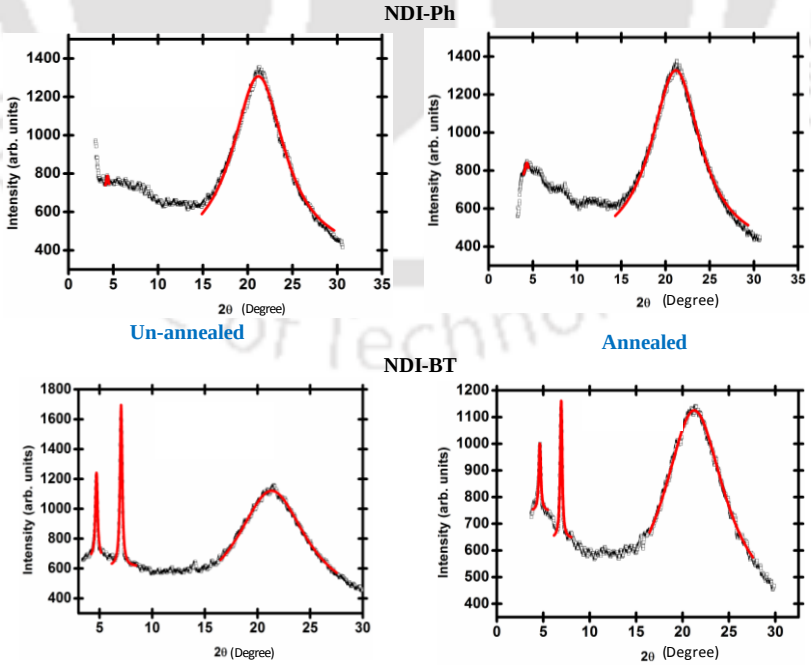

Figure 3.5. XRD spectra of the annealed (right side) and as spun (left side) polymer films fitted with Lorentzian to correctly estimate the peaks.

TH-1703_11612241

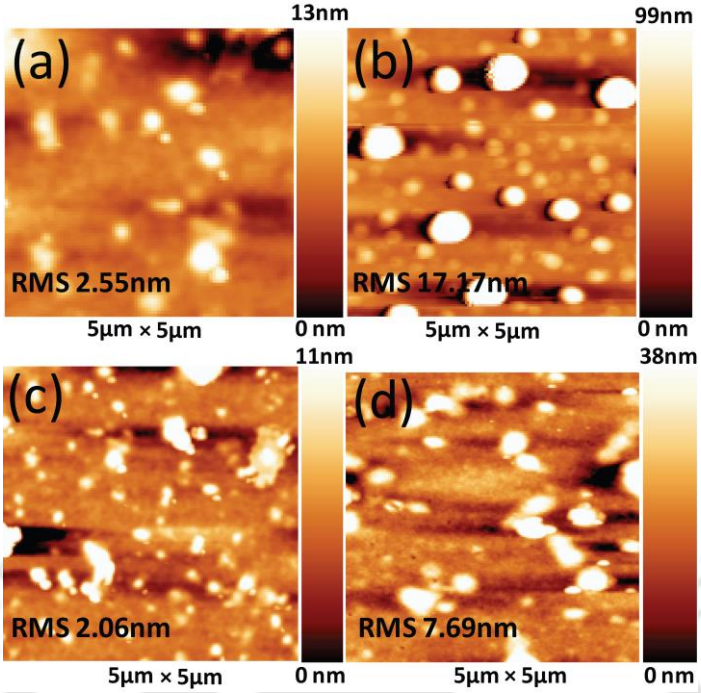

Figure 3.6. AFM topography image (5 μm × 5 μm) for the copolymer films: NDI-Ph (a) as spun (b) annealed; NDI-BT (c) as spun (d) annealed.

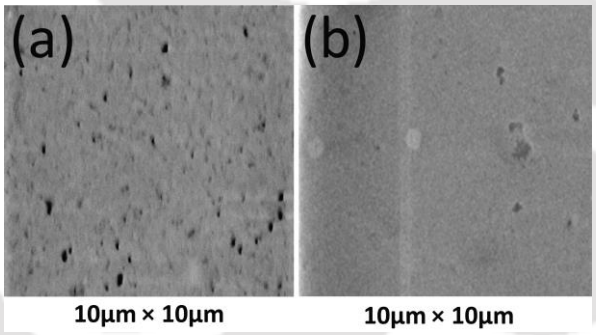

Figure 3.7. Typical FESEM images (10 μm × 10 μm) of (a) NDI-Ph (b) NDI-BT

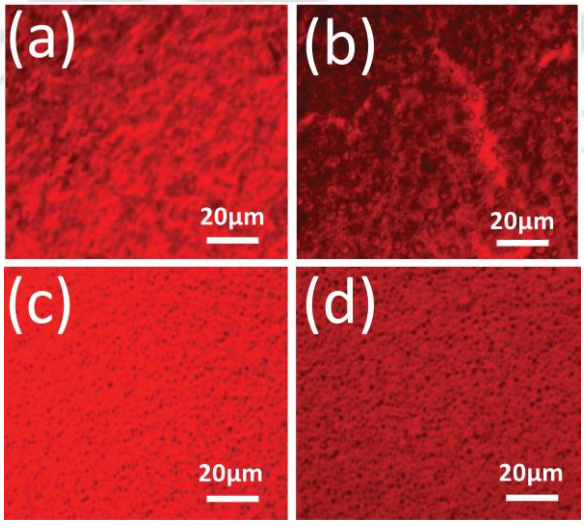

Figure 3.8. Polarizable Optical Microscope images of NDI-Ph (a) before annealing, (b) after annealing, (c) NDI-BT before annealing (d) after annealing.

TH-1703_11612241

3.3.6. OFET Measurements

Top contact bottom gate OFETs were fabricated using newly synthesized NDI-Ph and NDI-BT copolymers as active layers. The devices demonstrated well defined linear and saturation behavior with electron only mobility and On/Off ratio exceeding 10^4 (Figure 3.9). Typical plot showing FET characteristics measured under inert condition is shown in Figure 3.9. Although molecules with phenylene substitution are of D-A type, hole transport was not observed even with Au S-D electrodes. This feature can be attributed to weaker electron donating ability of phenylene group. NDI-Ph showed the highest electron OFET~0.8 cm^2/Vs whereas FETs fabricated with NDI-BT had OFET~0.2 cm^2/Vs after annealing at 150°C. Annealing increases the OFET by several orders, which are amongst the highest enhancement values for NDI based copolymers (Table 3.5). The observed enhancement of μ_{FET} is consistent with the occurrence of crystallites with annealing in the microscopic images and a crystalline transition temperature in DSC. In addition, XRD measurements on these thin films also indicate a decrease in d-spacing and π- π stacking distance with annealing for all the polymers. Specifically, it was also observed that with annealing the decrease in d-spacing and π-π stacking distance is higher for benzothiadiazole based molecules compared to phenylene substituted co-polymers which corroborates with a larger change in the μ_{FET}.

Upon comparing the NDI with PDI derivatives, it is evident that the NDI derivatives exhibit μ_{FET} values which are at least an order of magnitude higher than the corresponding PDI derivatives. This can be attributed to the enhanced interdigitated lamellar packing and better π-π stacking in NDI polymers. Annealed films of NDI polymers exhibit d-spacing in the range of 18.26 Å - 19.82 Å compared to 25.81 Å - 28.02 Å for PDI based polymers. Similarly, the π-π stacking distance increases from 4.06 Å in NDI-Ph to 4.12 Å in PDI-Ph polymer (Table 3.3). Importantly, the observed μ_{FET} values are higher than other non-thiophene based NDI polymers and are comparable to NDIOD-T2.[36,45] This comparable μ_{FET} can be attributed to a combination of factors, ranging from the molecular level to an optimum dielectric-semiconductor interface.

TH-1703_11612241

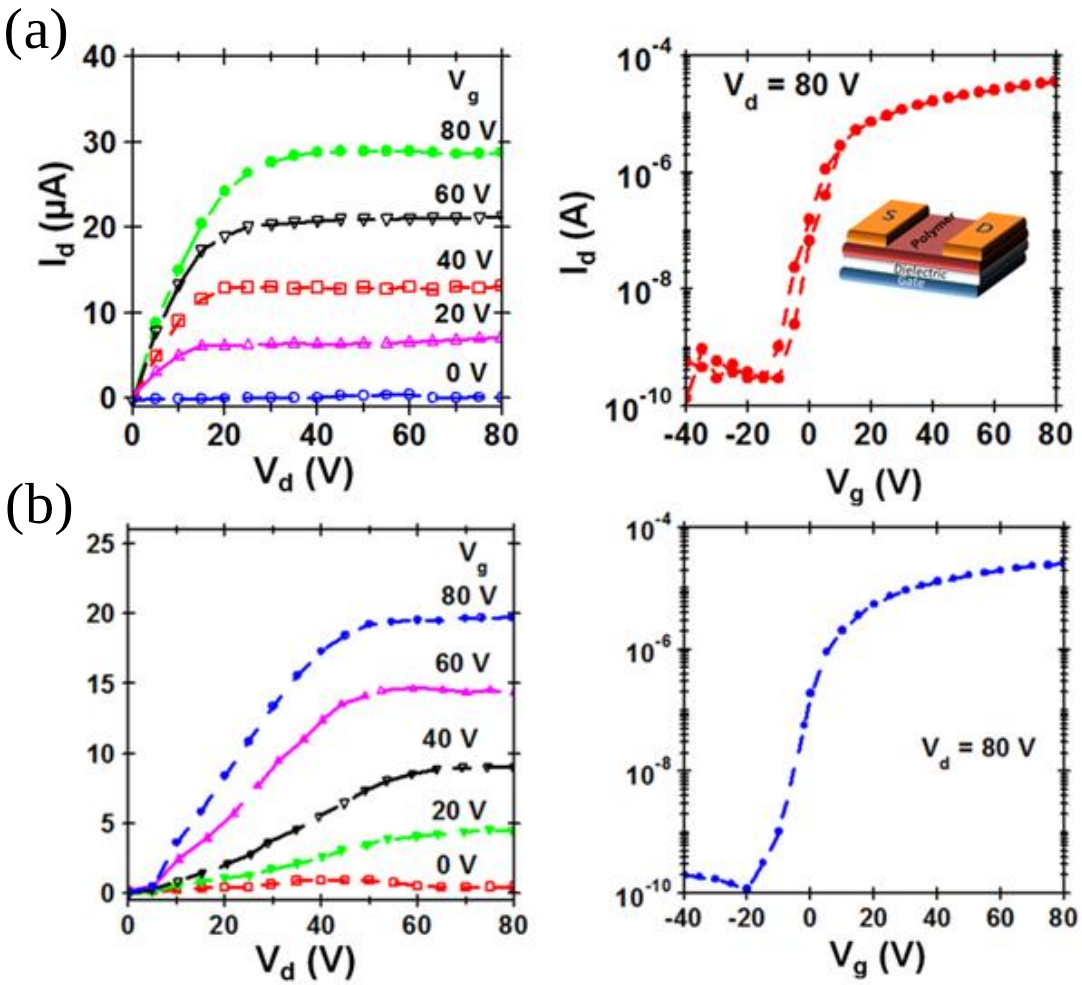

Figure 3.9. Typical output and transconductance characteristics for OFETs fabricated with (a) NDI-Ph (b) NDI-BT active layer and BCB as the dielectric (C_i ~ 4 nF/cm^2). Typical device dimensions are W ≈ 1 mm and L ≈ 60-100 μm.

The presence of linear alkyl chains in NDI-Ph and NDI-BT polymer improves the polymer packing and the π-π stacking. In comparison to the typical d-spacing of 23 Å - 24 Å observed for non-thiophene based NDI the d-spacing in these NDI polymer films were obtained to be 18.26 Å - 19.82 Å[35] indicating better lamellar structure and closely packed inter-digitated structure. In addition, the π-π stacking distance of the NDI co-polymers is in the range of 4.00 Å - 4.06 Å which is comparable to NDIOD-T2 (3.93 Å)[46] and better than other non-thiophene based NDI molecules (4.51 Å).[35] Hence, these molecules have a higher propensity to form ordered crystallites and interconnected aggregates which support enhanced transport as observed for other high mobility polymers reported recently.[43,47] Another interesting observation in the transport measurement is the enhanced performance of the D-A type molecules (NDI-Ph or PDI-Ph) compared to A-A

TH-1703_11612241

type (NDI-BT or PDI-BT molecule). This indicates the apparent importance of the intermolecular D-A type interaction on the charge transport compared to the geometry and microstructure of the molecule which can be a general way to achieve high mobility in NDI or PDI polymeric materials.

Table 3.5. Performance parameters of OFETs obtained under different annealing conditions

Polymers	Annealing temperature (°C)	Average μ_{FET} (cm^2/Vs)	Maximum μ_{FET} (cm^2/Vs)	I_{on}/I_{off}
NDI-Ph	as spun	0.1	0.8	~ 10^5
	110	0.4		
	150	0.6		
NDI-BT	as spun	0.007	0.2	> 10^4
	110	0.05		
	150	0.08		

3.4. Conclusions

In summary, these solution processable n-type copolymers having NDI backbone were synthesized in high yields (84, 85%) by palladium catalyzed Suzuki coupling reactions and their excellent solubility in several organic solvents allowed their deposition in organic thin film transistor (OTFT) devices from solution directly. We demonstrated the importance of the correlation between the conjugated backbone macro structure and anisotropy behavior in spin-coated aligned thin films of naphthalene diimide copolymers. The thin film structures and electronic anisotropic properties in conjugated copolymers can be regulated, which results in efficient intermolecular interactions and the formation of crystalline domains over large area after annealing, thereby facilitating large enhancement in charge carrier transport. The optical, thermal and redox characterization of the copolymers indicate good polymeric aggregates, high thermal stability with tendency to form crystalline domains and suitable energetic which support efficient electron injection. This was further supported by the morphology patterns observed in the AFM, FESEM and POM images. The transport studies performed under different

TH-1703_11612241

annealing conditions up to 150°C demonstrated huge enhancement in electron μ_{FET} with maximum values of 0.8 cm^2/Vs for the NDI-Ph and 0.2 cm^2/Vs for the NDI-BT polymers. The extended conjugation and efficient intermolecular interactions observed in thin films, especially in NDI copolymers along with the formation of crystalline domains as also confirmed by DSC analysis after annealing are collectively responsible for the enhanced device characteristics. This study conclusively illustrates that D-A copolymers display better properties compared to A-A copolymers and demonstrates a route to develop high-performing, solution processable copolymers.

3.5. References

1. Cheng, C. H. W.; Lonergan, M. C. *J. Am. Chem. Soc.* **2004,** *126* (34), 10536-10537.
2. Robinson, S. G.; Lonergan, M. C. *J. Phys. Chem. C.* **2013,** *117* (4), 1600-1610.
3. Sommer, M.; Huettner, S.; Thelakkat, M. *Adv. Polym. Sci.* **2010,** *228*, 123-153.
4. Bhuwalka, A.; Mike, J. F.; He, M.; Intemann, J. J.; Nelson, T.; Ewan, M. D.; Roggers, R. A.; Lin, Z. Q.; Jeffries-El, M. *Macromolecules* **2011,** *44* (24), 9611-9617.
5. Yan, H.; Chen, Z. H.; Zheng, Y.; Newman, C.; Quinn, J. R.; Dotz, F.; Kastler, M.; Facchetti, A. *Nature* **2009,** *457* (7230), 679-686.
6. Humphries, M. J.; Wilson, R. J.; Fernandez, O.; Archer, R. A. *J. Photon Energy* **2011,** *1*.
7. Chiba, T.; Pu, Y. J.; Sasabe, H.; Kido, J.; Yang, Y. *J. Mater. Chem.* **2012,** *22* (42), 22769-22773.
8. Shao, M.; He, Y. J.; Hong, K. L.; Rouleau, C. M.; Geohegan, D. B.; Xiao, K. *Polym. Chem.* **2013,** *4* (20), 5270-5274.
9. Marszalek, T.; Wiatrowski, M.; Dobruchowska, E.; Jung, J.; Ulanski, J. *J. Mater. Chem. C.* **2013,** *1* (19), 3190-3193.
10. Ben-Sasson, A. J.; Chen, Z. H.; Facchetti, A.; Tessler, N. *Appl. Phys. Lett.* **2012,** *100* (26), 263306.
11. Li, C. H.; Huang, C. H.; Kuo, M. Y. *Phys. Chem. Chem. Phys.* **2011,** *13* (23), 11148-11155.
12. Zhao, X. G.; Zhan, X. W. *Chem. Soc. Rev.* **2011,** *40* (7), 3728-3743.
13. Hwang, Y. J.; Murari, N. M.; Jenekhe, S. A. *Polym. Chem.* **2013,** *4* (11), 3187-3195.
14. Kim, R.; Amegadze, P. S. K.; Kang, I.; Yun, H. J.; Noh, Y. Y.; Kwon, S. K.; Kim, Y. H. *Adv. Funct. Mater.* **2013,** *23* (46), 5719-5727.
15. Chen, H. J.; Guo, Y. L.; Mao, Z. P.; Yu, G.; Huang, J. Y.; Zhao, Y.; Liu, Y. Q. *Chem. Mater.* **2013,** *25* (23), 4835-4835.
16. Huttner, S.; Sommer, M.; Thelakkat, M. *Appl. Phys. Lett.* **2008,** *92* (9), 093302.
17. Ge, C. W.; Mei, C. Y.; Ling, J.; Zhao, F. G.; Li, H. J.; Liang, L.; Wang, J. T.; Yu, J. C.; Shao, W.; Xie, Y. S.; Li, W. S. *J. Polym. Sci. Pol. Chem.* **2014,** *52* (16), 2356-2366.
18. Hu, C.; Zhang, Q. *Polym. Bull.* **2012,** *69* (1), 63-69.
19. Patil, D. R.; Kops, J. *J. Polym. Sci. Pol. Chem.* **1990,** *28* (2), 443-445.

TH-1703_11612241

20. Katz, H. E.; Lovinger, A. J.; Johnson, J.; Kloc, C.; Siegrist, T.; Li, W.; Lin, Y. Y.; Dodabalapur, A. *Nature* **2000,** *404* (6777), 478-481.
21. Mukhopadhyay, P.; Iwashita, Y.; Shirakawa, M.; Kawano, S.; Fujita, N.; Shinkai, S. *Angew. Chem. Int. Edit.* **2006,** *45* (10), 1592-1595.
22. Stewart, W. W. *Nature* **1981,** *292* (5818), 17-21.
23. Wurthner, F.; Ahmed, S.; Thalacker, C.; Debaerdemaeker, T. *Chem. Eur. J.* **2002,** *8* (20), 4742-4750.
24. Heinrich V.; Becker H.; Martin C.; Hans S.; *Eur. J. Org. Chem.* **1937**, *531*(1), 1-159
25. Fallon, G. D.; Lee, M. A. P.; Langford, S. J.; Nichols, P. J. *Org. Lett.* **2004,** *6* (5), 655-658.
26. Zhan, X. W.; Facchetti, A.; Barlow, S.; Marks, T. J.; Ratner, M. A.; Wasielewski, M. R.; Marder, S. R. *Adv. Mater.* **2011,** *23* (2), 268-284.
27. Langhals, H. *Heterocycles* **1995,** *40* (1), 477-500.
28. Choi, D.; Jeong, B. S.; Ahn, B.; Chung, D. S.; Lim, K.; Kim, S. H.; Park, S. U.; Ree, M.; Ko, J.; Park, C. E. *ACS. Appl. Mater. Inter.* **2012,** *4* (2), 702-706.
29. Li, C.; Wonneberger, H. *Adv. Mater.* **2012,** *24* (5), 613-636.
30. Bhosale, S. V.; Jani, C. H.; Langford, S. J. *Chem. Soc. Rev.* **2008,** *37* (2), 331-342.
31. Polander, L. E.; Romanov, A. S.; Barlow, S.; Hwang, D. K.; Kippelen, B.; Timofeeva, T. V.; Marder, S. R. *Org. Lett.* **2012,** *14* (3), 918-921.
32. Yan, Q. F.; Zhao, D. H. *Org. Lett.* **2009,** *11* (15), 3426-3429.
33. Babel, A.; Jenekhe, S. A. *J. Am. Chem. Soc.* **2003,** *125* (45), 13656-13657.
34. Guo, X. G.; Watson, M. D. *Org. Lett.* **2008,** *10* (23), 5333-5336.
35. Hu, X. L.; Zuo, L. J.; Pan, H. B.; Hao, F.; Pan, J. Y.; Fu, L.; Shi, M. M.; Chen, H. Z. *Sol. Energ. Mat. Sol. C.* **2012,** *103*, 157-163.
36. Chen, Z. H.; Zheng, Y.; Yan, H.; Facchetti, A. *J. Am. Chem. Soc.* **2009,** *131* (1), 8-9.
37. Zhan, X. W.; Tan, Z. A.; Domercq, B.; An, Z. S.; Zhang, X.; Barlow, S.; Li, Y. F.; Zhu, D. B.; Kippelen, B.; Marder, S. R. *J. Am. Chem. Soc.* **2007,** *129* (23), 7246-7247.
38. Zhou, W. Y.; Wen, Y. G.; Ma, L. C.; Liu, Y. Q.; Zhan, X. W. *Macromolecules* **2012,** *45* (10), 4115-4121.
39. Zhang, S. M.; Wen, Y. G.; Zhou, W. Y.; Guo, Y. L.; Ma, L. C.; Zhao, X. G.; Zhao, Z.; Barlow, S.; Marder, S. R.; Liu, Y. Q.; Zhan, X. W. *J. Polym. Sci. Pol. Chem.* **2013,** *51* (7), 1550-1558.
40. Kim, Y.; Hong, J.; Oh, J. H.; Yang, C. *Chem. Mater.* **2013,** *25* (15), 3251-3259.

TH-1703_11612241

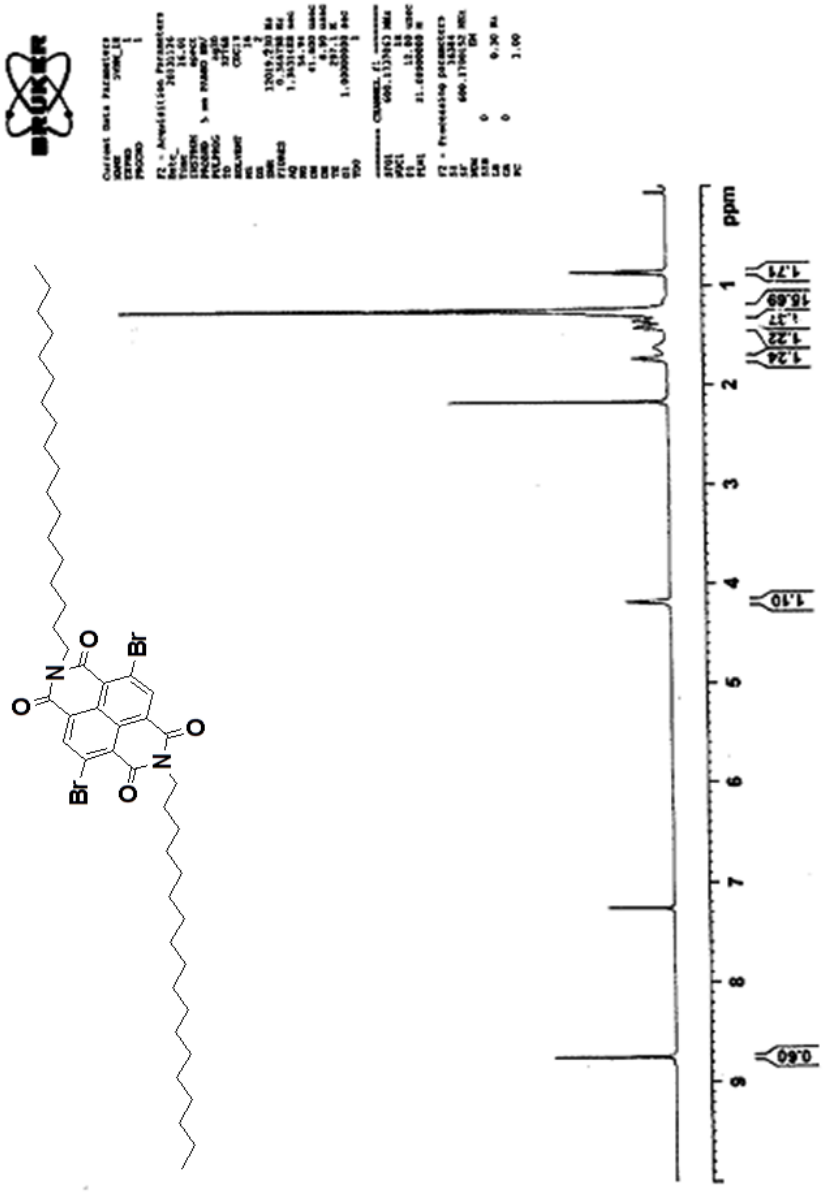

Figure 3.10. ^{1}H NMR Spectrum of Br_2-NDIOD ($CDCl_3$, 600MHz)

TH-1703_11612241

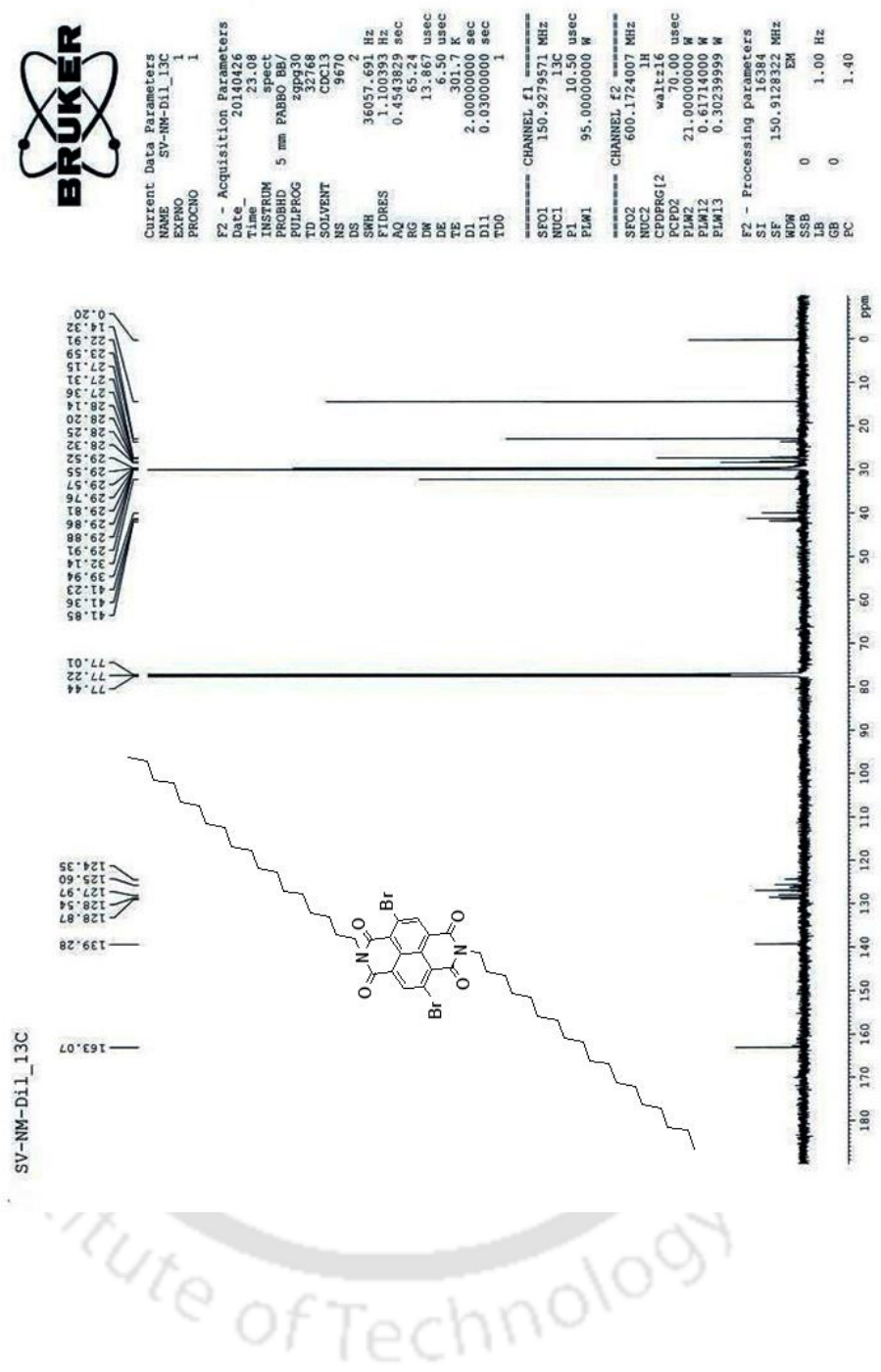

Figure 3.11. ^{13}C NMR Spectrum of Br_2-NDIOD ($CDCl_3$, 600MHz)

TH-1703_11612241

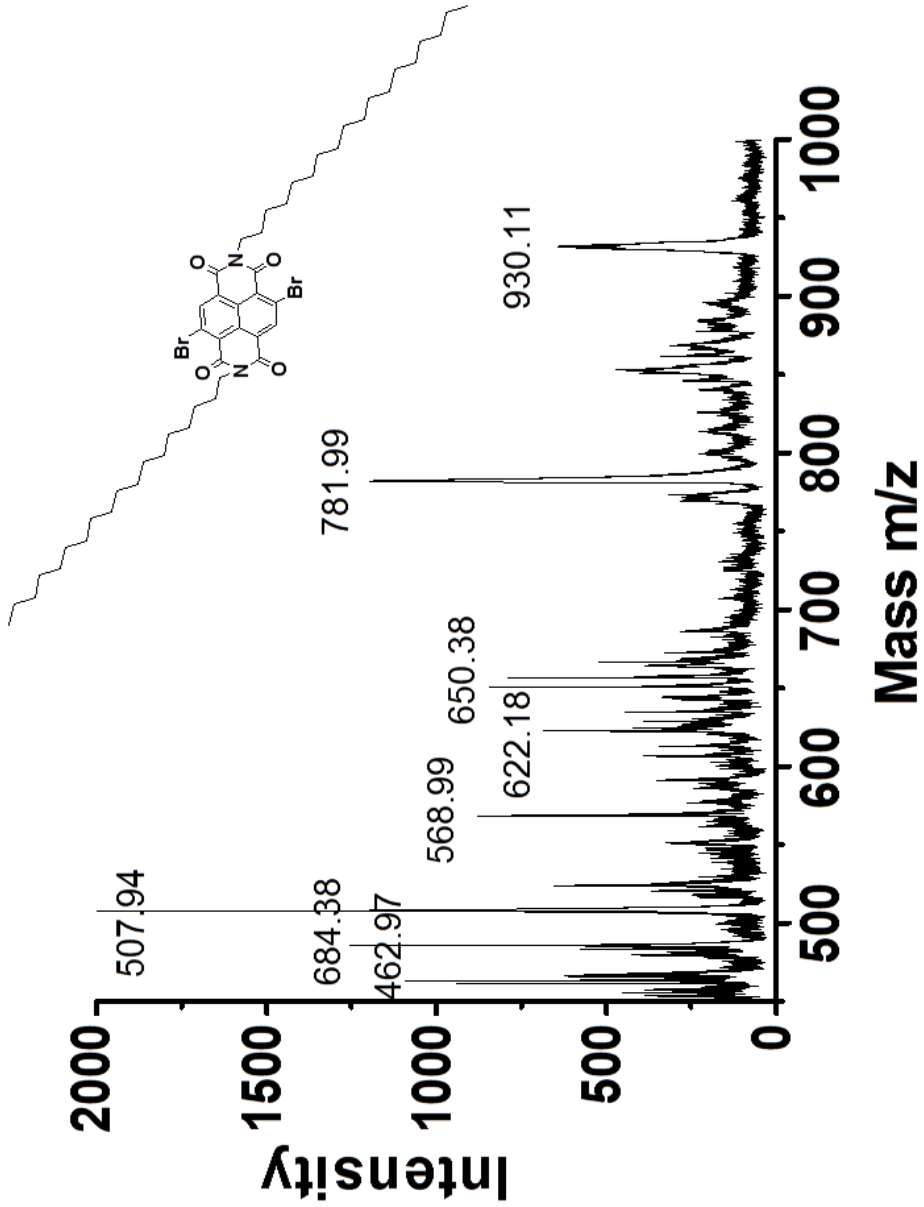

Figure 3.12. MALDI-TOF Spectrum of Br_2-NDIOD

TH-1703_11612241

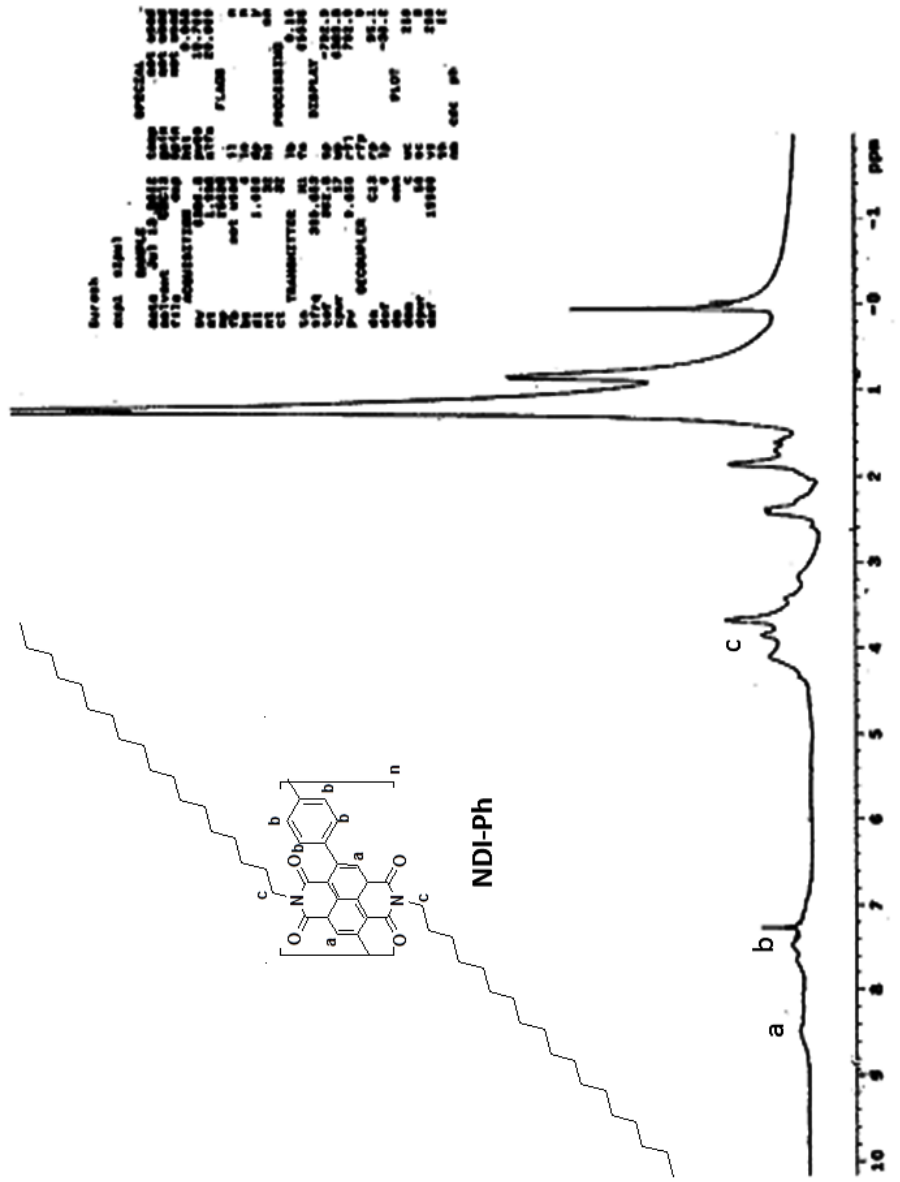

Figure 3.13. ^{1}H NMR Spectrum of NDI-Ph ($CDCl_3$, 400MHz)

TH-1703_11612241

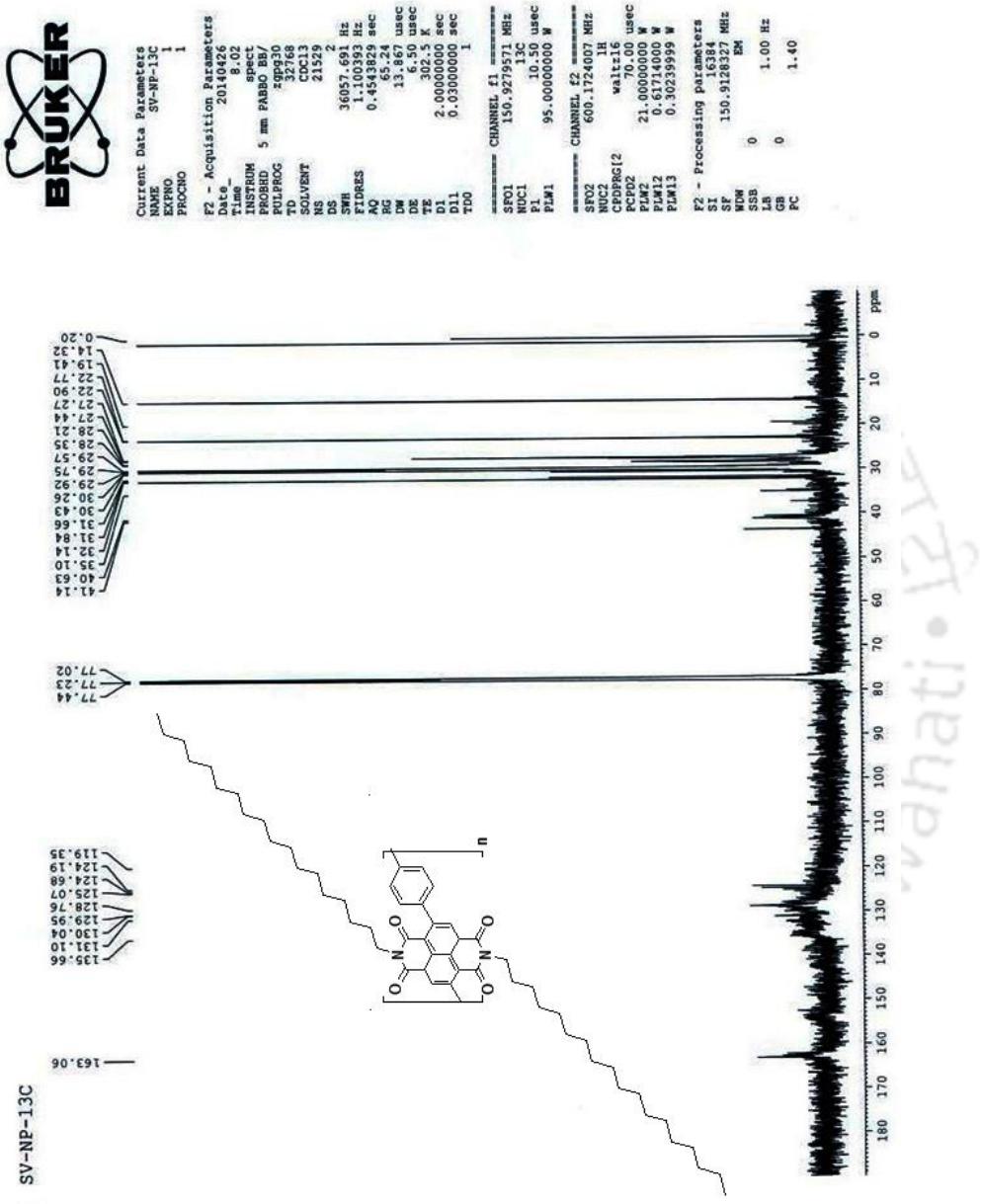

Figure 3.14. ^{13}C NMR Spectrum of NDI-Ph ($CDCl_3$, 600MHz)

TH-1703_11612241

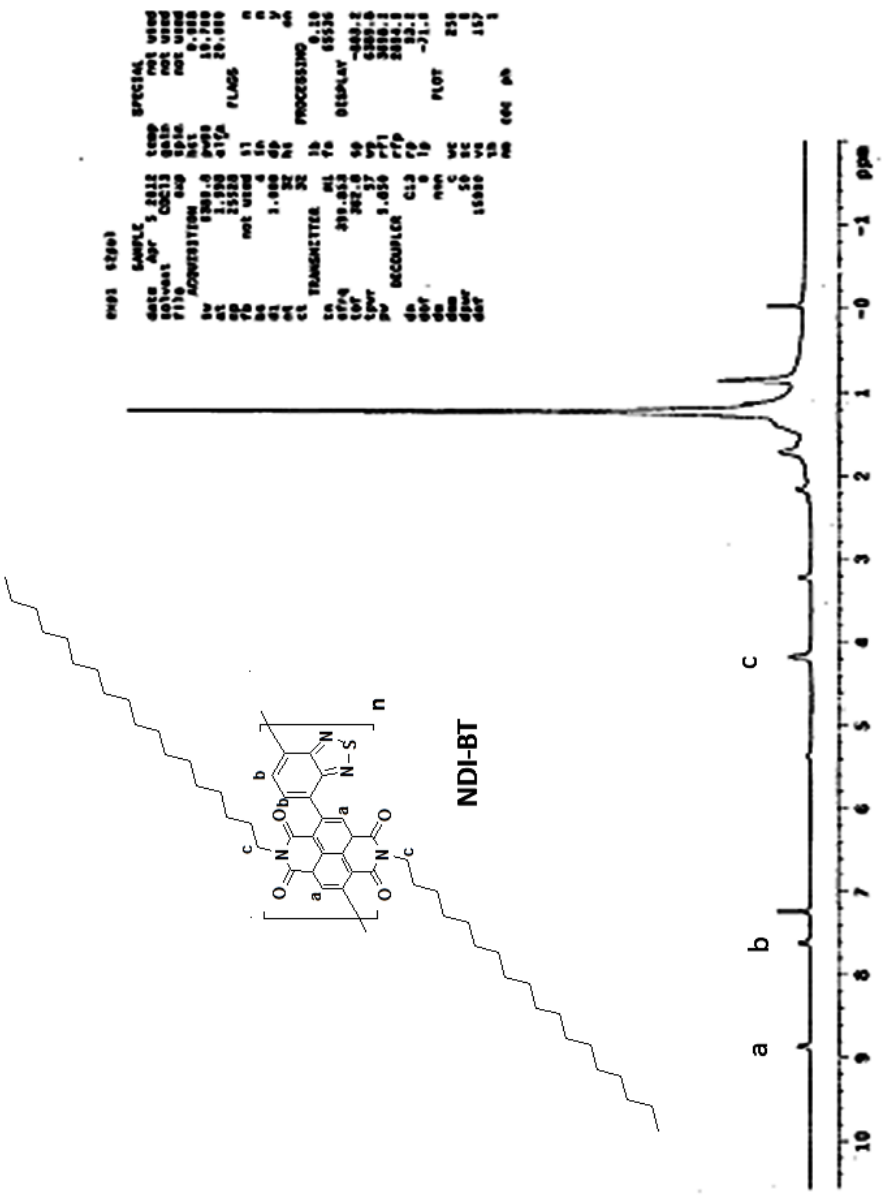

Figure 3.15. ^{1}H NMR Spectrum of NDI-BT ($CDCl_3$, 400MHz)

TH-1703_11612241

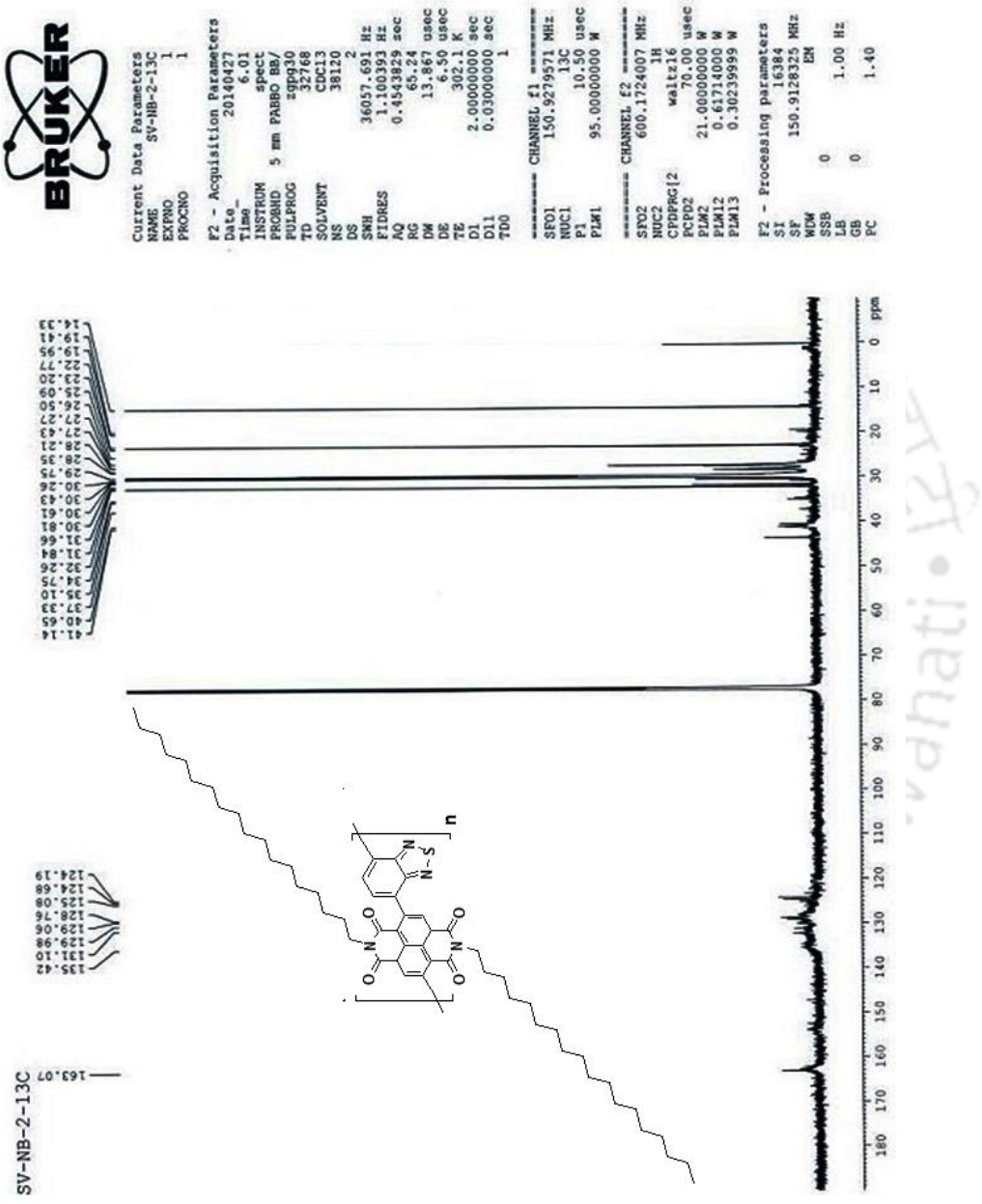

Figure 3.16. ^{13}C NMR Spectrum of NDI-BT ($CDCl_3$, 600MHz)

TH-1703_11612241

Chapter 4

Effect of dielectric material, HMDS and channel length on the performance of the Perylenediimide based OFETs

4.1. Introduction

Organic electronic devices are fascinating and receiving steady and increasing attention in recent years due to their versatile applications in optoelectronics, biomedical and digital electronics. Organic semiconductors are the active components in electronic devices including, solar cells,[1,2] light-emitting diodes (LEDs)[3] and organic field-effect transistors (OFETs).[4,5] OFETs are of interest for a wide range of low-cost, large-area and flexible electronic applications.[6-8] Such applications include active-matrix displays,[9] radio-frequency identification tags,[10] smart cards, smart price and inventory tags, and large-area sensor arrays.[11] OFETs provide two principle advantages over inorganic semiconductor based FETs. The former can be fabricated at lower temperatures and significantly lowers the cost. Low temperature processing in particular may allow OFETs to be integrated on inexpensive plastic substrates, rather than glass and the prospect of flexible, unbreakable, extremely low-weight flat panel displays at low cost has spurred significant commercial interest.

Despite the considerable progress made in recent years in improving the performance of OFETs, many of the designs, material and process parameters impacting OFET performance are still poorly understood and poorly controlled. One such parameter is contact resistance.[12] Consequently, OFET performance typically suffers from large

TH-1703_11612241

contact resistance, perhaps to the point where the speed of organic integrated circuits may not be limited by the intrinsic carrier mobility of the organic semiconductor, but by the contact resistance of the FETs. In contrast to the field-effect transistors based on single-crystalline silicon, polycrystalline silicon, or hydrogenated amorphous silicon, the source and drain contacts in OFETs cannot be easily optimized by conventional processes, such as semiconductor doping or metal alloying. In OFETs, the energy mismatch between Fermi-level of metal contact and HOMO or LUMO level of the organic semiconductor and morphology of the semiconductor determines the contact resistance value. It includes gate modulation of the bulk resistivity of the semiconductor to explain the experimentally observed gate voltage dependence of the contact resistance for different thicknesses of the semiconducting film. The contact resistance is found to be Ohmic. For thick semiconducting films, a significant asymmetry between source and drain contact resistances were observed with the drain resistances increasing more rapidly with thickness than the source resistance, reflecting the importance of diffusion at the drain contact.

Historically, the performance of n-type organic semiconductors was outmatched by that of the more intensively investigated p-type materials.[13,14] Nevertheless, both kinds of semiconductors are required for the fabrication of complementary integrated circuits,[15-17] bipolar transistors, or organic p/n junctions. During the past few years a larger number of organic materials have been reported that surpass the electron mobility of amorphous silicon.[18-20] In most cases, these electron deficient semiconductors have been designed by introducing electron withdrawing groups to extended aromatic π-systems with good p-channel activity.[21,22] Molecules of perylenetetracarboxylic diimides (PTCDI) and its derivatives form a unique class of n-type organic semiconductors.[23,24] The PTCDI were extensively studied due to their high molar absorptivity, high quantum yield of fluorescence with excellent photochemical and thermal stabilities. Self-assembly of π-conjugated molecules from solution provides a powerful approach for generating supramolecular nanostructures with long-range order, which are of great importance in the development of organic optoelectronic devices. PTCDIs or PDIs (Perylene diimides) are particularly attractive building blocks for self-assembly because chemical modifications of the PDI core at either imide,[25,26] ortho[27,28] or bay[29] positions offer immense opportunities to modify the molecular packing in the solid state, resulting in

TH-1703_11612241

exciting electronic and optical properties. The solid-state molecular packing has a significant effect on both exciton migration and carrier mobility, which are central for optoelectronic devices, viz., OLEDs,[30,31] FETs,[32] and photovoltaics.[33]

In order to inject more carriers into the organic layer, applying a high voltage to the gate electrode or utilizing a gate insulator having a high dielectric constant is required.[34] In many cases OFETs have been fabricated on thermally oxidized SiO_2 surfaces of heavily doped conductive Si substrates.[35] Although SiO_2 is a good insulator and has a very high dielectric strength, approximately 10 MV/cm, the dielectric constant of SiO_2 is not very high (~4). Thus, many groups have been trying to fabricate an OFET on a high-k high dielectric constant gate insulator to inject more carriers.[36,37] Another advantage of high-k materials is a lower working voltage.[38] The present study was focused on PVA and PMMA among various polymer dielectric materials. The dielectric constant of PVA and PMMA are approximately 8 and 3. Therefore, it will be possible to inject three times higher amount of carriers into the organic layer on PVA than on PMMA if the thickness of the dielectrics is same, and the best dielectric breakdown characteristics are really achieved. It is difficult, however, to fabricate a good polymer film with a high dielectric strength and a smooth surface on which a good morphology organic film could be grown.

In many cases, dielectric films are grown by the e-beam evaporation, sputtering, chemical vapor deposition, or laser ablated molecular beam epitaxy (MBE) method, but they require expensive equipment and highly complicated techniques to grow a stoichiometric, low-defect smooth film. Instead, herein, an Al_2O_3 film was grown using the anodic oxidation (anodization) method, withoug requiring vacuum apparatus or high temperature process. In this method, an Al_2O_3 film grows on the Al surface. During the anodization, growth of the Al_2O_3 film proceeds under "negative feedback" conditions i.e., more electrochemical current flows at thinner or defective parts in the growing oxide film, so that these defects are automatically restored. Herein, an attempt to produce a smooth surface on a thermally deposited Al is presented. On the anodized Al_2O_3/Al gate substrates, bottom-gate type OFETs using n-type Br_2PTCDI-C18 were fabricated with different channel length. It was found that OFETs worked exceedingly well and showed consistency in results with the varying channel length. In this chapter, the fabrication process and device performance with the variation in channel length and the surface modification of the dielectric layer were demonstrated.

TH-1703_11612241

4.2. Experimental section

4.2.1. Synthesis of Br_2PTCDI-C18

The Br_2-PTCDI-C18 molecule was synthesized and purified according to previously published report.[39]

4.2.2. Fabrication of OFET

OFETs were fabricated on glass substrates with top-contact and bottom-gate configuration, which offers a low contact resistance than other configurations. The schematic diagram of the device structure is shown in Figure 4.1(a). Initially, glass slide were sliced into pieces of 1 cm x 2.5 cm using diamond cutter pen. The slides were cleaned by soaking in piranha solution, degreased with acetone, methanol and washed with high purity deionized water (Millipore Q, resistance Rs > 18 MΩ cm) several times. A 150 nm thick patterned aluminum layer was deposited by thermal evaporation technique and this layer served as a gate electrode. The top surface of the aluminum was converted into Al_2O_3 (13 nm) by anodization process in order to reduce the leakage current and to enhance the gate field. Anodization was carried out with a constant current j = 0.6 mA/cm^2 driven through the electrolyte. A 0.001 M citric acid monohydrate ($C_6H_8O_7.H_2O$) electrolyte was prepared using ultrapure (18 MΩ cm) water. The contacted aluminum gates were then immersed into the electrolyte to form the working electrode (anode), and a platinum mesh served as counter electrode (cathode). A Keithley 2400 source meter was used to supply constant voltage source 10 V. The anodization potential was applied for several minutes until the current dropped below ~1 μA. A ~13 nm aluminum oxide layer was grown with an oxide formation factor or anodization ratio of 1.3 nm/V. The substrates were subsequently rinsed in 60 °C hot water several times and heated on a hot plate to remove the water content in the aluminum and alumina films. Generally, the anodized surfaces were found to be rough due to etching and oxidation process in the anodization. For the fabrication of OFETs, smooth surface morphology was needed to reduce the interface trap states. Poly vinyl alcohol (PVA, Sigma Aldrich, M_W = 76500 - 81000 kg/mol) dielectric solution was prepared by dissolving 30mg/mL in water and spun onto the pre-prepared anodized alumina substrates at 3000 rpm for 60 sec, followed by annealing at 100°C for 1h in vacuum oven. In another case, ~100 nm Poly

TH-1703_11612241

methyl methacrylate (PMMA, Sigma Aldrich, M_W = 5,50,000 kg/mol, dissolved in anisole 30 mg/mL) film was grown on the top of anodized substrate and vacuum annealed at 120°C for 2 h to remove the residual solvent and to improve the film quality. Another set of PVA or PMMA substrates were coated with HMDS to study the effect on the growth of overlayer and on the performance of the device. HMDS was spin coated on the surface at 6000 rpm for 60 sec. The substrates were then baked at 120 °C for 30 min to evaporate the additional HMDS. Synthesized and purified Br_2PTCDI-C18 was chosen as the n-type organic semiconductor and thermally evaporated on top of the bilayer dielectric system of about 50 nm. The molecular structure is shown in the Figure 4.1(b). To ensure the quality of active layer, the optimized substrate temperature, 50 °C and growth rate of 0.2 Å/s have been maintained throughout the deposition at a base pressure of 10^{-6} Torr. With the help of surface profilometer (Dektak), the individual layer thicknesses have been approximated. Device fabrication was concluded by patterning 50 nm thick silver source-drain electrodes with defined channel width (W = 750 µm) and different channel length (L) (channel length L = 25, 50, 100, 190 µm), using shadow masks. AFM measurements for the films of organic semiconductor deposited on different dielectrics were performed by using Agilent 5500 AFM/SPM microscope instrument in tapping mode. To characterize capacitance of the resulting films, 100 nm thick 2 mm x 2 mm aluminum squares were evaporated as top electrodes. The capacitance measurements were carried out at 1 kHz and 10 mV modulation voltages with a Keithley 4200 SCS. The electrical characteristics of OFET devices were measured under accumulation mode using a Keithley 4200-SCS semiconductor parameter analyzer. The measurements were carried out on a Lakeshore probe station under vacuum (10^{-5} mbar) immediately after they were fabricated. The key device parameters, including charge carrier mobility (µ), on/off current ratio (I_{on}/I_{off}), and threshold voltage (V_{Th}), were calculated.

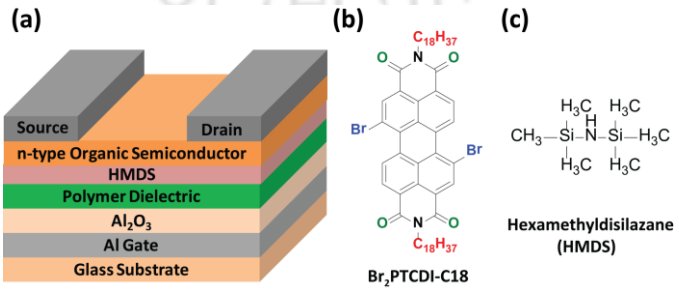

Figure 4.1. (a) Schematic diagram of the device structure, Structures of (b) N, N′-Dioctadecyl-1,7-Dibromo-3, 4, 9, 10-perylenetetracarboxylic diimide (Br_2PTCDI-C18) molecule and (c) HMDS

TH-1703_11612241

4.3. Results and Discussion

4.3.1. Morphological studies of different dielectric layers

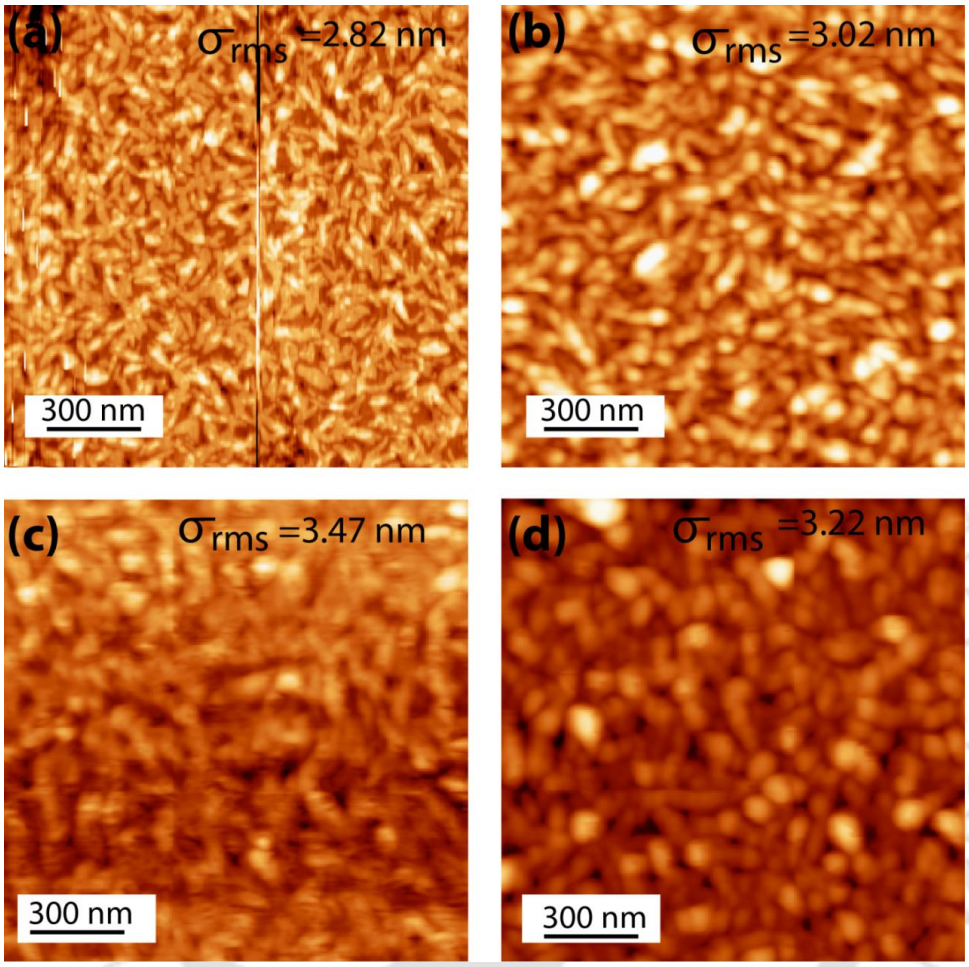

Figure 4.2. AFM topography images of Br_2PTCDI-C18 n-type semiconductor molecule deposited on (a) PVA (b) PMMA (c) PVA/HMDS (d) PMMA/HMDS surfaces.

Figure 4.1(a) shows a schematic diagram of the OFETs prepared on an anodized Al_2O_3, employed in this study with different dielectric materials and HMDS surface modifying layer. OFETs were fabricated using 13 nm-thick anodized Al_2O_3/100 nm PVA, Al_2O_3/100 nm PVA/HMDS, Al_2O_3/100 nm PMMA and Al_2O_3/100 nm PMMA/HMDS on glass substrate. All the four devices were tested to identify the effect of channel length on the performance and stability of the OFETs. A thin HMDS layer has been grown to study the effect of HMDS on the growth of PVA or PMMA surfaces. In general, anodized aluminum films have extremely high rough surfaces. To reduce the surface roughness, a

TH-1703_11612241

100 nm PVA or PMMA film was spin coated on the anodized surfaces. The semiconductor films deposited on different dielectric materials were characterized using the AFM (Figure 4.2). The temperature and pressure during deposition were 50°C and ~10^{-6} mbar respectively. On to these films, organic semiconductor films were thermally deposited and characterized by the AFM.

The surface morphology of the Br_2PTCDI-C18 films on different substrates was characterized using AFM (Figure 4.2). The growth of Br_2PTCDI-C18 films on all HMDS treated substrates exhibited high structural order and displayed grain formation than the untreated films. However, the grain size was greatly varied from the substrates with different surface energy and surface roughness. Figure 4.2(a) shows the topography image of Br_2PTCDI-C18 deposited on PVA surface with an RMS roughness (σ) of 2.82 nm while on PMMA the RMS roughness was 3.02 nm (Figure 4.2(b)) within the 1.5 × 1.5 μm^2 scan scale. On the HMDS modified surface of PVA and PMMA, the RMS roughness (σ) was found to be 3.47 nm and 3.22 nm, respectively (Figure 4.2(c) & 4.2(d)). It was observed that the grain size increased with the modification of dielectric surface with HMDS due to the increased hydrophobicity that made the surface more favorable for the organic molecule growth. Although the RMS roughness of all the films were comparable (see Figure 4.2), the grain size was reduced on untreated substrates (approximately 100-120 nm).

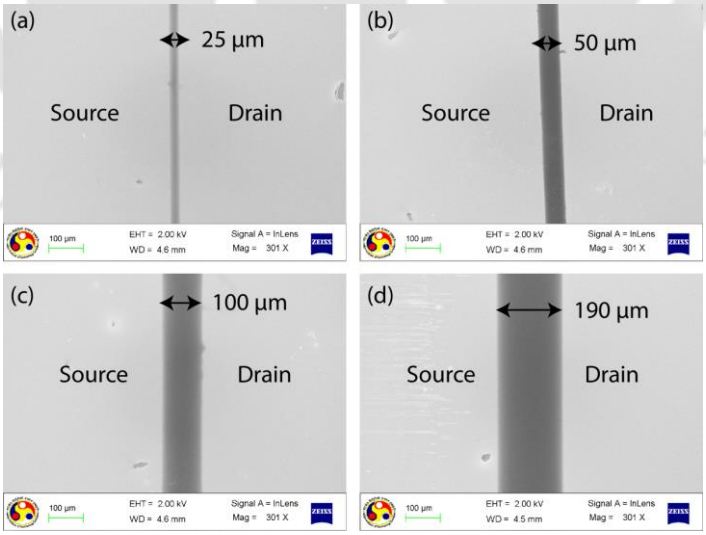

Figure 4.3. FESEM images of different channel lengths on the fabricated devices with same channel width 750 µm with channel length (a) 25 µm (b) 50 µm (c) 100 µm (d) 190 µm.

TH-1703_11612241

Br_2PTCDI-C18 OFETs were fabricated on different dielectric materials with varying channel length and characterized in the saturation regime, defined by the standard MOSFET models. To explore the influence of the different dielectric materials (13 nm Al_2O_3/100 nm PVA, 13 nm Al_2O_3/100 nm PMMA) and HMDS treatment on device performance, transistors with a channel length L = 25, 50, 100, 190 µm and a channel width W = 750 µm were compared. The FESEM images of the different channel length are shown in the Figure 4.3(a) - (d). Different diameters of copper wires were used as masks to define the varying channel length.

4.3.2. Devices fabricated with Al_2O_3/PVA as dielectric

Figure 4.4 depicts the output and transfer characteristic curves of the OFET devices fabricated using Al_2O_3/PVA as the dielectric material with different channel lengths. It can be clearly seen that the drain current (I_{DS}) decreased when the channel length increased. At 25 µm channel length, the I_{DS} at V_{DS} = 10V is 500 nA and which decreased to 380 nA at a channel length of 50 µm. It was further decreased to 250 nA and 120 nA for the 100 µm and 190 µm channel length, respectively. The data were analyzed by plotting the square root of the I_{DS} as a function of gate voltage (V_{GS}). The slope of a fit to the linear portion of this plot, above threshold, yields the field effect electron mobility (µ), while the gate voltage intercept of the fit line determines the threshold voltage (V_{Th}). The (inverse) sub-threshold slope is determined by a linear fit to the log(I_{DS}) just as the current begins to increase. $I_{on/off}$ ratios were determined using the minimum observed I_{DS} in the off region and the maximum current observed in the on region. The field-effect mobilities (µ) were obtained from the slope of a plot of $(I_{DS})^{1/2}$ against V_{GS}, using the equation,

$$I_{DS} = \frac{\mu_{FE} C_{diel} W}{2L} (V_{GS} - V_{Th})^2$$

Where, V_{Th} and C_{diel} are the threshold voltage and capacitance per unit area, respectively. The OFETs using Al_2O_3/PVA gate dielectrics exhibited mobility in the range of 0.012-0.025 cm^2/Vs for the different channel lengths. The threshold voltages were in the range of 0.23 V to -3.12 V. The averaged transistor parameters for OFETs for different channel lengths are summarized in Table 4.1. The µ value of the 25 µm channel length device was

TH-1703_11612241

2 times lower than OFET with μ of the 190 μm channel length prepared using same dielectric material.

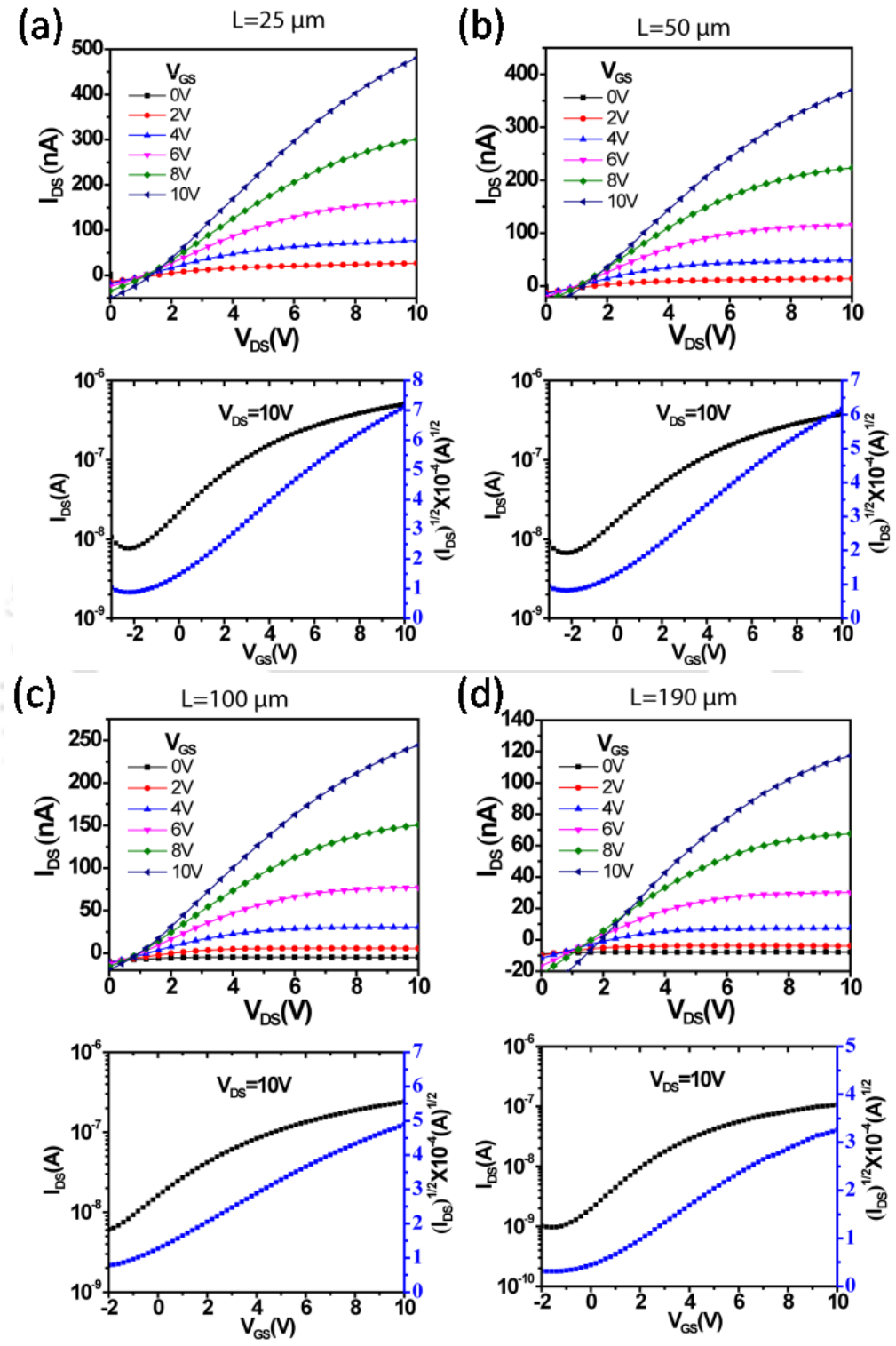

Figure 4.4. Output and transfer characteristics of the OFET device fabricated on the Al_2O_3/PVA as the dielectric material with different channel lengths (a) L= 25 μm (b) L= 50 μm (c) L=100 μm (d) L=190 μm.

TH-1703_11612241

Table 4.1. Summary of the electrical parameters of the Al_2O_3/PVA dielectric and Br_2PTCDI-C18 organic semiconductor based organic field effect transistors fabricated with different channel lengths measured under vacuum conditions inside the probe station.

Device	Al_2O_3/PVA/Br_2PTCDI-C18			
	L=25 µm	**L=50 µm**	**L=100 µm**	**L=190 µm**
µ(cm^2/Vs)	0.012	0.014	0.024	0.025
V_{Th}(V)	-2.15	-2.01	-3.12	0.23
S(V/dec)	3.95	4.02	4.15	4.36
$I_{on/off}$ ×10	1.7	1.5	1.3	1.5

4.3.3. Devices fabricated with Al_2O_3/PVA/HMDS as dielectric

Figure 4.5 shows the output and transfer characteristic curves of the OFET devices fabricated by surface modifying the Al_2O_3/PVA dielectric material with the HMDS layer for different channel lengths. It can be seen that the drain current (I_{DS}) slightly decreased compared to the unmodified layer (Figure 4.4). At 25 µm channel length, the I_{DS} at V_{DS} = 10V is 400 nA and is decreased to 350 nA at a channel length of 50 µm. It was further decreased to 320 nA and 80 nA for 100 µm and 190 µm channel length respectively. The OFETs using Al_2O_3/PVA/HMDS gate dielectrics exhibited high performance and mobility in the range of 0.011-0.013 cm^2/Vs for the different channel lengths. The threshold voltages are in the range of 0.15 V to 2.25 V. In addition, the threshold voltage and sub-threshold slope are improved compared to the unmodified device. The ‘‘on-off current ratio’’ also increased in these devices. The averaged transistor parameters for OFETs for different channel lengths are summarized in Table 4.2.

4.3.4. Devices fabricated with Al_2O_3/PMMA as dielectric

Figure 4.6 shows the output and transfer characteristic curves of the OFET devices fabricated using the Al_2O_3/PMMA dielectric material and Br_2PTCDI-C18 as the dielectric material at different channel lengths. Here also, it was observed that the drain current (I_{DS}) decreased compared to the PVA dielectric layer based devices but the threshold voltages and other properties improved. At 25 µm channel length, the I_{DS} at V_{DS} = 10V

TH-1703_11612241

was 80 nA and it decreased to 70 nA at a channel length of 50 µm. It was further decreased to 60 nA and 50 nA for the 100 µm and 190 µm channel length respectively. Field effect mobility was extracted for all the four transistors and was in the range of 0.0025 - 0.0045 cm^2/Vs. All the device parameters are tabulated in Table 4.3.

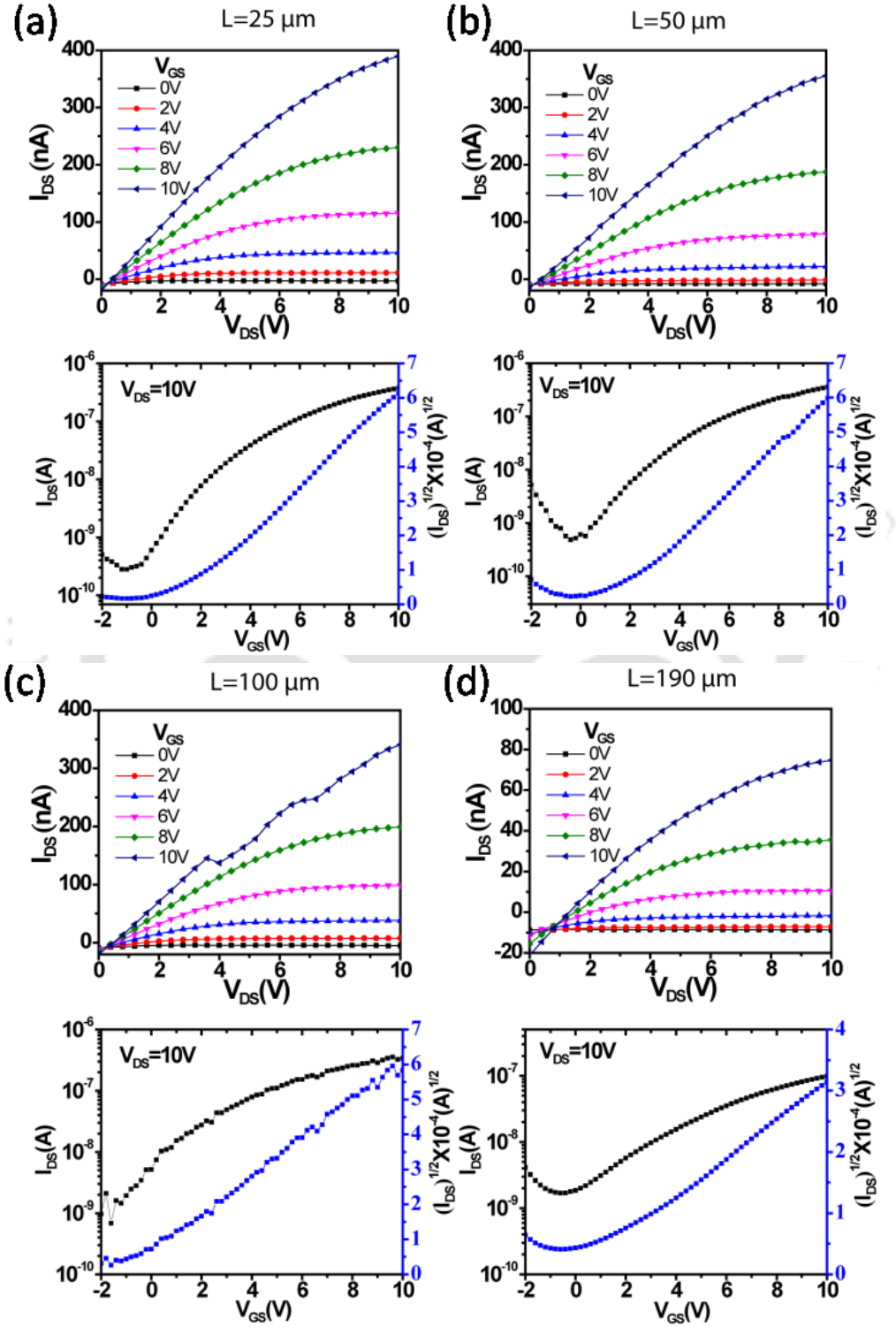

Figure 4.5. Output and transfer characteristics of the OFET device fabricated on the Al_2O_3/PVA/HMDS as the dielectric material with different channel length (a) L= 25 µm (b) L= 50 µm (c) L=100µm (d) L=190µm.

TH-1703_11612241

Table 4.2. Summary of the electrical parameters of the Al_2O_3/PVA/HMDS dielectric and Br_2PTCDI-C18 organic semiconductor based organic field effect transistors fabricated with different channel length measured under vacuum conditions inside the probe station.

	Al_2O_3/PVA/HMDS/Br_2PTCDI-C18			
Device	**L=25 µm**	**L=50 µm**	**L=100 µm**	**L=190 µm**
µ(cm^2/Vs)	0.011	0.012	0.012	0.013
V_{Th}(V)	2.25	2.14	0.15	0.29
S(V/dec)	2.75	2.52	3.15	3.37
$I_{on/off} \times 10^3$	3	2	2	1.6

Table 4.3. Summary of the electrical parameters of the Al_2O_3/PMMA dielectric and Br_2-PTCDI-C18 organic semiconductor based organic field effect transistors fabricated with different channel length measured under vacuum conditions inside the probe station.

	Al_2O_3/PMMA/ Br_2PTCDI-C18			
Device	**L=25 µm**	**L=50 µm**	**L=100 µm**	**L=190 µm**
µ(cm^2/Vs)	0.0025	0.0039	0.0042	0.0045
V_{Th}(V)	3.25	3.55	3.5	3.92
S(V/dec)	1.75	2.35	2.55	2.62
$I_{on/off} \times 10^4$	1	1	0.8	0.2

TH-1703_11612241

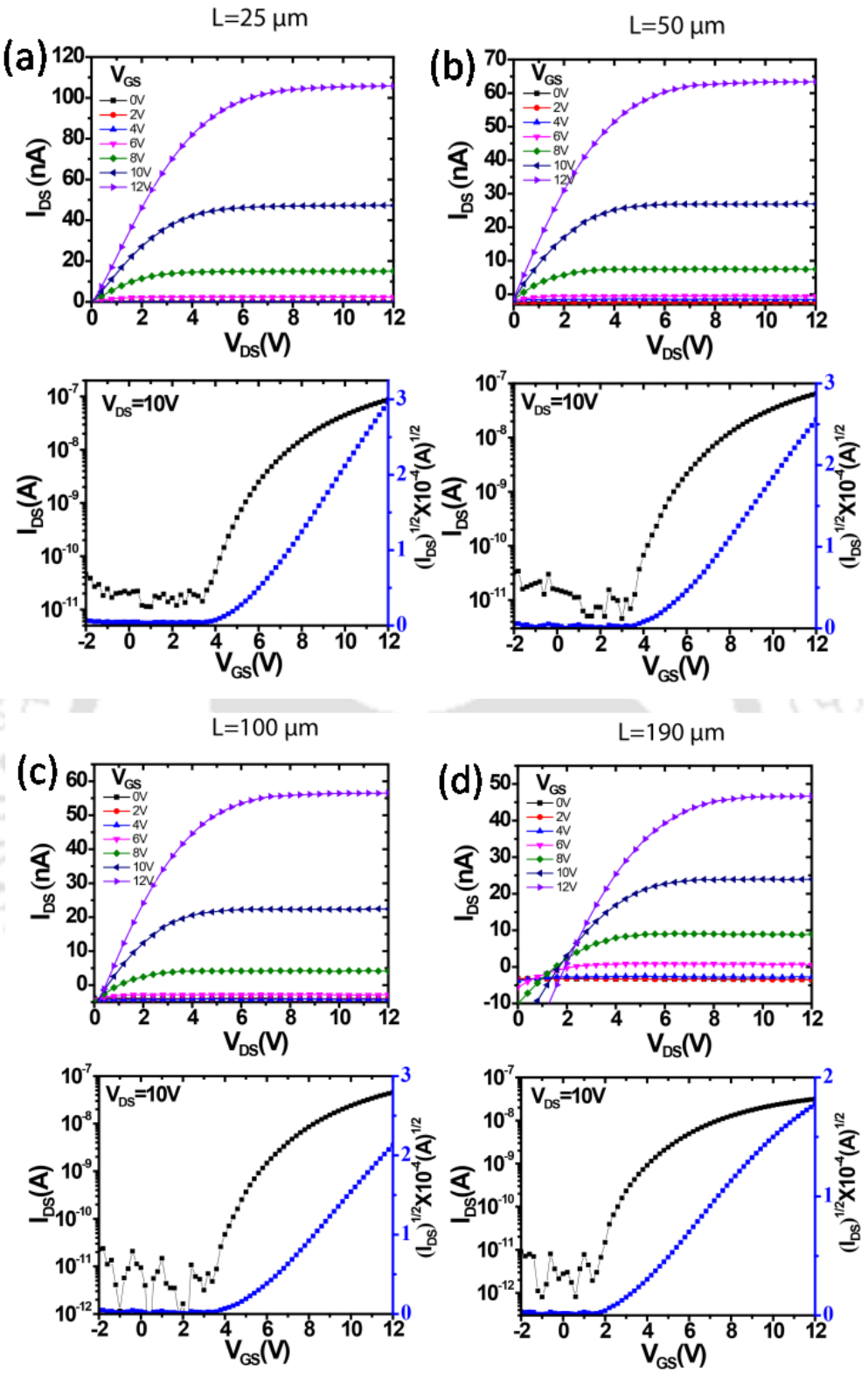

Figure 4.6. Output and transfer characteristics of the OFET device fabricated on the Al_2O_3/PMMA as the dielectric material with different channel length (a) L= 25 µm (b) L= 50 µm (c) L=100 µm (d) L=190 µm.

TH-1703_11612241

4.3.5. Devices fabricated with Al_2O_3/PMMA/HMDS as dielectric

Figure 4.7 shows the output and transfer characteristics curves of the OFET devices fabricated using the Al_2O_3/PMMA/HMDS dielectric material and Br_2PTCDI-C18 as the dielectric material at different channel lengths. It can be observed that the drain current (I_{DS}) increased compared to the PMMA dielectric layer based devices but the threshold voltages and other properties were also improved. At 25 µm channel length, the I_{DS} at V_{DS} = 10V is 120 nA and it decreased to 80 nA at a channel length of 50 µm. It was further decreased to 50 nA and 20 nA for the 100 µm and 190 µm channel length respectively. Field effect mobility was extracted for all the four transistors were in the range of 0.0015 - 0.0025 cm^2/V s. All the device properties were tabulated in Table 4.4.

Table 4.4. Summary of the electrical parameters of the Al_2O_3/PMMA/HMDS dielectric and Br_2PTCDI-C18 organic semiconductor based organic field effect transistors fabricated with different channel length measured under vacuum conditions inside the probe station.

	Al_2O_3/PMMA/HMDS/ Br_2PTCDI-C18			
Device	**L=25 µm**	**L=50 µm**	**L=100 µm**	**L=190 µm**
µ(cm^2/Vs)	0.0015	0.0023	0.0025	0.0014
V_{Th}(V)	-2.15	-2.01	-3.12	0.23
S(V/dec)	3.95	4.02	4.15	4.36
$I_{on/off} \times 10^4$	1.7	1.5	1.3	1.5

4.3.6. Variation of I_{DS} and Contact resistance with Channel length

Figure 4.8(a) shows the resistance vs channel length of the devices. All the devices exhibited linear increase in the resistance with the channel length. The contact resistances are extracted using the linear fitting of these curves by TLM (Transmission Line Method) and are shown in the Table 4.5. The contact resistance depends on the morphology of the organic semiconductor, nature of the dielectric material, grain size and density of the grain boundaries at the source/drain electrode.

TH-1703_11612241

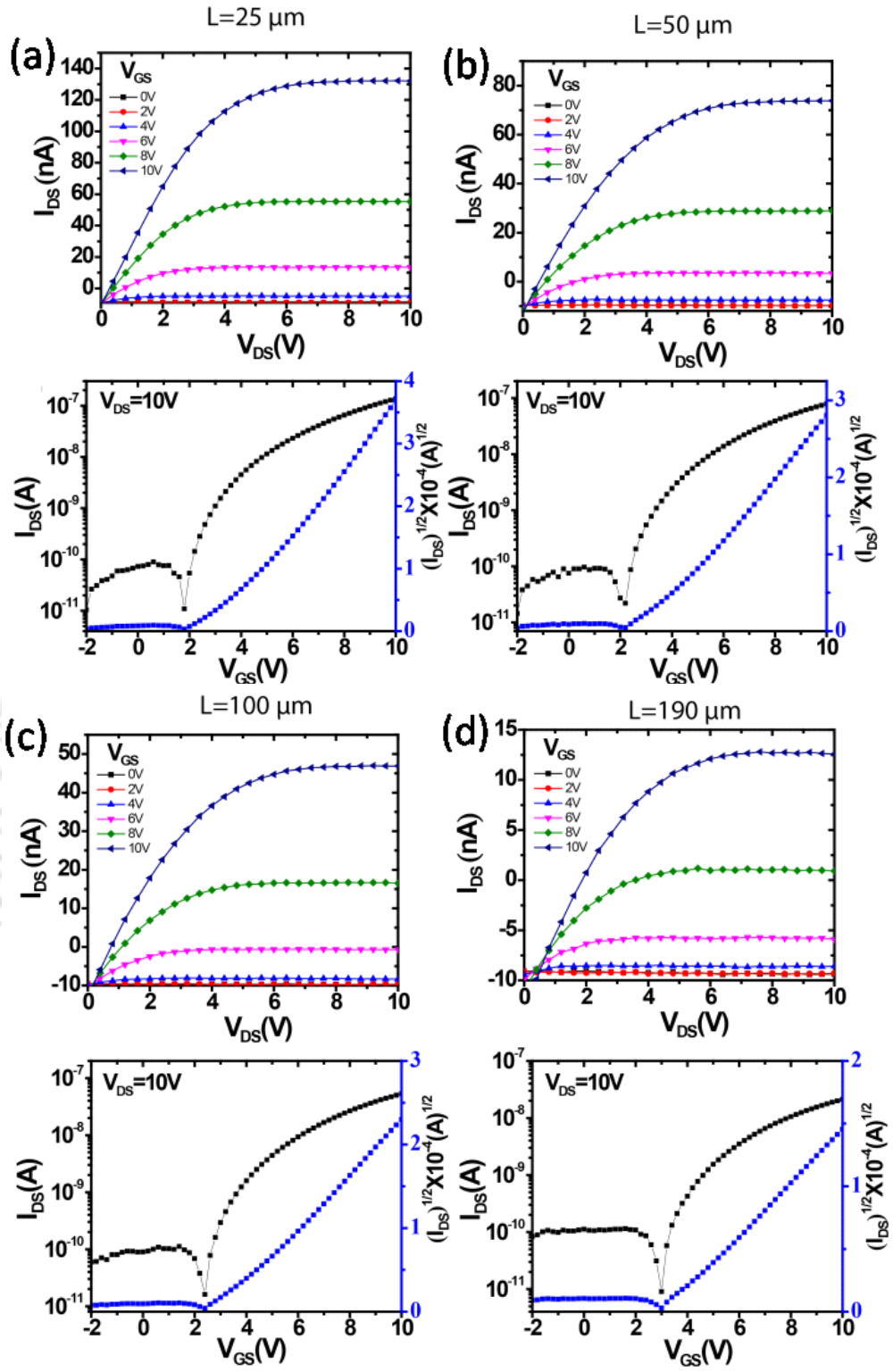

Figure 4.7. Output and transfer characteristics of the OFET device fabricated on the Al_2O_3/PMMA/HMDS as the dielectric material with different channel length (a) L= 25 µm (b) L= 50 µm (c) L=100 µm (d) L=190 µm.

TH-1703_11612241

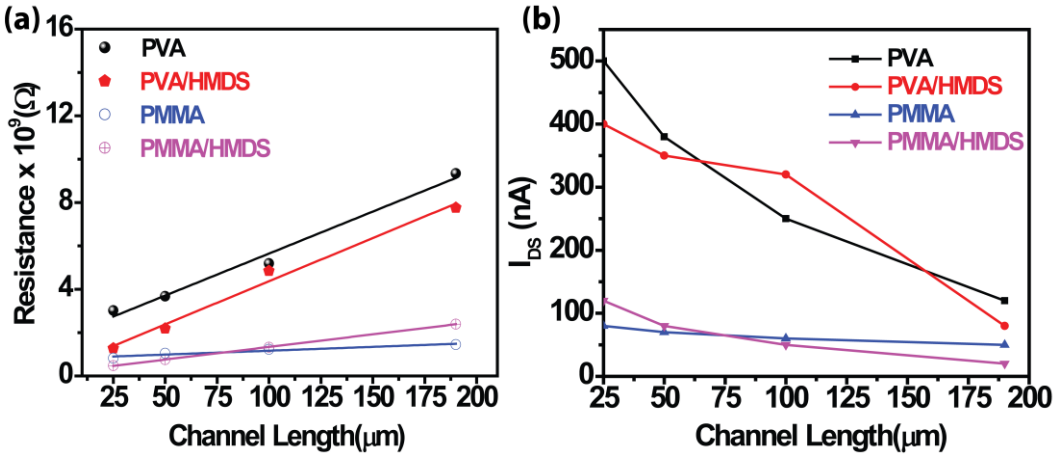

Figure 4.8. (a) Resistance vs channel length graph for the devices fabricated with different dielectric materials (b) I_{DS} vs Channel Length graph for the devices fabricated with different dielectric materials with channel lengths (L) 25 μm, 50 μm, 100 μm and 190 μm.

As number of charge traps in the channel of organic semiconductor increases the contact resistance also increases (Figure 4.8(b)). In case of the PVA dielectric the grain size of the deposited Br_2PTCDI-C18 is less compared to the HMDS treated one. This results in the higher density of grain boundaries at the electrode and OSC interface compared to HMDS treated device which causes high contact resistance.

Table 4.5. Summary of contact resistances calculated for the OFETs fabricated on different dielectrics Al_2O_3/PVA, Al_2O_3/PVA/HMDS, Al_2O_3/PMMA, Al_2O_3/PMMA/HMDS by Transmission line method.

Sl. No	Dielectric material used	Contact resistance(R_C)
1	Al/Al_2O_3/PVA/ Br_2PTCDI-C18	$R_C = 7.89\times10^8\ \Omega$
2	Al/Al_2O_3/PVA/HMDS/ Br_2PTCDI-C18	$R_C = 6.22\times10^8\ \Omega$
3	Al/Al_2O_3/PMMA/ Br_2PTCDI-C18	$R_C = 1.98\times10^8\ \Omega$
4	Al/Al_2O_3/PMMA/HMDS/ Br_2PTCDI-C18	$R_C = 1.38\times10^8\ \Omega$

After HMDS treatment the contact resistance reduced due to increase in the grain size. Because of the hydrophobic nature of the PMMA dielectric, the contact resistance is less than in case of PVA. After modification with the HMDS the contact resistance further

TH-1703_11612241

decreased as in the PVA dielectric. In all the above conditions, the PMMA/HMDS showed very low contact resistance, $1.38\times10^{8}\ \Omega$. The contact resistance also depends on the vertical overlap between gate with source - drain contacts. In this work, the overlaps of the contacts are kept same for all the devices.

4.3.7. Bias Stress measurements

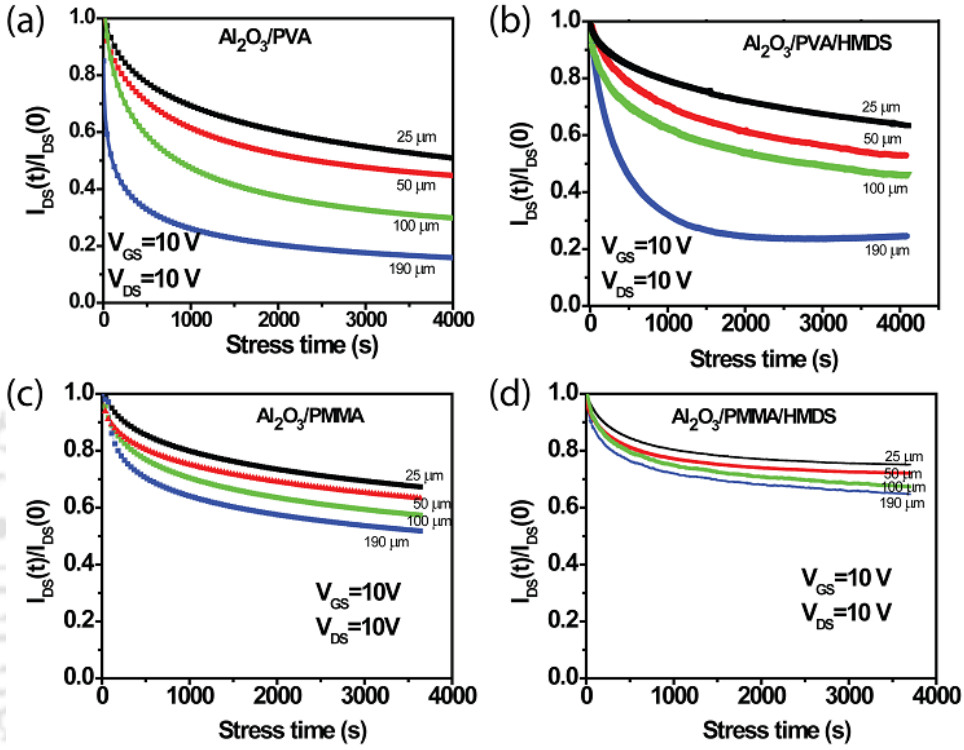

Figure 4.9. Bias stress measurements of the devices fabricated with different dielectric materials (a) Al_2O_3/PVA (b) Al_2O_3/PVA/HMDS (c) Al_2O_3/PMMA (d) Al_2O_3/PMMA/HMDS at different channel lengths 25 µm, 50 µm, 100 µm and 190 µm

In order to study the electrical stability of the devices under vacuum conditions, the bias stress measurements were performed on the devices for the different channel length. The device exhibited decay behavior of I_{DS} for 1h bias stress under vacuum conditions as shown in Figure 4.9(a) - (d). As channel length increases the increase in decay of the current is due to the more number of charge traps present in the higher channel length. For 25 µm channel length, in case of Al_2O_3/PVA the decay in the current is about 45% (Figure 4.9(a)), which reduced to 30% (Figure 4.9(b)) in case of Al_2O_3/PVA/HMDS. When the surface of the dielectric is modified by HMDS the decay is more due to the hydrophilic nature of PVA dielectric material. In contrast, for the device fabricated with

TH-1703_11612241

PMMA the decay in the current significantly reduced to 25% (Figure 4.9(c)) and upon surface modification of the dielectric with HMDS it is further decreased to below 20% (Figure 4.9(d)). The same trends were observed for all the devices fabricated with different channel lengths. Thus the device fabricated on Al_2O_3/PMMA/HMDS with 25 µm channel length show better stability among all the devices.

4.4. Conclusions

In conclusion, it was demonstrated that OFETs fabricated using oxide gate dielectrics modified with polymer dielectric materials and HMDS have greatly improved electrical properties compared to those fabricated using without HMDS layers. High-performance low-voltage operating Br_2PTCDI-C18 based OFETs on low cost glass substrates were fabricated and the effect of channel length, dielectric material and HMDS on the electrical properties of the OFETs with high stability with different channel lengths was studied. An anodized Al_2O_3 gate dielectric was developed. As the channel length of the device decreases the I_{DS} also increased. The devices fabricated on Al_2O_3/PVA/HMDS have shown better performance compared to other devices. HMDS layer significantly improved the $I_{on/off}$ ratios and electrical stability of the device. Electrical stabilities of the device were tested by stressing the device for one hour at 10 V. The device fabricated on the Al_2O_3/PMMA/HMDS show better stability due to hydrophobic nature of PMMA.

4.5. References

1. Heeger, A. J. *Adv. Mater.* **2014,** *26* (1), 10-28.
2. Hwang, Y. J.; Courtright, B. A. E.; Ferreira, A. S.; Tolbert, S. H.; Jenekhe, S. A. *Adv. Mater.* **2015,** *27* (31), 4578-4584.
3. Kalyani, N. T.; Dhoble, S. J. *Renew. Sust. Energ. Rev.* **2012,** *16* (5), 2696-2723.
4. Newman, C. R.; Frisbie, C. D.; da Silva, D. A.; Bredas, J. L.; Ewbank, P. C. *Chem. Mater.* **2004,** *16* (23), 4436-4451.
5. Dong, H. L.; Fu, X. L.; Liu, J.; Wang, Z. R.; Hu, W. P. *Adv. Mater.* **2013,** *25* (43), 6158-6182.
6. Lee, B. H.; Hsu, B. B. Y.; Patel, S. N.; Labram, J.; Luo, C.; Bazan, G. C.; Heeger, A. J. *Nano. Lett.* **2016,** *16* (1), 314-319.
7. Kaltenbrunner, M.; Sekitani, T.; Reeder, J.; Yokota, T.; Kuribara, K.; Tokuhara, T.; Drack, M.; Schwodiauer, R.; Graz, I.; Bauer Gogonea, S.; Bauer, S.; Someya, T. *Nature* **2013,** *499* (7459), 458-463.
8. Ji, D. Y.; Jiang, L.; Cai, X. Z.; Dong, H. L.; Meng, Q.; Tian, G. F.; Wu, D. Z.; Li, J. Z.; Hu, W. P. *Org. Electron.* **2013,** *14* (10), 2528-2533.

TH-1703_11612241

9. McCarthy, M. A.; Liu, B.; Donoghue, E. P.; Kravchenko, I.; Kim, D. Y.; So, F.; Rinzler, A. G. *Science* **2011,** *332* (6029), 570-573.
10. Subramanian, V.; Chang, P. C.; Lee, J. B.; Molesa, S. E.; Volkman, S. K. *Ieee. T. Compon. Pack. T.* **2005,** *28* (4), 742-747.
11. Zhang, C. C.; Chen, P. L.; Hu, W. P. *Chem. Soc. Rev.* **2015,** *44* (8), 2087-2107.
12. Reese, C.; Bao, Z. *Adv. Funct. Mater.* **2009,** *19* (5), 763-771.
13. Tseng, H. R.; Phan, H.; Luo, C.; Wang, M.; Perez, L. A.; Patel, S. N.; Ying, L.; Kramer, E. J.; Nguyen, T. Q.; Bazan, G. C.; Heeger, A. J. *Adv. Mater.* **2014,** *26* (19), 2993-2998.
14. Zhang, C.; Zhang, J.; Zeng, W. X.; Zheng, N. H.; Li, W.; Gao, W.; Yu, G.; Yang, C. L. *Polym. Chem.* **2016,** *7* (16), 2808-2814.
15. Kraft, U.; Sejfic, M.; Kang, M. J.; Takimiya, K.; Zaki, T.; Letzkus, F.; Burghartz, J. N.; Weber, E.; Klauk, H. *Adv. Mater.* **2015,** *27* (2), 207-214.
16. Usta, H.; Facchetti, A.; Marks, T. J. *Accounts. Chem. Res.* **2011,** *44* (7), 501-510.
17. Klauk, H.; Zschieschang, U.; Pflaum, J.; Halik, M. *Nature* **2007,** *445* (7129), 745-748.
18. Sirringhaus, H. *Adv. Mater.* **2014,** *26* (9), 1319-1335.
19. Zhao, Y.; Guo, Y. L.; Liu, Y. Q. *Adv. Mater.* **2013,** *25* (38), 5372-5391.
20. Zhan, X. W.; Facchetti, A.; Barlow, S.; Marks, T. J.; Ratner, M. A.; Wasielewski, M. R.; Marder, S. R. *Adv. Mater.* **2011,** *23* (2), 268-284.
21. Jones, B. A.; Facchetti, A.; Wasielewski, M. R.; Marks, T. J. *J. Am. Chem. Soc.* **2007,** *129* (49), 15259-15278.
22. Tang, M. L.; Oh, J. H.; Reichardt, A. D.; Bao, Z. N. *J. Am. Chem. Soc.* **2009,** *131* (10), 3733-3740.
23. Jiang, W.; Li, Y.; Wang, Z. H. *Accounts. Chem. Res.* **2014,** *47* (10), 3135-3147.
24. Piliego, C.; Cordella, F.; Jarzab, D.; Lu, S.; Chen, Z.; Facchetti, A.; Loi, M. A. *Appl. Phys. A.* **2009,** *95* (1), 303-308.
25. Piliego, C.; Jarzab, D.; Gigli, G.; Chen, Z. H.; Facchetti, A.; Loi, M. A. *Adv. Mater.* **2009,** *21* (16), 1573.
26. Jones, B. A.; Facchetti, A.; Wasielewski, M. R.; Marks, T. J. *Adv. Funct. Mater.* **2008,** *18* (8), 1329-1339.
27. Clikeman, T. T.; Bukovsky, E. V.; Wang, X. B.; Chen, Y. S.; Rumbles, G.; Strauss, S. H.; Boltalina, O. V. *Eur. J. Org. Chem.* **2015,** (30), 6641-6654.
28. Zhao, D. L.; Wu, Q. H.; Cai, Z. X.; Zheng, T. Y.; Chen, W.; Lu, J.; Yu, L. P. *Chem. Mater.* **2016,** *28* (4), 1139-1146.
29. Vajiravelu, S.; Lygaitis, R.; Grazulevicius, J. V.; Gaidelis, V.; Jankauskas, V.; Valiyaveettil, S. *J. Mater. Chem.* **2009,** *19* (24), 4268-4275.
30. Li, G.; Zhao, Y. B.; Li, J. B.; Cao, J.; Zhu, J.; Sun, X. W.; Zhang, Q. C. *J. Org. Chem.* **2015,** *80* (1), 196-203.
31. Costa, R. D.; Cespedes-Guirao, F. J.; Orti, E.; Bolink, H. J.; Gierschner, J.; Fernandez-Lazaro, F.; Sastre-Santos, A. *Chem. Commun.* **2009,** (26), 3886-3888.
32. Liu, C. M.; Xiao, C. Y.; Li, Y.; Hu, W. P.; Li, Z. B.; Wang, Z. H. *Chem. Commun.* **2014,** *50* (83), 12462-12464.

TH-1703_11612241

33. Rajaram, S.; Shivanna, R.; Kandappa, S. K.; Narayan, K. S. *J. Phys. Chem. Lett.* **2012,** *3* (17), 2405-2408.
34. Ortiz, R. P.; Facchetti, A.; Marks, T. J. *Chem. Rev.* **2010,** *110* (1), 205-239.
35. Park, S.; Lim, B. T.; Kim, B.; Son, H. J.; Chung, D. S. *Sci. Rep.* **2014,** *4*.
36. Facchetti, A.; Yoon, M. H.; Marks, T. J. *Adv. Mater.* **2005,** *17* (14), 1705-1725.
37. Peng, J.; Sun, Q. J.; Wang, S. D.; Wang, H. Q.; Ma, W. L. *Appl. Phys. Lett.* **2013,** *103* (6), 061603.
38. Xu, W. T.; Rhee, S. W. *J. Mater. Chem.* **2009,** *19* (29), 5250-5257.
39. Vasimalla, S.; Senanayak, S. P.; Sharma, M.; Narayan, K. S.; Iyer, P. K. *Chem. Mater.* **2014,** *26* (13), 4030-4037.

TH-1703_11612241

Chapter 5

Low voltage, low cost, flexible ambipolar OFETs based on Br_2PTCDI-C18/CuPc fabricated on Al foil gate substrates

5.1. Introduction

The application of organic field effect transistors (OFETs) increased drastically in recent years due to their low cost and easy fabrication process compared to the inorganic transistors, where highly sophisticated equipments and clean room facility are prerequisites.[1,2] OFETs are used to understand the fundamental physics of charge transport, existence of trap states and also in light emitting field-effect transistors for organic active matrix displays[3,4] radio frequency identification components,[5] bio/chemical sensors,[6] and inverters.[7,8] Fabrication of devices on low cost, flexible substrates is highly desirable for biosensor applications, which need low operating voltage, disposable devices. The stability of the OFETs is the main hindering factor preventing the use of these devices for real applications. There are three stability parameters, viz., electrical stability, environmental stability and long term stability/durability. For electrical stability the performance of the device is studied by stressing the device for longer periods with the application of constant gate and drain voltages. For environmental stability the device performance is studied under ambient conditions like humidity, temperature, etc. The above stability parameters can be optimized by choosing suitable material candidates and by proper device engineering. Generally, n-type materials are unstable as compared to the p-type materials under ambient conditions due to their interaction with the water and oxygen molecules in the atmosphere and their high lying lowest unoccupied molecular orbital (LUMO) energy levels.[9] Numerous stable and innovative organic semiconducting

TH-1703_11612241

materials were synthesized by tuning the highest occupied molecular orbital (HOMO) and (LUMO) energy levels with different structural modifications or functionalizations. In any device, besides the prominent role of organic semiconductor the overall stability and performance is also dependent on other material/layers used in the fabrication. In addition to the above parameters, the fabrication cost and the fabrication time are equally vital parameters required for sustainable and large scale production. Various attempts have been made to reduce the cost of the OFET devices by fabricating them on economical glass and flexible plastic substrates by replacing the conventional silicon substrates.[10-12]

OFETs have been utilized in the fabrication of inverters and logic circuit in the digital electronics applications.[13-16] For such applications both n-type and p-type transistors are needed to transport the electrons and holes. Achieving balanced and high hole and electron mobility with a single component organic semiconductor is difficult because of the problem of unequal charge carrier injection into the semiconductor.[17] Ambipolar OFETs have shown moderate progress in the last three decades after the first report on ambipolar OFET based on phthalocyanine derivative appeared.[18] For an ambipolar OFET to be competent, a single semiconducting material must be able to transport both charge carriers in the accumulation channel of the device. Hence, different approaches have been used to achieve this goal such as using different source and drain electrodes for same organic semiconductor,[19,20] the formation of layer by layer heterojunction structures by depositing electron and hole transporting organic layers of different thicknesses,[21-23] the composite blending of p-type and n-type organic semiconductors in an appropriate ratio[24,25] and the synthesis of polymers containing both n-type and p-type molecules in the same chain.[26] These ambipolar OFETs which can exhibit both n-type and p-type behavior to enable efficient transport of both electrons and holes in the single device simultaneously are becoming highly desirable for the fabrication of organic integrated electronic circuits with potential industrial applications. Device stability is also a major challenge to achieving air stable ambipolar OFETs.[27] In addition to the organic molecule, the dielectric material also plays a crucial role in the stability of the ambipolar devices. Most of the ambipolar characteristics reported in the literature are based on bottom contact SiO_2 gate dielectrics, where a heavily doped Si wafer serve as gate electrode and substrate with Au as a source/drain contacts. Such a rigid substrate requirement limits the flexibility of the composed circuits. Further, SiO_2 layers may contain a high density of

TH-1703_11612241

hydroxyl groups known as electron traps, which significantly suppresses the device characteristics and degrade the performance. With newer applications requiring portable and light weight materials the prerequisite of fabricating these devices on flexible and inexpensive substrates remains an immediate goal.[28] Low cost and high dielectric constant PVA polymer and hydrophobic PMMA layers can provide stable performance with less degradation even under ambient high humidity conditions. Low band gap organic semiconductors, especially small molecule based semiconductors, are more promising candidates for achieving low cost ambipolar OFETs than polymers because of their higher purity and ease of processing. Among all the deposition methods, vacuum-deposited small molecules exhibit certain advantages in terms of purity, growth, morphology and control in the thickness in the nm range. Small molecule materials are also easier to synthesize and high chemical purity can be achieved using techniques such as vacuum sublimation. Therefore, bilayer heterojunction structures appear to be one of the most promising approaches presently for ambipolar OFET device fabrication.

In this chapter, the fabrication and characterization of ambipolar OFETs on flexible Al foil gated OHP sheet substrate, which makes the device inexpensive with easy and rapid fabrication yet achieving very low operating voltages of 3V is presented for the first time. The anodized Al foil is coated with a PMMA/PVA and C-PVA dielectric material. These devices are stable in air and operate in the hole and the electron transporting regime. The fabrication of top contact bottom gate ambipolar OFETs with a bilayer structure using Br_2PTCDI-C18 as n-type and CuPc as p-type semiconducting materials is discussed elaborately. To reduce the leakage current and operating voltage, anodized Al_2O_3 modified with PVA and PMMA in first case and C-PVA in the other device, as a buffer gate dielectric layer, is used instead of the commonly used SiO_2 layer. Br_2PTCDI-C18/CuPc heterostructure ambipolar OFETs were optimized for reducing the operating voltage, a prerequisite for using such devices for several practical applications including biomedical devices. Very low operating voltages of 3V were achieved by using the cross linked PVA as the gate dielectric both in the p-type and n-type modes. The electrical, ambient and long-term stabilities of the devices were also significantly improved overcoming several major challenges in ambipolar OFETs.

TH-1703_11612241

5.2. Experimental section

5.2.1. Synthesis of Br_2PTCDI-C18

The n-Channel molecule Br_2PTCDI-C18 was synthesized and characterized using the reported procedure[29] whereas CuPc was commercially procured. The structure of the molecules and their energy diagrams are shown in the Figure 5.1(a) & (b).

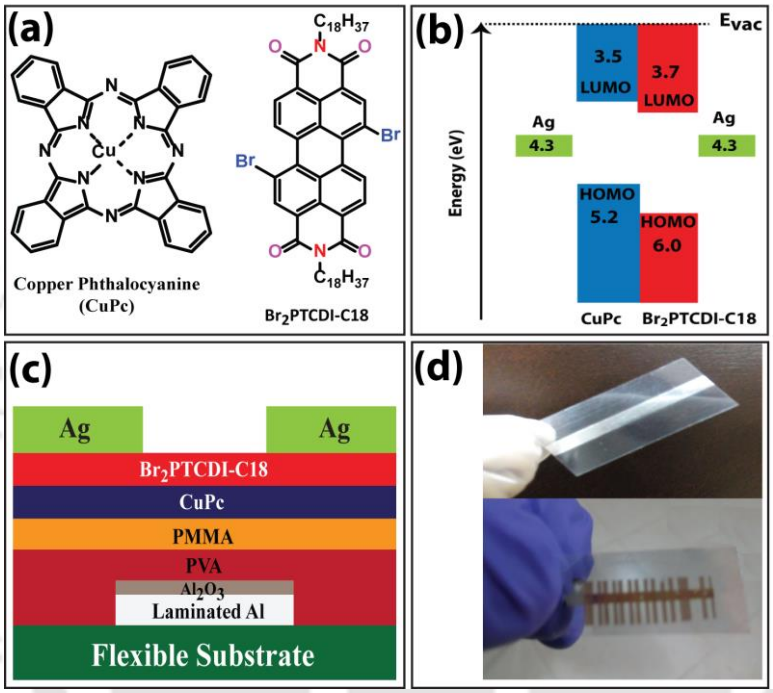

Figure 5.1. (a) Structures of the molecules (b) Energy level diagram (c) Schematic illustration of the OFET device (d) Photograph Images of flexible substrate with Al foil as gate and final device.

5.2.2. Fabrication of ambipolar OFET devices

Ambipolar OFETs with top contact bottom gate configurations were fabricated on a readily available pristine OHP plastic sheet which is less than a fraction of the cost of any reported commercial substrate. The schematic illustration of the device is shown in the Figure 5.1(c). Additionally it can be cut into desired shape and size by a knife or scissors for a device. Furthermore, an economical gate electrode using the aluminum foil (~30 µm thick) commonly found in laboratory/kitchen, was cut using a scissors into strips and laminated on top of the OHP sheet at ~100 °C using a lamination machine at a general book store. The Al laminated plastic strips were degreased through cleaning in soap solution and water repeatedly several times and finally were sonicated in deionized water

TH-1703_11612241

thrice to remove the contaminants. The films were dried under vacuum conditions at 70-80 °C for 2h to remove the solvent residues. The top surface of the Al was anodized to get 30 nm Al_2O_3 by anodization technique. Al_2O_3 layer has high dielectric constant and acts as a barrier layer to reduce the leakage current. The anodization process was carried out using 0.001M citric acid monohydrate ($C_6H_8O_7.H_2O$) as electrolyte and the laminated gates on flexible substrates were then immersed into aqueous electrolyte solution to form the working electrode (anode), whereas the platinum mesh served as a counter electrode (cathode). To perform the anodic oxidation, a constant current density j = 0.4 mA/cm^2 was driven through the electrolyte using Keithley 2400 source meter as constant voltage source. A constant current across the growing insulating Al_2O_3 layer was maintained by ramping up the voltage up to a limiting anodization voltage V_A, which was then maintained for several minutes until the current had completely decayed to below ~6μA. From electrochemical theory, the thickness of the oxide layer per unit applied voltage is called Anodization ratio (C_{Al}). For aluminum the anodization ratio is C_{Al} = 1.3 nm/V. Here we used 30 nm Al_2O_3 as the barrier dielectric layer. At 23V, the thickness will be ~30nm. We also confirmed this thickness by using a profilometer by etching the anodized layer using sodium hydroxide solution. The removed alumina layer forms step with the un-anodized film and measured using the profilometer to know the thickness of the oxidized layer. These results were compared with the calculated values using the formula: thickness = $C_{Al} \times V_A$. The samples were rinsed in high-purity hot milli Q water and dried on a hot plate to remove the acid traces and water. To further make the surface smooth and reduce the number of interface traps, thin polymer films were spin coated without any electro or mechanical polishing. Here, PMMA/PVA and C-PVA were used as the polymer dielectric materials with anodized Al_2O_3. A PVA (Sigma Aldrich, M_W = 76,500 - 81,000 kg/mol) solution was prepared by dissolving it in 30 mg/mL de-ionized water. Ammonium dichromate was used as the cross-linking agent for PVA dielectric. The polymer and cross-linking agent mixed in 6:1 mass ratio were dissolved in deionized water. The insulator films were spin coated from the polymer/cross-linking agent solution at 3000 rpm, and the spin-coated films were cross linked for 60 min using an ultraviolet UV lamp followed by annealing at 60°C for 1h in a vacuum oven. The thickness of the C-PVA dielectric layer was found to be 30 nm measured using Dektak profilometer (Dektak-150). On another substrate, 70 nm thick PVA layer was deposited using spin coating at 3000 rpm for 60 sec, followed by vacuum annealing at 70°C for 2h to remove

TH-1703_11612241

residual solvent and to improve the film quality. As a second layer, PMMA (Sigma Aldrich, M_W = 5,50,000 kg/mol) 10 mg/mL dissolved in anisole (Sigma Aldrich) was deposited using spin coating to get ~30 nm thick layer, followed with vacuum annealing at 70°C for 2h. A 30 nm thick CuPc film was deposited followed by vacuum deposition of 20 nm Br_2PTCDI-C18 layer on to the PMMA/PVA/Al_2O_3 and C-PVA dielectrics under identical conditions at a rate 0.8 nm/min using thermal evaporation at a base pressure of ~10^{-6} mbar at 60°C substrate temperature. Finally, using a thermal vacuum deposition chamber, 50 nm thick silver (Ag) source/drain (S/D) electrodes was deposited. The channel length (L) and channel width (W) were predefined as 25 µm and 750 µm respectively with width/length (W/L) ratio as 30. Images of the laminated Al foil on pristine OHP sheet and the final devices were shown in the Figure 5.1(d). The surface morphology of the dielectric and semiconducting films were characterized in air using atomic force microscopy (Agilent AFM/STM 5500) in tapping mode and the dielectric thickness was measured by using a Dektak profilometer (Dektak-150). Electrical characterization of the OFETs were carried out in a probe station (Lake Shore, <1×10^{-4} mbar). All the capacitance-electric field (C-E) measurements, current-voltage (I-V) characteristics and bias-stress measurements of OFETs were collected with a Keithley 4200-SCS semiconductor parameter analyser. The key device parameters such as μ_{FE}, on/off current ratio (I_{on}/I_{off}) and threshold voltage (V_{Th}), were extracted using equations of drain currents in the saturation region:

$$I_{DS} = \frac{\mu_{FE} C_{diel} W}{2L} \left(V_{GS} - V_{Th}\right)^2$$

Where, C_{diel} is the capacitance of the dielectric layer per unit area, V_{GS} and V_{Th} are the gate voltage and threshold voltage, respectively. A linear fit was applied in the saturation region of V_{GS} vs $(I_{DS})^{1/2}$ curve in order to calculate the mobility.

5.3. Results and discussions

5.3.1. Leakage current and capacitance measurements

The device properties are critically dependent on the thickness, surface roughness and morphology of the different layers in these devices. The thicknesses of the individual

TH-1703_11612241

layers were optimized to achieve low leakage current and high capacitance with good performance. MIM structures were fabricated by depositing the top Al onto the gate dielectrics to prepare the capacitors. The leakage current measurements and capacitance-voltage measurements were performed by Keithley 4200 source/measure unit. Figure 5.2(a) shows the leakage current characteristics of the PMMA/PVA and cross-linked PVA (C-PVA) dielectric materials used for the fabrication of ambipolar OFETs. The leakage current densities for PMMA/PVA and C-PVA films were typically in the range of 10^{-9} A/cm^2 which is low to be used as films in the fabrication of OFETs. Figure 5.2(b) shows the variation of capacitance of the PMMA/PVA and C-PVA MIM capacitor structures with applied voltage measured at 100 kHz. The capacitance of the PMMA/PVA was found to be 13 nF/cm^2, whereas for the C-PVA the value was 82 nF/cm^2. The high capacitance of the C-PVA is due to the high dielectric constant of PVA (k = 10) and less thickness (30 nm).

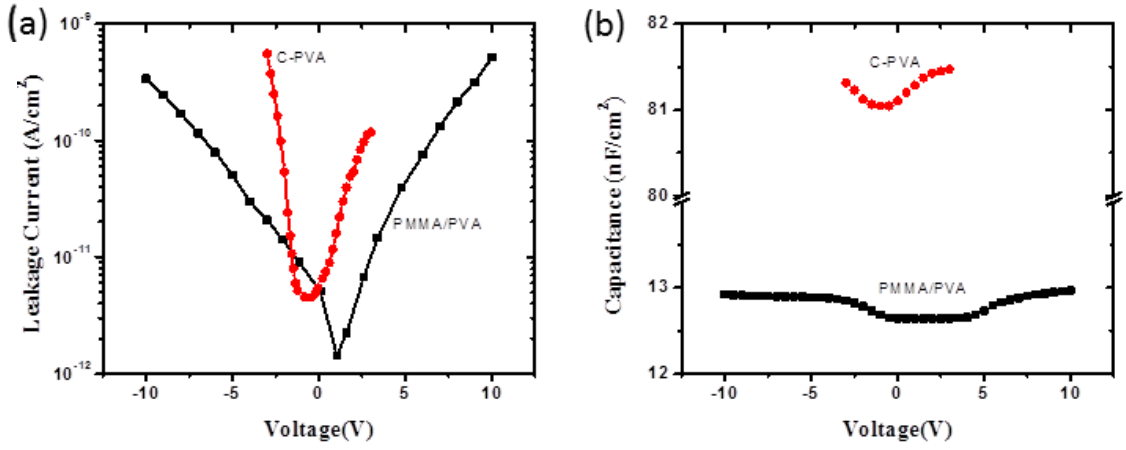

Figure 5.2. (a) I-V characteristics of bilayer polymer (PMMA/PVA) dielectrics and cross-linked PVA (C-PVA) dielectric materials. (b) Capacitance of polymer dielectrics films. Measurements were carried out at 100 kHz.

5.3.2. Morphology of different layers in the flexible OFET device

Ambipolar OFET devices were fabricated on flexible substrates by laminating the patterned Al foil as the gate electrode. Pristine Al foil was used without any further treatment, such as mechanical or electro polishing. The morphologies of gate surfaces and polymer thin films were characterized by using AFM in tapping mode. The morphology and RMS roughness of the laminated Al was measured by using AFM images and analyzed using WSXM software. The morphology and RMS roughness of the dielectric

TH-1703_11612241

layers directly related to the density of the trap states at the interface. A higher trap density at interface can significantly reduce the carrier mobility and device performance. Highly smooth interfaces are preferable for the fabrication of the OFETs. Figure 5.3(a) shows the AFM topography image of the laminated Al surface and the RMS roughness is found to be 21 nm. These films were anodized in order to grow the barrier oxide layer to reduce the leakage current. After anodization, it could be seen (Figure 5.3(b)) that the corresponding RMS roughness of the anodized Al surface was 33 nm, which is increased due to the oxidation and etching processes in anodization. After spin coating the PMMA/PVA layer on the anodized Al, the surface becomes smooth and the roughness was reduced to 5.8 nm (Figure 5.3(c)). For the fabrication of OFETs, organic layers were deposited on the smooth dielectric material surface. Figure 5.3(d) shows the morphology of the thermally deposited organic molecules bilayer top surface, having RMS roughness 1.3 nm.

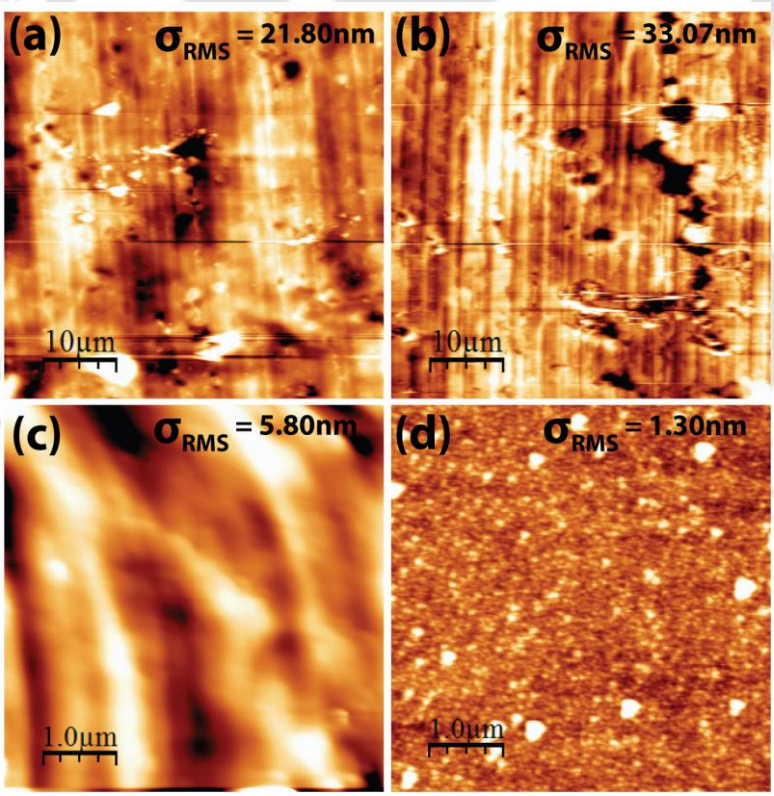

Figure 5.3. AFM topographical images of (a) Laminated Al foil (b) Anodized Al foil (c) PMMA/PVA spin coated on the anodized surface (d) after the deposition of the organic molecules CuPc and Br_2PTCDI-C18.

TH-1703_11612241

5.3.3. Device Characterization under vacuum conditions

5.3.3.1. Transfer and Output Characteristics

OFET devices were fabricated with CuPc and Br_2PTCDI-C18 heterostructure on a PMMA/PVA coated flexible substrate. The devices showed typical ambipolar (both p-channel and n-channel) characteristics measured under vacuum conditions.

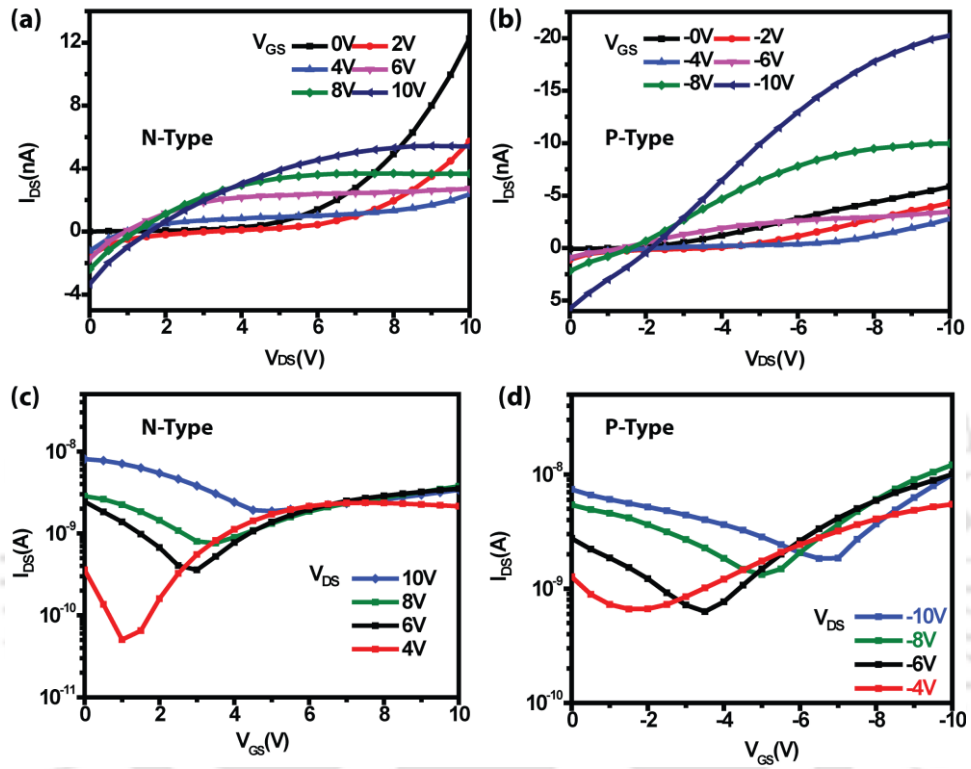

Figure 5.4. Output characteristics of the ambipolar device fabricated using PMMA/PVA as the dielectric material (a) n-type (b) p-type. Transfer characteristics of the ambipolar device fabricated using PMMA/PVA as the dielectric material (c) n-type (d) p-type measured under vacuum conditions.

Typical output characteristics of the ambipolar PMMA/PVA dielectric based OFETs measured under vacuum conditions are shown in Figure 5.4(a) and 5.4(b). For positive gate voltages, the transistor is in the electron-enhancement mode and for negative gate voltages the transistor is in the hole-enhancement mode. The magnitude of the drain currents in both regimes differs for these devices. The p-channel (negative V_{GS}) shows a current which is three times in magnitude higher than the current in the n-channel (positive V_{GS}). This is a clear signature of ambipolar behavior. Electrons are injected at higher drain voltages into the electron-conducting channel, and *vice versa*. In both

TH-1703_11612241

measurements the curvature in the output characteristics did not originate from the zero of the I−V diagram which suggests the existence of injection barriers with nonlinear contact resistances. Herein, this contact resistance is also visible in the electron channel and is even more pronounced in the hole channel because the conductivity of both channels is reduced due to mutual dilution of the conducting material by the other species.[30,31]

It can be observed that the current and transfer behavior of the devices depended on the applied drain voltage. Figure 5.4(c) and Figure 5.4(d) shows the transfer transistor characteristics measured under vacuum for the PMMA/PVA device. The transfer characteristics show the off regime behavior and it was dependent on the applied gate voltage. The corresponding mobilities were calculated and are tabulated in Table 5.1.

Table 5.1. Summary of the electrical parameters of the PMMA/PVA dielectric based organic field effect transistor measured under vacuum conditions.

Device	V_{DS}	μ(cm^2/Vs)	V_{Th}(V)	S(V/dec)	$I_{on/off}$ ×10
n-type	10	8.8×10^{-5}	-7.25	8.52	1
	8	2.6×10^{-3}	-2.01	5.02	1
	6	1.2×10^{-2}	1.11	3.14	2
	4	2.5×10^{-3}	0.66	1.01	2
p-type	-10	2.7×10^{-3}	-4.98	6.75	~1
	-8	3.4×10^{-3}	-3.64	3.13	~1
	-6	5.5×10^{-3}	-2.52	2.25	1.5
	-4	7.3×10^{-3}	0.85	1.21	1.5

As shown in Figure 5.4(a) - (d) the device exhibited ambipolar behavior for the n- and p-type measurements. Ambipolar behavior was observed for all devices with electron and hole mobilities with values as high as 1.2×10^{-2} cm^2/Vs and 5.5×10^{-3} cm^2/Vs, respectively, which were derived from saturated currents. For the electron conduction, large negative value of the threshold voltage was observed. Furthermore, the mobility variations with the applied V_{GS} are shown in the Table 5.1. The current on/off ratios are

TH-1703_11612241

in the range of 10^1-10^2 for the p- and n-channel transport. This is the first example for the flexible ambipolar organic field-effect transistor fabricated on the low cost Al laminated substrate for applications in low-cost organic electronics with such high mobility values.

5.3.3.2. Dual Sweep Characteristics of PMMA/PVA device

Figure 5.5(a) & (b) shows the dual sweep transfer characteristic curves of the device for the n- and p-type transport measured under vacuum conditions. The p-type transport exhibited severe hysteresis, whereas n-type transport showed negligible hysteresis. In addition both the transports exhibited the anti-clockwise hysteresis (ACH). Clock wise hysteresis is due to the charge traps at the dielectric and semiconductor interface, where as in this case it may be due to the slow polarization of polar dipoles in the dielectric materials with the applied gate voltage under vacuum conditions.

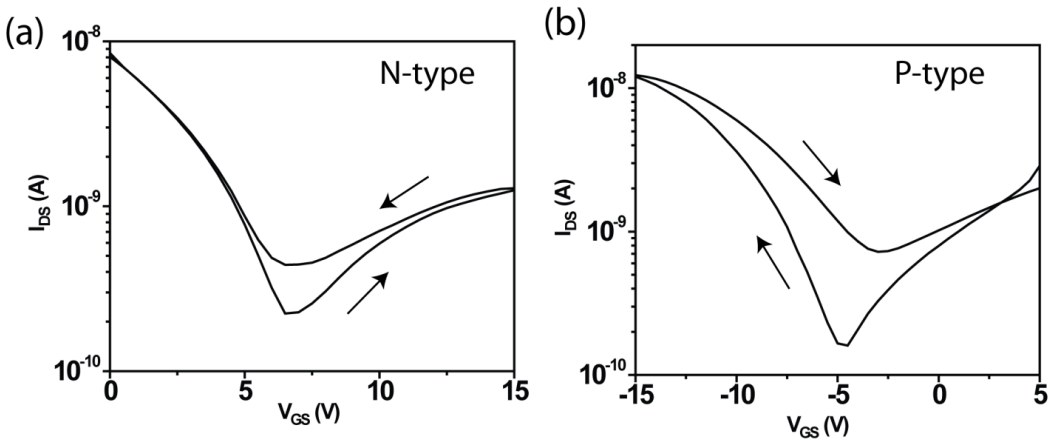

Figure 5.5. Dual sweep transfer characteristics of the ambipolar device fabricated using PMMA/PVA as the dielectric material (a) n-type (b) p-type measured under vacuum conditions.

To realize the sustainability of these devices, and the stability, reproducibility and performance of the laminated gate device under vacuum conditions, back to back scan measurements were analyzed ten times (Figure 5.6(a) & (b)). In back to back scan measurements the transfer curves were collected several times continuously without interruption. A threshold shift was observed in the n-type behavior, while it was negligible in the p-type. Generally, the shift in threshold is due to the charge trapping at the interface of organic semiconductor and dielectric material. More the shift in n-type transfer characteristic curve indicates that more electrons are trapped in the channel in the n-type measurement than the holes in the p-type measurements. These devices showed

TH-1703_11612241

less dispersion in the curves in the p-type behavior (Figure 5.6(b)). The measured threshold voltage shift values for the n-type and p-type transports of the OFETs are 3 V and 0.5 V. Moreover, sub threshold slope improved and the on/off-current ratio also increased by more than an order of magnitude, due to less trapping of holes than electrons.

5.3.3.3. Back to back scan measurements of PMMA/PVA device

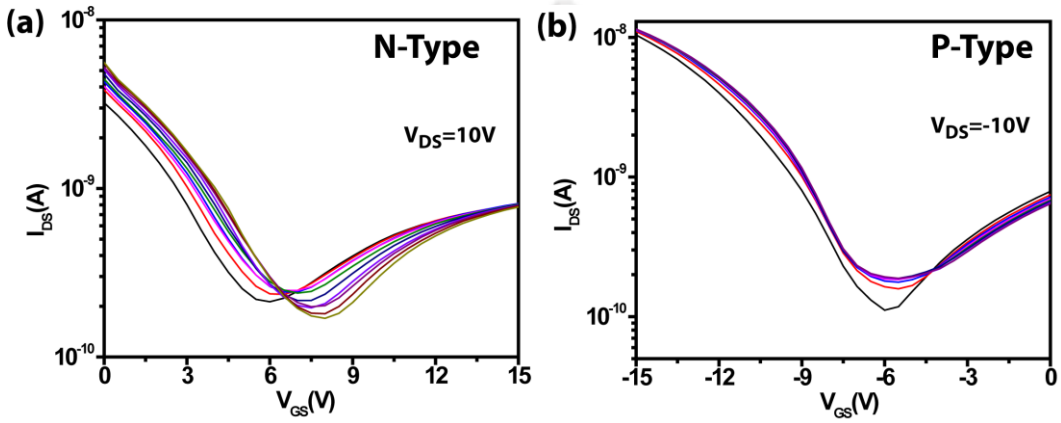

Figure 5.6. Set of 10 transfer curves of ambipolar organic field-effect transistors fabricated using PMMA/PVA as the dielectric material measured under vacuum conditions for (a) n-type (b) p-type, measured for 10 times.

5.3.4. Device Characterization under humidity conditions

In order to study the performance of the Al laminated flexible ambipolar devices under ambient conditions, the measurements were performed at ~60% RH (normal lab RH) conditions (Figure 5.7) for both electron and hole transport. Interestingly, under humidity conditions the device exhibited balanced ambipolar nature on either side of the applied voltage. The drain currents also increased by one order compared to the vacuum conditions. In addition, the switching of the n-type to p-type occurs at almost near zero for both electron and hole transport currents (Figure 5.7). Moreover, a drastic improvement was observed in the threshold voltage and sub-threshold slope due to less trapping of holes than electrons. The device parameters such as field-effect mobility, threshold voltage, sub-threshold voltage and on-off ratio are summarized in Table 5.2. The ambient atmosphere shifted the threshold voltage towards zero voltage and indicating the reduced traps in the interface. The reason for the improved performance of the

TH-1703_11612241

ambipolar characteristics is due to interaction of water molecules with the polar dipoles that exist in the PVA dielectric. In the presence of water molecules the polarization of the dipoles become faster and induce more charges in the interfaces leading to the decrease in the charge trapping and increase in the drain current. This may be due to the complete polarization of polar dielectric dipoles (–OH groups) in the presence of water molecules from ambient conditions.[32] However, in the vacuum, slow polarization of dipoles takes place and the number of charges induced in the interface is low. This situation leads to the faster degradation of the device. The enhancement of the ambipolar performance under the ambient condition is unique and an interesting phenomena. Generally, the performance and stability of the organic device is diminished under ambient conditions.[33-36] On the contrary to this general trend, these devices showed enhanced performance under ambient conditions.

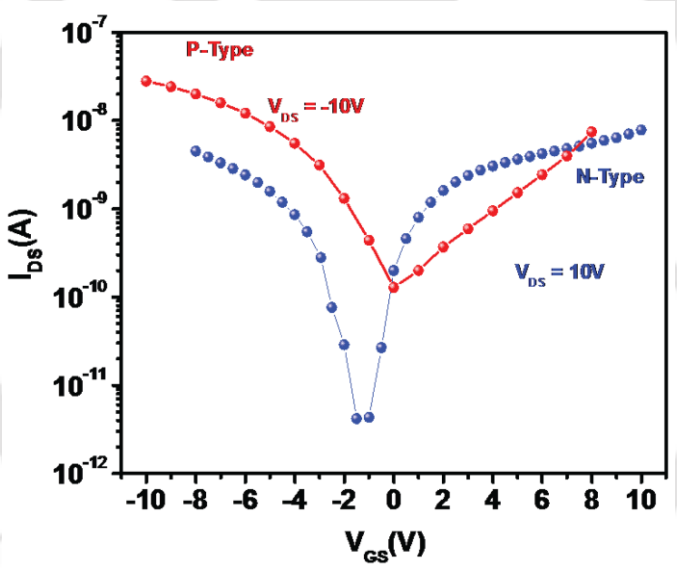

Figure 5.7. Balanced ambipolar behavior of the OFET device fabricated using PMMA/PVA as the dielectric material measured under humidity condition.

Table 5.2. Summary of the electrical parameters of the PMMA/PVA dielectric based organic field effect transistor measured under humidity conditions.

Device	V_{DS}	μ(cm^2/Vs)	V_{Th}(V)	S(V/dec)	$I_{on/off} \times 10^3$
n-type	10	5.4×10^{-4}	-1	0.63	1.63
p-type	-10	2.1×10^{-3}	0.6	1.85	0.21

TH-1703_11612241

5.3.5. Bias stability of PMMA/PVA based OFET under vacuum and ambient conditions

The electrical stability of the device was further studied by measuring the bias-stress for 1h under vacuum and ambient conditions. The normalized results for the bias stress of both n-type and p-type currents were shown in the Figure 5.8. The p-type transport behavior measured under vacuum conditions exhibited the anomalous bias-stress effect, where the current increased to higher value for some time followed by decay. The n- type transport exhibited as usual current decay with little increase in the drain current initially (Figure 5.8(a)). The current in the hole transport initially increased by four orders at 1000s bias stress time and then started to decay. In the electron transport, the current initially increased and starts decaying to 50% of the initial value at the end of 1h measurement time. Generally, the current decay under bias is due to the charge trapping at the interface and in the semiconductor/dielectric material. On the other hand, in the anomalous bias-stress the current enhancement with the bias time is due to the slow polarization of the dipoles in the polar dielectric material. These curves reveal that the electron charge trapping is higher than the hole trapping in these ambipolar devices.

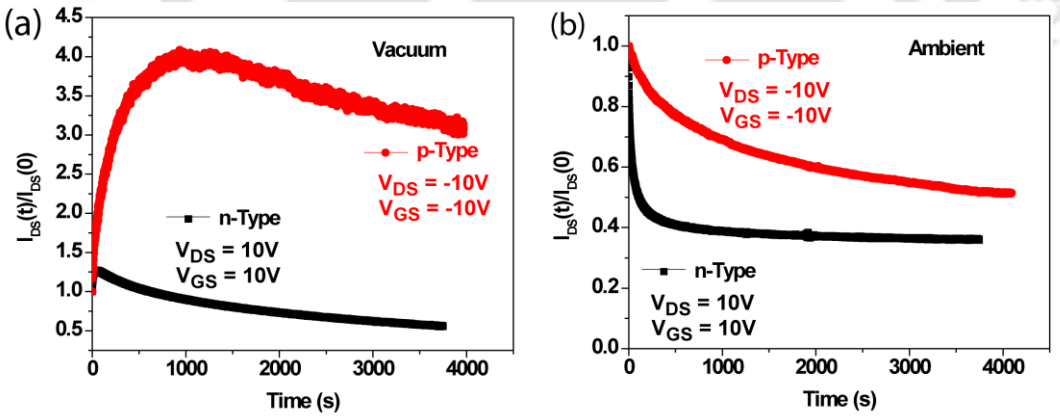

Figure 5.8. Bias stress measurements of the PMMA/PVA based OFET for 1h in (a) vacuum and (b) ambient.

Under ambient conditions in contrast to vacuum, both the charge transports decayed (Figure 5.8(b)) which was more pronounced for the hole current than the electron current. For the electron transport, the current decayed immediately to 40% and remained almost constant in the rest of the measurement time. The decay of both the currents under ambient conditions is due to the interaction of water and oxygen molecules and acts like

TH-1703_11612241

charge trapping sites leading to the degradation of the electron and hole currents (Figure 5.8(b)). Even though, both the curves decayed with time, the overall decay is 45% in the p-type transport and 60% in the n-type transport for 1h of bias stress measurement under ambient conditions. These results confirm the stability of the device under ambient conditions with 60% RH. For the n-type transport under ambient conditions, the rapid decay that occurred immediately after the device had been turned on suggested that the charge trap sites at the semiconductor/gate dielectric interface predominantly and rapidly interacted with the mobile carriers available in the channel region. Here, in this case there is no slow polarization of dipoles of dielectric. Hence, as in vacuum, p-type transistor shows the anomalous bias-stress effect, for n-type normal decay of I_{DS} observed, but in ambient condition both the currents decayed due to interaction of water molecules.

5.3.6. Ambipolar OFET fabrication and characterization using the cross linked PVA

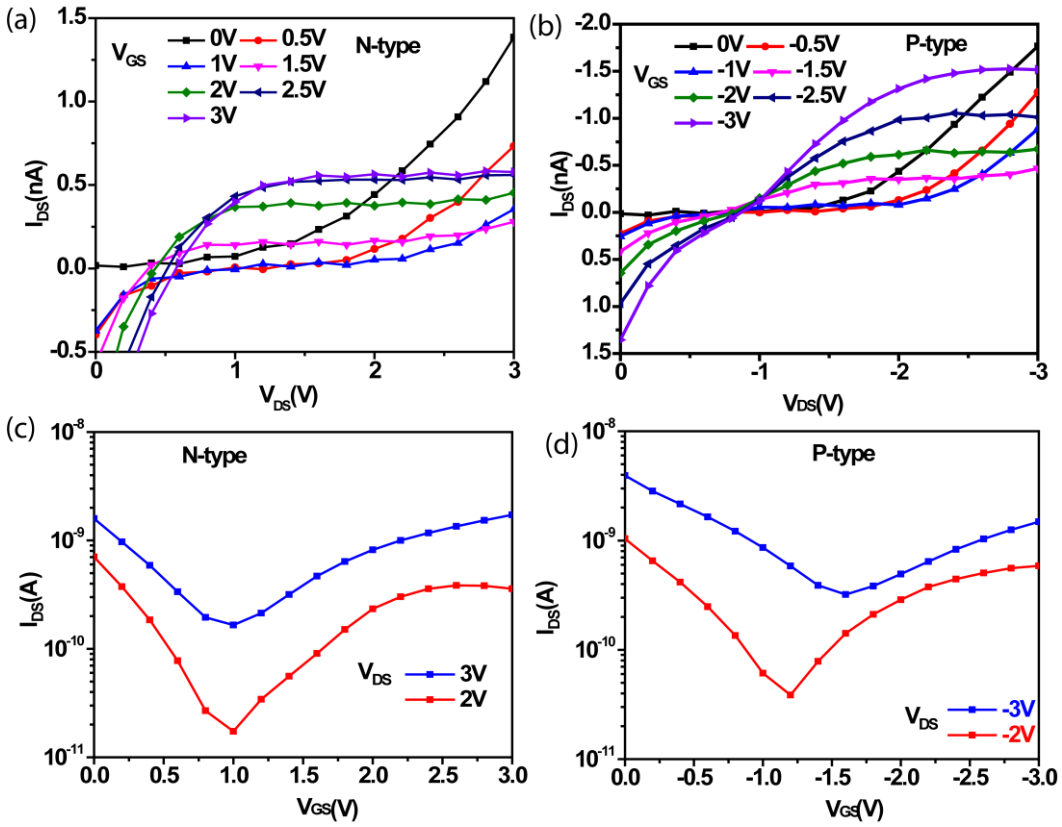

Figure 5.9. Output characteristics of the ambipolar device fabricated using cross linked PVA (C-PVA) as the dielectric material (a) n-type (b) p-type. Transfer characteristics of the ambipolar OFET (c) n-type (d) p-type

TH-1703_11612241

In addition to the PMMA/PVA dielectric based devices, low operating voltage ambipolar OFET devices on the Al laminated flexible plastic substrates using cross linked PVA (C-PVA) as the dielectric material were also fabricated. Typical output characteristics of the ambipolar OFET in hole-enhancement mode and electron-enhancement mode operations are shown in Figure 5.9(a) and 5.9(b). With the C-PVA, the operating voltage of the device was drastically reduced to below 3 V. The device parameters were calculated and tabulated in Table 5.3. The devices exhibited clear signature of ambipolar behavior which changed with the applied drain voltage and gate voltages like the previous devices. Figure 5.9(c) and 5.9(d) showed the transfer characteristics of the ambipolar transistor measured under vacuum. Ambipolar behavior for all devices with hole and electron mobilities of 3.4×10^{-4} cm^2/Vs and 2.0×10^{-4} cm^2/Vs were observed respectively, derived from the saturated currents.

Table 5.3. Summary of the electrical parameters of the C-PVA dielectric based organic field effect transistor measured under vacuum conditions.

Device	**V_{DS}**	**μ(cm^2/Vs)**	**V_{Th}(V)**	**S(V/dec)**	**$I_{on/off}$ ×10**
n-type	3	2.3×10^{-4}	0.35	1.60	1
	2	2.0×10^{-4}	0.75	0.81	2
p-type	-3	3.0×10^{-4}	-0.81	1.60	~1
	-2	3.4×10^{-4}	-1.62	0.82	1.5

5.3.7. C-PVA device bias stability under vacuum and humidity conditions

In order to exclude the effects of oxygen or water present in air, the bias stress measurement were performed under vacuum (~10^{-4} Torr). The fast degradation of the device current was clearly observed when gate bias stress was applied. The drain current as a function of time under the constant gate and drain bias was measured (Figure 5.10). Both the devices exhibited a decrease in I_{DS} as a function of time, indicating that the mobile carriers in the channel region were immobilized by gate bias. The faster decay in

TH-1703_11612241

the drain current may be due to the direct interaction charge trapping groups (-OH) in the PVA dielectric material with the organic semiconductor and channels. In the case of PMMA/PVA dielectric based device, the PVA and organic semiconducting material interfaces were separated by the hydrophobic PMMA layer. It was found that the hydrophilic / hydrophobic nature of the gate dielectric strongly determined the electrical stability of the device as the decay of $I_{DS}(t)/I_{DS}(0)$ intensified with the only PVA layer. In this case there is no PMMA layer which covers the PVA, the hydrophilic dielectric. The value of I_{DS} after applying 1h bias stress decreased to a very low value (Figure 5.10). As observed in the PMMA/PVA dielectric based device, the C-PVA based device did not show any visible anomalous bias stress effect, which may be due to the direct interaction of –OH groups with the charges at the interface. These low operating voltage ambipolar devices can be used in integrated circuits and for bio-sensor applications.

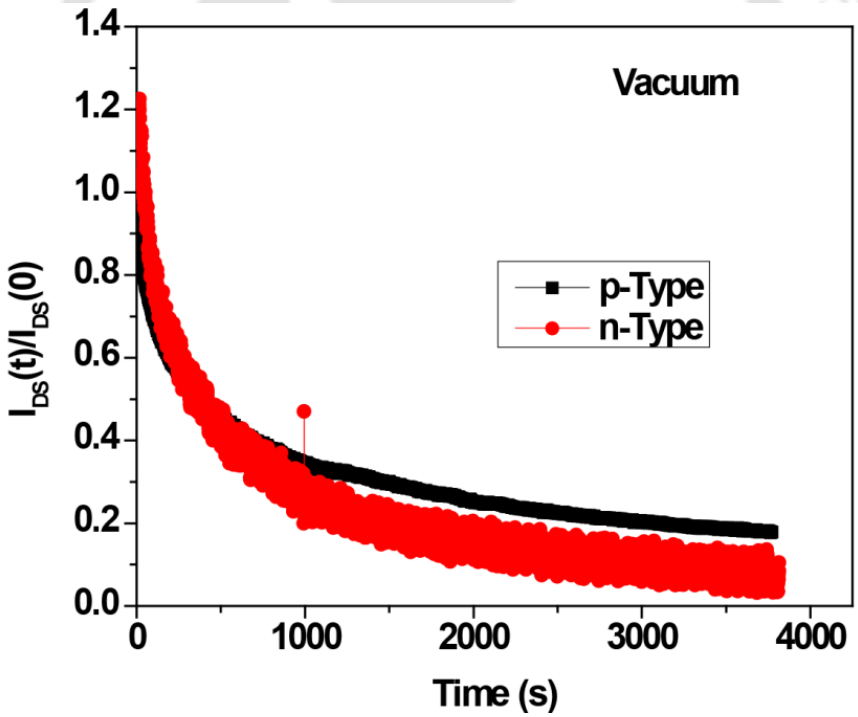

Figure 5.10. Time-dependent I_{DS} decay under a constant bias stress under vacuum conditions for the ambipolar organic field-effect transistors fabricated using C-PVA as the dielectric material. Both n-type and p-type transports measured for 1h.

TH-1703_11612241

5.3.8. Long term Stability of PMMA/PVA based ambipolar OFET

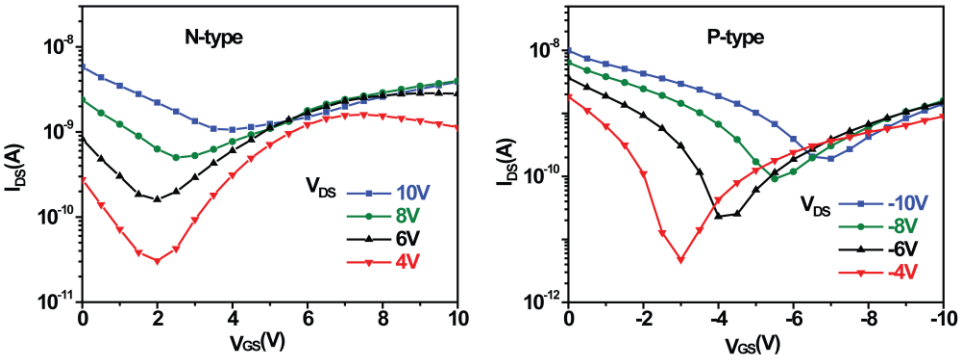

Figure 5.11. Transfer characteristics of the ambipolar device fabricated using PMMA/PVA as the dielectric material for n-type and p-type behaviors measured after 8 months under vacuum conditions.

Long term stability of the device is a crucial factor for the practical application of the OFET devices. In order to check the long term stability of the device, the measurements of the device were performed after 8 months of the fabrication. The transfer and output characteristics of the PMMA/PVA were shown in Figure 5.11. Except a small decrease in the I_{DS}, the devices were working well conforming that the devices fabricated on the low cost Al foil are very stable over extended time and can be useful for practical applications.

5.4. Conclusion

In summary, sustainable ambipolar OFET devices fabricated with a commercial Al foil laminated on a pristine low cost OHP flexible sheet without any electro or mechanical polishing showed good ambient stability. The top surface of the Al foil was anodized and PMMA/PVA dielectric material was spin coated to make the surface smooth and to increase the capacitance of the bilayer and then Br_2PTCDI-C18/CuPc hetero structure were deposited as active layer. The devices were operated at a low operating voltage of 10 V. The performance and dual polarity nature of the ambipolar devices were studied systematically under vacuum and humidity conditions. The device stability was also tested by performing the bias stress measurements at these conditions. The C-PVA gate dielectric on the low cost laminated Al foil was also used to fabricate high performance and ambient stable ambipolar OFETs with a simple architecture comprising Br_2PTCDI-C18/CuPc heterostructure as active layer within few hours and the operating voltages still

TH-1703_11612241

reduced to 3 V. The high performing, charge balanced, low operative voltage ambipolar behavior for all OFETs were demonstrated with electron and hole mobility values of 1.2 × 10^{-2} cm^2/Vs and 5.5 × 10^{-3} cm^2/Vs, respectively. The reproducibility and stability of these flexible, light-weight and low-cost devices were also studied so as to extend their practical utility in biosensors, electronic skin and nose. These ambipolar devices were also studied in different conditions (vacuum and ambient) and are described in this chapter. The hole currents exhibited anomalous bias stress effect whereas the electron currents decayed with time under vacuum. However, under humidity, both the currents decayed due to the charge trapping at the interface by the absorbed water molecules. The devices exhibited reproducible results in the ambient even after several days of exposure. All the electrical, ambient and long-term stabilities of the devices were systematically studied and presented here. These results demonstrate very easy fabrication of ambipolar device on low cost substrate and gate with good ambient and electrical stability, which are highly desirable for practical applications.

5.5. References

1. Dimitrakopoulos, C. D.; Malenfant, P. R. L. *Adv. Mater.* **2002,** *14* (2), 99.
2. Chua, L. L.; Zaumseil, J.; Chang, J. F.; Ou, E. C. W.; Ho, P. K. H. *Nature* **2005,** *434* (7030), 194-199.
3. Gelinck, G. H.; Huitema, H. E. A.; Van Veenendaal, E.; Cantatore, E.; Schrijnemakers, L.; Van der Putten, J. B. P. H.; Geuns, T. C. T.; Beenhakkers, M.; Giesbers, J. B.; Huisman, B. H.; Meijer, E. J.; Benito, E. M.; Touwslager, F. J.; Marsman, A. W.; Van Rens, B. J. E.; De Leeuw, D. M. *Nat. Mater.* **2004,** *3* (2), 106-110.
4. Capelli, R.; Toffanin, S.; Generali, G.; Usta, H.; Facchetti, A.; Muccini, M. *Nat. Mater.* **2010,** *9* (6), 496-503.
5. Myny, K.; Steudel, S.; Smout, S.; Vicca, P.; Furthner, F.; van der Putten, B.; Tripathi, A. K.; Gelinck, G. H.; Genoe, J.; Dehaene, W. *Org. Electron.* **2010,** *11* (7), 1176-1179.
6. Anthopoulos, T. D. *Appl. Phy. Lett.* **2007,** *91* (11), 113513.
7. Wei, Q.; Tajima, K.; Hashimoto, K. *ACS. Appl. Mater. Inter.* **2009,** *1* (9), 1865-8.
8. Anthopoulos, T. D.; de Leeuw, D. M.; Cantatore, E.; Setayesh, S.; Meijer, E. J.; Tanase, C.; Hummelen, J. C.; Blom, P. W. M. *Appl. Phy. Lett.* **2004,** *85* (18), 4205-4207.
9. Jones, B. A.; Facchetti, A.; Wasielewski, M. R.; Marks, T. J. *J. Am. Chem. Soc.* **2007,** *129* (49), 15259-15278.
10. Lee, B. H.; Hsu, B. B.; Patel, S. N.; Labram, J.; Luo, C.; Bazan, G. C.; Heeger, A. J. *Nano. Lett.* **2016,** *16* (1), 314-9.
11. Huang, J.; Zhu, H. L.; Chen, Y. C.; Preston, C.; Rohrbach, K.; Cumings, J.; Hu, L. B. *ACS. Nano.* **2013,** *7* (3), 2106-2113.

TH-1703_11612241

12. (a) Kaltenbrunner, M.; Sekitani, T.; Reeder, J.; Yokota, T.; Kuribara, K.; Tokuhara, T.; Drack, M.; Schwodiauer, R.; Graz, I.; Bauer-Gogonea, S.; Bauer, S.; Someya, T. *Nature* **2013,** *499* (7459), 458-63; (b) Dumitru, L. M.; Manoli, K.; Magliulo, M.; Sabbatini, L.; Palazzo, G.; Torsi, L. *ACS. Appl. Mater. Interfaces.* **2013,** *5* (21), 10819-23.
13. Taylor, D. M.; Patchett, E. R.; Williams, A.; Neto, N. J.; Ding, Z. Q.; Assender, H. E.; Morrison, J. J.; Yeates, S. G. *IEEE. T. Electron. Dev.* **2014,** *61* (8), 2950-2956.
14. Smits, E. C. P.; Mathijssen, S. G. J.; van Hal, P. A.; Setayesh, S.; Geuns, T. C. T.; Mutsaers, K. A. H. A.; Cantatore, E.; Wondergem, H. J.; Werzer, O.; Resel, R.; Kemerink, M.; Kirchmeyer, S.; Muzafarov, A. M.; Ponomarenko, S. A.; de Boer, B.; Blom, P. W. M.; de Leeuw, D. M. *Nature* **2008,** *455* (7215), 956-959.
15. Klauk, H.; Zschieschang, U.; Pflaum, J.; Halik, M. *Nature* **2007,** *445* (7129), 745-8.
16. Huang, C.; West, J. E.; Katz, H. E. *Adv. Funct. Mater.* **2007,** *17* (1), 142-153.
17. Shim, H.; Kumar, A.; Cho, H.; Yang, D.; Palai, A. K.; Pyo, S. *ACS. Appl. Mater. Inter.* **2014,** *6* (20), 17804-14.
18. Guillaud, G.; Alsadoun, M.; Maitrot, M.; Simon, J.; Bouvet, M. *Chem. Phys. Lett.* **1990,** *167* (6), 503-506.
19. Anthopoulos, T. D.; Setayesh, S.; Smits, E.; Cölle, M.; Cantatore, E.; de Boer, B.; Blom, P. W. M.; de Leeuw, D. M. *Adv.Mater.* **2006,** *18* (14), 1900-1904.
20. Seo, S.; Park, B. N.; Evans, P. G. *Appl. Phy. Lett.* **2006,** *88* (23), 232114.
21. Chang, J.-F.; Chen, W.-R.; Huang, S.-M.; Lai, Y.-C.; Lai, X.-Y.; Yang, Y.-W.; Wang, C.-H. *Org. Electron.* **2015,** *27*, 84-91.
22. Gao, D.; Zhang, X.; Kong, X.; Chen, Y.; Jiang, J. *ACS. Appl. Mater. Inter.* **2015,** *7* (4), 2486-93.
23. Hu, Y.; Zhang, N.; Lin, J.; Qin, L.; Liu, X. *Appl. Phy. Express.* **2012,** *5* (9), 095601.
24. Shkunov, M.; Simms, R.; Heeney, M.; Tierney, S.; McCulloch, I. *Adv. Mater.* **2005,** *17* (21), 2608-2612.
25. Smith, J.; Hamilton, R.; McCulloch, I.; Stingelin-Stutzmann, N.; Heeney, M.; Bradley, D. D. C. *J. Mater. Chem.* **2010,** *20* (13), 2562.
26. Xu, X.; Xiao, T.; Gu, X.; Yang, X.; Kershaw, S. V.; Zhao, N.; Xu, J.; Miao, Q. *ACS. Appl. Mater. Inter.* **2015,** *7* (51), 28019-26.
27. Sirringhaus, H. *Adv. Mater.* **2009,** *21* (38-39), 3859-3873.
28. Yan, Y.; Huang, L. B.; Zhou, Y.; Han, S. T.; Zhou, L.; Zhuang, J.; Xu, Z. X.; Roy, V. A. *Sci. Rep.* **2015,** *5*, 15770.
29. Vasimalla, S.; Senanayak, S. P.; Sharma, M.; Narayan, K. S.; Iyer, P. K. *Chem. Mater.* **2014,** *26* (13), 4030-4037.
30. Schwartz, G.; Ke, T.-H.; Wu, C. C.; Walzer, K.; Leo, K. *Appl. Phy. Lett.* **2008,** *93* (7), 073304.
31. Opitz, A.; Bronner, M.; Brütting, W. *J. Appl. Phys.* **2007,** *101* (6), 063709.
32. Subbarao, N. V.; Gedda, M.; Iyer, P. K.; Goswami, D. K. *ACS. Appl. Mater. Inter.* **2015,** *7* (3), 1915-24.
33. Knopfmacher, O.; Hammock, M. L.; Appleton, A. L.; Schwartz, G.; Mei, J.; Lei, T.; Pei, J.; Bao, Z. *Nat. Commun.* **2014,** *5*, 2954.

TH-1703_11612241

34. Chen, H. Z.; Ling, M. M.; Mo, X.; Shi, M. M.; Wang, M.; Bao, Z. *Chem. Mater.* **2007,** *19* (4), 816-824.
35. Li, L. Q.; Li, H. X.; Song, Y. B.; Xu, W.; Hu, W. P.; Zhu, D. B. *Res. Chem. Intermediate.* **2008,** *34* (2-3), 147-153.
36. Handa, S.; Miyazaki, E.; Takimiya, K. *Chem. Commun.* **2009,** (26), 3919-21.

TH-1703_11612241

Conclusions

Chapter 1 gives the brief introduction about Organic Field Effect Transistors, fabrication and working principles of OFETs and some recent developments in the synthesis of new materials for the fabrication of high performance n-type organic semiconducting materials. Particularly, the development of PDI and NDI based materials as the alternatives for the fullerenes was discussed.

Chapter 2 describes the synthesis of two new n-channel Perylenediimide (PDI) copolymers PDI-Ph, and PDI-BT. Remarkable enhancements in the electron transport behavior for copolymers were achieved on improving the intermolecular interactions in their thin film structures. These solution processable n-type copolymers having PDI backbone was synthesized in high yields (83-86%) by palladium catalyzed Suzuki coupling reactions. Since these copolymers possess crystalline domains, annealing their films induced crystalline phases in the thin film structures with a very high degree of enhancement in crystallinity. The annealing of films resulted in significant enhancement in the intermolecular interactions in the thin film state on the macro scale, facilitating improved and higher charge carrier transport in annealed devices as compared to the as-spun devices which are having lesser crystalline phases. It is observed that the extended conjugation in the copolymer structures, the efficient intermolecular interactions in the thin film state, and the formation of crystalline domains in the copolymers after annealing are responsible for the enhanced device performance. These copolymers demonstrated electron mobility as high as 0.04 cm^2 V/s and 0.032 cm^2 V/s for PDI-Ph and PDI-BT are, respectively, with I_{on}/I_{off} ratios of 10^3-10^4.

Chapter 3 demonstrates synthesis of two new n-channel Naphthalene diimide (NDI) based copolymers NDI-Ph, NDI-BT and fabrication of solution processed thin film transistor (TFT) devices are reported. These solution processable n-type copolymers were synthesized in high yields (83-86%) by Suzuki coupling reactions. As in case of PDI polymers the annealing of thin films of these polymers also results enhancement in the intermolecular interactions in the thin film state on the macro scale, facilitating improved and higher charge carrier transport in annealed devices as compared to the as-spun devices that have lesser crystalline phases. The enhancement in μ_e values for all four copolymers is very large for any reported n-type copolymers. The extended conjugation

TH-1703_11612241

in the copolymer structures, the efficient intermolecular interactions in the thin film state, and the formation of crystalline domains in the copolymers after annealing improved the device performance. These copolymers have shown electron mobility enhancement of several orders and are reported to be as high as 0.8 cm^2 V/s and 0.2 cm^2 V/s for NDI-PH and NDI-BT respectively, with I_{on}/I_{off} ratios of 10^3-10^4.

Chapter 4 provides the study of variation of the device parameters by changing the dielectric layer, modification of the dielectric layer at different channel lengths of the OFET. We fabricated the low cost OFET with a new molecule Br_2PTCDI-C18 on glass substrate. In this study we used a bilayer dielectric system Al_2O_3/ PVA and Al_2O_3/PMMA. The effect of HMDS as SAM was also studied. The devices were fabricated at 25 µm, 50 µm, 100 µm, 190 µm channel lengths with all the combinations of different dielectric systems Al_2O_3/PVA, Al_2O_3/PMMA, Al_2O_3/PVA/HMDS, Al_2O_3/PMMA/HMDS. It was observed that as the channel length decreases the I_{DS} increases and the HMDS layer increases the I_{on}/I_{off} ratios of the device.

Chapter 5 presents the fabrication of low cost, flexible, ambient stable, low operating voltage and balanced ambipolar organic field-effect transistors on plastic over-head projecter (OHP) sheets as transparent substrates using laminated Al foil as gate electrode without any mechanical or electro polishing for the first time. Br_2PTCDI-C18 is used as n-channel and copper phthalocyanine (CuPc) as p-channel semiconductors. In the first device PMMA/PVA used as the dielectric layer and achieved electron and hole mobilities as high as 1.2×10^{-2} cm^2 V/s and 5.5×10^{-3} cm^2 V/s respectively, with the operating voltages ± 10V. Then in the second device we used C-PVA (Crosslinked PVA) as the dielectric material and the operating voltages are further reduced to ± 3V. The electrical, ambient and long-term stabilities of the devices were studied. These results demonstrate very easy fabrication of ambipolar device on low cost substrate and gate with good ambient and electrical stability, which are highly desirable for practical applications.

TH-1703_11612241

List of Publications

1. **Suresh Vasimalla**, Satyaprasad P. Senanayak, Meenakshi Sharma, K. S. Narayan, Parameswar K. Iyer, Improved performance of Solution Processed n-type Organic Field-Effect Transistors by Regulating the Intermolecular Interactions and Crystalline Domains on Macroscopic Scale" ***Chem. Mater.***2014, 26, 4030-4037.

2. Nimmakayala V. V. Subbarao, Murali Gedda, **Suresh Vasimalla**, Parameswar K. Iyer and Dipak K. Goswami, Effect of thickness of bilayer dielectric on 1,7-dibromo-N,N′-dioctadecyl-3,4,9,10-perylenetetracarboxylic diimide based organic field-effect transistors, ***Physica Status Solidi (A).*** Applications and Materials Science.2014, 211, 2403-2411.

3. Nimmakayala V. V. Subbarao, Murali Gedda, **Suresh Vasimalla**, Anamika Dey, Parameswar K. Iyer and Dipak K. Goswami, Growth and characterization of N, N'-dioctadecyl-1,7-dibromo-3,4,9,10-perylenetetracarboxylicdiimide micron/nano wires for organic field effect transistors, ***AIP Conf. Proc.*** 2014, 1576, 42-45.

4. **Suresh Vasimalla,** Nimmakayala V. V. Subbarao, Parameswar K. Iyer, Low voltage, low cost, flexible and balanced ambipolar OFETs based on Br_2PTCDI-C18/CuPc fabricated on an Al foil gate substrate with good ambient stability, ***J. Mater. Chem C***, 2016, 4, 7102-7109.

5. **Suresh Vasimalla,** Nimmakayala V. V. Subbarao.; Parameswar K. Iyer, Effect of dielectric material, HMDS and channel length on the performance of the Perylenediimide based Organic Field-Effect Transistors, ***J. Mater. Chem C***, (Minor revision)

6. **Suresh Vasimalla**, Parameswar K. Iyer, Synthesis and characterization of Naphthalenediimide and Benzo Selenadiazole based Donor-Acceptor polymers by direct C-H arylation. (Manuscript prepared)

TH-1703_11612241

Conferences

1. "2nd International Conference on Advanced Nanomaterials and Nanotechnology (ICANN-2011)" held at IIT Guwahati, Guwahati, during Dec 8- 10, 2011.
2. "3rd International Conference on Advanced Nanomaterials and Nanotechnology (ICANN-2013)" held at IIT Guwahati, Guwahati, during Dec 1-3, 2013.
3. "International Symposium on Polymer Science and Technology, Macro 2015" held at IACS Kolkata, Kolkata during January 23-26.
4. "INUP Familiarization Workshop" especially for the North East at IIT-Guwahati" during 28-29 September 2012, India.
5. "INUP Hands on training and work shop" held in Center for Nanotechnology and Nano Science, IISc Bangalore during 24 June - 3 July 2014.
6. "The Annual Chemical Engineering Symposium Reflux 2015" held in Department of Chemical Engineering, IIT Guwahati on March 27-29, 2015.
7. "4th International Conference on Advanced Nanomaterials and Nanotechnology (ICANN-2015)" held at IIT Guwahati, Guwahati, during Dec 8-10, 2015.

TH-1703_11612241